Home of the 1996 Olympic Village
Georgia Institute of Technology

Office of Contract Administration
Contracting Support Division
Atlanta, Georgia 30332-0420 U.S.A.
PHONE 404·894·6944
FAX 404·894·5285

June 22, 1999

In reply refer to: E-16-X38

IN-25
077248
p 137

Dr. Howard Ross/ 6711
NASA Lewis Research Center
Microgravity Combustion Branch
Mail Stop 500-115
21000 Brookpark Road
Cleveland, OH 44135

Subject: Summary of Research (Final Report)
Project Director(s): Dr. Suresh Menon
Telephone No.: (404)894-9126
Contract No.: NAG3-1610
Prime No.: N/A
"PREMIXED TURBULENT FLAME PROPAGATION IN MICROGRAVITY"
Period Covered: 940525 - 980824

The subject report is forwarded in conformance with the contract/grant specifications.

Should you have any questions or comments regarding this report(s), please contact the Project Director or the undersigned at 404-894-4763.

/tw

Sincerely,

Thelma Woods
Customer Service Representative

Distribution:
Addressee: 1 copy
1 copy to: Ms. Mira Alberto, Grants Office , Mail Stop 500-315
1 copy to: NASA, Center for Aerospace Information (CASI) ***Final Technical Report Under Grant NAG3-1610 and Grant NAG3-2192

SUMMARY

A combined numerical-experimental study has been carried out to investigate the structure and propagation characteristics of turbulent premixed flames with and without the influence of buoyancy. Experimentally, the premixed flame characteristics are studied in the wrinkled regime using a Couette flow facility and an isotropic flow facility in order to resolve the scale of flame wrinkling. Both facilities were chosen for their ability to achieve sustained turbulence at low Reynolds number. This implies that conventional diagnostics can be employed to resolve the smallest scales of wrinkling. The Couette facility was also built keeping in mind the constraints imposed by the drop tower requirements. Results showed that the flow in this Couette flow facility achieves full-developed turbulence at low Re and all turbulence statistics are in good agreement with past measurements on large-scale facilities. Premixed flame propagation studies were then carried out both using the isotropic box and the Couette facility. Flame imaging showed that fine scales of wrinkling occurs during flame propagation. Both cases in 1g showed significant buoyancy effect. To demonstrate that micro-g can remove this buoyancy effect, a small drop tower was built and drop experiments were conducted using the isotropic box. Results using the Couette facility confirmed the ability to carry out these unique reacting flow experiments at least in 1g. Drop experiments at NASA GRC were planned but were not completed due to termination of this project.

The parallel numerical study developed a new subgrid combustion modeling approach for large-eddy simulation (LES) of turbulent combustion. This LES model was then applied to simulate both non-reacting and reacting flows in the Couette flow facility. Validation of the non-reacting LES was accomplished by comparison with past data and it was demonstrated that the present LES could capture all turbulence statistics using very coarse grid resolution. Simulation of reacting Couette flow with and without buoyancy showed that the effect of gravity is quite significant at low Reynolds number. Analysis showed that heat release significantly changes the flame-vortex interaction process. The buoyancy effect was found to depend strongly on the direction of propagation relative to the direction of gravity. Overall buoyancy increases the tangential strain in the plane of the flame. The overall fuel consumption is decreased but the contribution of the subgrid scales towards creation of the turbulent flame area is more in the presence of buoyancy.

These studies have established a unique experimental-computational capability to study fully resolved turbulent premixed flames. Many issues such as the impact of varying the Karlovitz, Damkohler, Lewis and Reynolds numbers can be studied using these facilities.

PREMIXED TURBULENT FLAME PROPAGATION IN MICROGRAVITY

Suresh Menon
School of Aerospace Engineering
Georgia Institute of Technology
Atlanta, GA 30332

Final Technical Report
under
Grant NAG3-1610
and
Grant NAG3-2192

Submitted to
Microgravity Combustion Program
NASA Glenn Research Center
Cleveland, OH

June 1999

1. Introduction

The structure and propagation of turbulent premixed flames have been investigated for some time. A regime which occurs in numerous combustion systems is called the wrinkled flamelet regime. In this regime, chemical reactions occur in thin sheets and the flame thickness is much smaller than the smallest turbulent (Kolmogorov) eddy. Thus, turbulence does not change the flame structure and only wrinkles the flame. The resulting increase in flame area has been used to estimate an effective "turbulent" flame speed u_t as a function of the laminar flame speed S_L and the turbulence intensity u'. However, the exact form of the relation: $u_t=(S_L, u')$ has not yet been fully resolved although many models have been proposed. A key reason for this uncertainty is the inability to experimentally resolve in a typical high Reynolds number (*Re*) flow, all the scales of motion that could contribute to flame wrinkling. Experimental verification in real devices is almost impossible to achieve both due the difficulty in resolving the entire range of turbulent scales and due to the complexity of the flow. As a result, most experiments are conducted using relatively "clean" flows such as stagnation point flows, premixed flames in diverging ducts, etc. The typical test conditions are such that the Reynolds number is too high to allow resolution of all the turbulent scales.

Experimentally, turbulent fluctuations at the small scales can be resolved only if the Re is reduced (e.g., by reducing the flow velocity). A flow field that provides sustained turbulent flow in a relatively low Re is Couette flow. As shown earlier, stationary turbulent Couette flow is achieved at Re (based on belt speed and spacing) as low as 1800. However, with heat release, the turbulent stresses responsible for momentum transport can be overwhelmed by the buoyant stresses in normal gravity. Since this phenomenon is not present in realistic high Reynolds number devices, a microgravity environment is required to suppress the buoyancy effects while still maintaining reasonable operating pressure, temperature and observable scales at all sizes.

The experiments carried out under this project were leading towards a series of drop experiments that would have been unique under the microgravity program. However, since this project was not renewed the final series of drop experiments were not possible. The delay in carrying out these experiments were due to the complexity of the test configuration and the problem attempted under this project. In spite of this, we have been successful in achieving all our goals except the final drop experiments. In fact, as a prelude to the planned drop experiments at NASA, an isotropic turbulence flow device was built and successfully dropped in our laboratory. This facility provided an additional capability to investigate premixed flame propagation in turbulent flow and was also used for some of the studies.

The present study investigated turbulent premixed flames in the *wrinkled flamelet regime* where the preheat zone is undisturbed by turbulence. The wrinkled flamelet regime can be characterized by high Re_l where l is the integral length), high Damkohler number Da >>1 and a Karlovitz number, Ka < 1. In practical combustion systems, other regimes can occur. A regime of interest is the *distributed reaction regime* which in its extreme range is characterized by low *Re*, low *Da* and Ka>>1. In this regime, the flame thickness is much larger than the integral scale and transport within the reaction zone is modified by the turbulence. An intermediate range within this regime, called *flamelets in eddies regime* or *thin reaction zones*, often occur in practical combustors. This regime, approximately characterized by moderate-to-high *Da*, high *Re* and Ka>1, contains turbulent eddies that penetrate into the preheat zone, but not into the reaction zone of the flame structure. Eddies mix the unburned reactants with the burnt products causing significant transport of heat upstream of the flame. This thin reaction zone regime falls within the operational range for the present Couette flow facility and therefore, provides us with a unique opportunity to extend the current investigation (possibly in the future) to this equally important regime in turbulent premixed combustion.

2. Experimental Facilities and Codes Developed Under this Project

Here, a brief description is given of the flow facilities that have been built and planned for this research. This report also summarizes all the effort carried out under this project. Most of the results were presented earlier (copies of all presentations are included as appendices).

2.1 Non-Reacting Couette Flow Facility:

A non-reacting Couette facility was built to carry out the turbulence measurements and to demonstrate that sustained turbulence can be achieved in this device. This device has been designed to fit inside the NASA Lewis 2.2's drop tower rig and therefore, is much smaller than the facilities used in laboratory Couette flow studies. For example, the current length to gap ratio is 14 compared to 30-158 of the earlier devices. In addition, the current device operates in a closed loop, (i.e., turbulent flow is forced to re-enter the test section) whereas, classical devices transition the flow from laminar to turbulent. In addition to demonstrating that turbulent Couette flow can be achieved in a compact device, the experience gained in this facility helped in the integration of the device into the drop rig.

The maximum Reynolds number (based on belt speed and spacing) that can be achieved in this device is 30,000 based on the belt speed and spacing. Thus, this device can achieve both low turbulent Re values where buoyancy is dominant and high Re values where buoyancy can be ignored. Details of this facility is reported in the papers included in the appendix (Menon et al., 1997, Disseau et al., 1997).

2.2 Constant Volume Reactor:

To investigate safety issues and to study issues involving flame measurement during the drop, a device that generates nominally isotropic turbulence was also built. This device is essentially a rectangular box with fans in the chamber that are used to churn the premixed reactants. This device is quite similar to devices used earlier by many researchers to study premixed flame propagation in isotropic turbulence. However, unlike the Couette facility, the turbulent decays in this device. Drop experiments have been carried out at Georgia Tech using an in-house facility that was recently built. Measurements indicate that we get low-gravity of around 0.01g for around 0.3 sec which is adequate. This device is another tool to address turbulent premixed flames.

Results were reported earlier (Menon et al., 1997; Disseau et al., 1998). These papers are included in the appendix.

2.3 Reacting Couette Flow Facility:

Using our experience with the non-reacting studies in the Couette facility and the drop experiments with the isotropic box, we built a reacting Couette facility. Due to the safety requirements that must be met during the drop experiments at NASA, some changes to the non-reacting design had to be carried out. However, in most aspects, this facility mimics the non-reacting facility. Unfortunately, this project was not renewed and the microgravity drop experiments had to be terminated. However, with some bridge funding support from NASA LERC we were able to carry out a limited series of tests in 1g of reacting Couette flow. The primary goal of this series was to demonstrate that (a) premixed flame propagation in Couette facility can be successfully accomplished and (b) imaging of the premixed flame in the flow can be carried out. Recent results obtained in this facility are summarized the appendix of this report later.

2.4 Subgrid Combustion based LES Methodology:

A parallel large-eddy simulation (LES) solver has also been developed and used to study turbulent premixed flames. In this methodology turbulent combustion is simulated in the subgrid. The key advantage of this method is that, given the subgrid turbulence and the laminar flame speed, the model predicts the turbulent flame brush structure and the effective propagation speed. Thus, the experimental data on the turbulence and reactant composition can be used for model validation. The results obtained so far with this method have demonstrated its ability to capture thin flames accurately without requiring exorbitant LES grid resolution (since the flame is resolved in the small-scales). This new subgrid combustion, model-based LES provides an unique new capability to study high Re wrinkled flames that cannot be fully resolved in the laboratory.

The current development of a new subgrid combustion model for LES has been reported in the past (Menon et al., 1997; Chakravarthy and Menon, 1997, 1998) and therefore, avoided here for brevity. Briefly, this approach simulates the flame propagation, molecular diffusion, chemical reactions, heat release and small-scale turbulent mixing as independent but concurrent processes all occurring within the subgrid. This approach is physically consistent with the actual process of combustion since molecular (both mass and heat) transport occurs at scales that cannot be resolved on a conventional grid. Furthermore, this process occurs only when the species have been mixed at the small scales. For premixed combustion using the G-equation approach, this translates to simulating laminar propagation and heat release (and volumetric expansion) within the subgrid while the subgrid eddies wrinkle and increase the local flame surface. Details of this approach have been given elsewhere (Menon et al., 1993; Menon and Calhoon, 1996; Smith and Menon, 1996; Chakravarthy and Menon, 1997).

Many fundamental issues had to be resolved to carry out accurate simulation of turbulent premixed flames using this approach. A key issue that had to be addressed was the coupling between the LES-resolved large-scale motion (obtained by dynamic simulation of the momentum equations) and the subgrid-resolved flame propagation, heat release and turbulent mixing processes. The problems in coupling occur primarily because an Eulerian scheme is used for the LES equations while the transport of the subgrid fields across LES cells is carried out using a Lagrangian approach. The latter approach is a key requirement in our approach since it allows us to capture both co- and counter-gradient effects on the flame without requiring any ad hoc modifications (in contrast, conventional LES would allow only gradient diffusion). Furthermore, the combination of the Lagrangian scheme for large-scale transport and the mixing and propagation models in the subgrid allows us to capture premixed flames within one-two LES cells (whereas, conventional approach would numerically diffuse the front).

Most of the earlier results were reported in the papers cited above. A more recent paper being revised for submission to a journal (Combustion Science and Technology) is also included in the appendix. This paper summarizes our results of LES of Couette premixed flames and the impact of buoyancy on the flame propagation characteristics. As reported, even in the configuration chosen for our experiments, significant buoyancy effects are encountered. This further justified our original project goal of doing these studies in microgravity environment.

3. Summary of Results from the Reacting Couette Experiments

The effect of gravity on turbulent pre-mixed flame propagation was investigated in two different facilities, a stirred, constant volume reactor and a Couette flow reactor. Results for these studies are summarized here. More details are in the papers included in the appendix (Disseau et al, 1999).

3.1 Premixed flame studies in the Constant Volume Reactor

In this device the flammable mixture was stirred with a fan in an enclosed cube with optical access. Once the flow was fully turbulent the fan was switched off and the mixture was ignited using a spark located at the center of the reactor. This combustion chamber could be dropped in a drop tower at the Aerospace Engineering Combustion Laboratory on the Georgia Tech campus.

The stirred reactor has the advantage of being relatively simple to operate and producing a comparatively simple flow field. The fact that it can be dropped in-house allows us to carry out orders of magnitude more runs at negligible cost compared to what could be done at NASA Lewis. However, the level of turbulence is harder to control since it starts to decay as soon as the fan is switched off. In addition, turbulence is no longer generated (by the fan) once the flammable mixture has been ignited. In the confined reactor, the propagating flame must then be expected to affect the level of turbulence ahead of itself. This must somehow be corrected for.

Because of the short duration of the drop, even in the NASA drop tower, the diagnostics that can be carried out under conditions of micro gravity are limited to imaging of flame radiation, Schlieren, shadow and, possibly, image velocimetry. It was, therefore, decided to fill the reactor with air and fully characterize the turbulent flow field under conditions of gravity using laser Doppler velocimetry. The air was then replaced by a flammable mixture, which was ignited. The ignition process as well as the flame spread was then imaged under conditions of gravity and micro gravity. From comparisons between the resultant images it was then anticipated that the effect of gravity on the turbulent, reacting flow field could be determined.

Laser Doppler velocimetry studies on the stirred reactor indicated the turbulence decayed relatively slowly. It was, therefore, possible to disconnect the fan just prior to the drop and still have relatively high turbulence intensities during ignition and propagation of the flame. Turbulence intensity, however, did decay throughout this time. In addition, the turbulence was not totally isotropic although very little mean flow remained during the tests. In addition, the degree to which the flame front propagating in the confined chamber affected the turbulence level ahead of the flame remains to be quantified. In light of the above it was concluded that it would be necessary to construct a four fan facility in order to obtain more reliable results.

Nevertheless, it was possible to obtain shadowgrams of lean, turbulent, premixed methane-air flames in 1g and micro gravity environments, Comparisons of the images obtained under the two conditions showed that the effect of gravity was essentially eliminated during the drop. The results also seem to indicate that gravity has an effect on the turbulent flame speed. However, the precise nature of the interaction between turbulent flame propagation and gravity appears to depend on the level of turbulence and the stoichiometry of the flame. This work is being continued. However, further studies are no longer funded under this contract.

3.2 Premixed flame studies in the Reacting Couette Flow Facility

The Couette flow was generated using an endless Mylar belt running between a set of rollers. The entire apparatus was enclosed in an explosion proof housing with optical access. This facility was designed to be dropped in the 2.2 second micro gravity drop tower on the

NASA LRC campus in Cleveland OH. It is too big to be dropped in the drop tower on the Georgia Tech campus.

The Couette reactor has a constant turbulence level across most of its flow field (unlike the constant volume reactor where turbulence always decays). Nearly constant turbulence is achieved in both space and time; the former because of the nature of the Couette flow and the latter because new turbulence is constantly being generated by the moving belt. The flow, however is much more complex and its interaction with the propagating flame is, therefore, more difficult to quantify.

The flow in the Couette facility was found to be largely two-dimensional with constant turbulence intensities near the core. Slight flow asymmetries were introduced by the non-symmetric recirculation of fluid outside the test region. Belt flutter was reduced by adding a pair of guide plates. The confined nature of the flow caused the turbulence level to be somewhat higher than previously observed in open Couette flows. The spatial resolutions of the experimental techniques used were determined to be sufficient to resolve flow structures down to the Kalmogorov scale for Reynolds numbers up to 10,000. For this flow condition the turbulent velocity fluctuations were four times the magnitude of the laminar flame speed for a lean methane-air mixture. Thus, a wrinkled, premixed turbulent flame could be produced in the Couette facility. When a low density plasma was introduced into the flow tracking its interface with the cold air showed that even for this turbulent flow buoyancy, and thus, the effect of gravity persists.

Ignition and flame spread in the turbulent Couette flow was visualized using high speed Schlieren. An in-house developed analysis program was used to identify the flame front in the images. This capability permitted us to follow the flame front as it progressed through the turbulent flow. It was noted that an initial, smooth flame kernel was formed by the ignition process which then transformed into a wrinkled, turbulent flame. The effects of the flow field and that of gravity were clearly noted. Work is continuing on these experiments to the extent possible without NASA support.

Results obtained so far are summarized in the appendix.

APPENDIX

The Appendix contains copies of the papers and presentations given during the course of this research project. Some of the papers are currently under revision for publication in archival journals.

PUBLICATIONS and PRESENTATIONS UNDER THIS GRANT

Menon, S., Jagoda, J. and Sujith, S. "Turbulent Premixed Flames in Microgravity," Proceedings of the Third International Microgravity Combustion, Cleveland, Ohio, April 1995.

Menon, S. and Chakravarthy, K., "Large-Eddy Simulations of Turbulent Premixed Flames in Couette Flow," AIAA Paper No. 96-3077, 32nd AIAA/ASME/SAE/ASEE Joint Propulsion Meeting, Orlando, FL, July 1-3, 1996.

Menon, S., Disseau, M., Chakravarthy, V. K., and Jagoda, J., "Turbulent Premixed Flame Propagation in Microgravity," Fourth International Microgravity Combustion Workshop, May 19-21, NASA CP 10194,pp. 155-160, 1997.

Disseau, M. L., Menon, S., and Jagoda, J., "The Effect of Gravity on Turbulent, Premixed Flame Propagation - A Preliminary Cold Flow Study," AIAA 97-0672, 35th Aerospace Sciences Meeting, Reno, NV, January 6-9, 1997.

Chakravarthy, V. K. and Menon, S., "Characteristics of a Subgrid Model for Turbulent Premixed Combustion," AIAA Paper No. 97-3331, 33rd AIAA/ ASME/SAE/ASEE Joint Propulsion Conference and Exhibit, Seattle, WA, July 6-9, 1997.

Disseau, M., Menon, S., Jagoda, J., and Lal, M., "The Effect of Gravity on Turbulent, Premixed Flame Propagation," AIAA Paper No. 98-0566, 36th Aerospace Sciences Meeting and Exhibit, Reno, NV, January 12-15, 1998.

Chakravarthy, V. K. and Menon, S. "Heat Release and Buoyancy Effects on Turbulent Premixed Flames," in preparation (to be submitted to Combustion Science and Technology), 1999.

APPENDIXES

- "Experimental Studies in Turbulent Premixed Combustion With and Without Buoyancy," M. Disseau, J. Jagoda and S. Menon. 27th Int'l Symposium on Combustion, Aug. 1998.

- "Heat Release and Buoyancy Effects on Turbulent Premixed Flames," V. K. Chakravarthy and S. Menon. Preparation for submission to *J. of CS&T.*

- "The Effect of Gravity on Turbulent Premixed Flame Propagation," M. Disseau, M. Lal, S. Menon and J. Jagoda. Poster Presentation AIAA 36th Aerospace Sciences Meeting, 1998.

- "The Effect of Gravity on Turbulent Premixed Flame Propagation," M. Disseau, D. McElhannon, M. Lal, S. Menon and J. Jagoda. AIAA 98-0566, 1998

- "Turbulent Premixed Flame Propagation in Microgravity", S. Menon, M. Disseau, V. K. Chakravarthy and J. Jagoda. 4th Int'l Microgravity Comb. Workshop, 1997

- "Turbulent Premixed Flame Propagation in Microgravity", S. Menon, M. Disseau, V. K. Chakravarthy and J. Jagoda. 4th Int'l Microgravity Comb. Workshop, 1997

- "Characteristics of a Subgrid Model for Turbulent Premixed Combustion," V. K. Chakravarthy and S. Menon. AIAA 97-3331

- "The Effect of Turbulent Premixed Flame Propagation – a Preliminary Cold Flow Study," M. Disseau S. Menon, J. Jagoda and R. Sujith. AIAA 97-0672

- "Large-Eddy Simulations of Premixed Flames in Couette Flow," S. Menon and V. K. Chakravarthy. AIAA 96-3077.

"Experimental Studies in Turbulent Premixed Combustion With and Without Buoyancy"
M. Disseau, J. Jagoda, S. Menon

Presentation
27th Symposium (International) on Combustion
Boulder, Colorado
August 2-7, 1998

1. Premixed flame studies in the Constant Volume Reactor

1.1 Experimental Facility and Methods

The stirred constant volume combustion chamber, which is used in the GT drop tower, is shown in Fig. 1. It was fabricated out of steel and designed to withstand pressures up to 150 psi. A stirrer (1), which consists of a 6 inch in diameter 4-blade fan, is mounted on one side. It is supported by two bearings, and sealed with an o-ring. A Lovejoy connector is attached to the end of the drive shaft to allow, not only easy alignment with the motor, but also quick disconnect. Two quartz windows (5) allow optical access to the turbulent flame in the chamber. The two mirrors (6) attached to the device are part of shadow-graph system described below. The stirred reactor is filled with a combustible mixture through a port located at the bottom (4). The partial pressure method was used to calculate the stoichiometry of the mixture. A homemade spark plug (1) and its ignition system are located on the side opposite the stirrer.

A small drop tower was designed and constructed in the Aerospace Engineering Combustion Laboratory on the Georgia Tech campus, see Fig. 2. The constant volume combustion chamber discussed above (1) is raised to its starting position using a winch (not shown for simplicity). Here it is lined up with an electromagnet (hidden in this view). Once the magnet is powered, its 175 lbs. lifting capacity holds the device tightly in place. The lifting cables are then disconnected. Turning off the power to the magnet results in a clean release of the combustor. At the end of the free-falling drop the device is decelerated in a box filled with expanded polystyrene pellets (2), kindly donated by TechPak, Inc. Also shown in Fig. 2 is the shadow-graph system that is used to track the flame front during the drop. Light from a 0.95mW HeNe laser (3) is expanded and collimated by a set of lenses (4), into a 4 inch beam. This beam is sent down, through the combustion chamber, and then back up, using 3 mirrors (5), one fixed on the drop tower and two attached to the tower. The beam is then imaged onto a screen (6). (The lines starting with the HeNe laser and ending on this screen represent the light path taken by the laser light) A Kodak Ektapro intensified digital camera (7) running at 1000 frames per second records the images. These images can then be downloaded to a PC where they can be enhanced and processed to obtain flame speeds, shapes, and thickness.

Once the device is in position, the overall drop procedure consists of first turning on the ignition circuit. This prevents a spark generated by turning on the circuit from igniting the flammable mixture prematurely. Next the methane is injected into the chamber, and the gasses are given time to mix. The pressure in the reactor is monitored by a pressure gauge. The external piping is then disconnected. The motor is connected to the shaft and turned on to the desired speed. After the flammable mixture has been stirred for about one minute, and the desired level of turbulence has been reached in the chamber, the motor is disconnected. Any excess pressure is then relieved. The camera is turned on, and the power to the electromagnet is turned off. Because the electromagnet does not release the experiment immediately after its power has been turned off, switching off the magnet could not be used to trigger the igniter. Instead, a Hall effect sensor, positioned on the magnet docking guide (Figs. 1 - 3), senses the instant the experiment is separated from the electromagnet, and triggers a pulse. After a 50 msec delay, during which the dropping experiment has ample time to stabilize, a pulse triggers the ignition transformer. A small neon light DC transformer connected to the spark plug is used to ignite the flammable mixture. It is powered by two 9 volts DC batteries and provides 1500 volts AC at 20KHz

and 5 mA, sufficient to create an ignition spark. After the run, the combustion chamber is retrieved, purged, checked for possible problems, hoisted back up in position, and prepared for a new run.

A Kistler K-BEAM capacitive accelerometer is attached to the device to be able to monitor the degree of microgravity experienced by the combustion process. This accelerometer has a range of +/- 1g with a sensitivity of 1959 $^{mV}/_{g}$ and can survive a maximum of +/- 40g. The manufacturer's guaranteed precision around 0 g, is +/- $3x10^{-2}$g.

1.2 Results

The mechanics of the drop tower facility were extensively tested and the microgravity environment was quantified. It was ascertained that the 60 inch drop of this facility provides 0.4 sec at ~ 10^{-3}g or better. Gravity level traces obtained during each of the runs show that levels of $3x10^{-3}$g and below are being achieved for all runs. The experimental device sinks about 30 inches into the polystyrene during its deceleration. Overall the facility behaved exactly as planned and was found to be relatively user friendly. Several vibration problems associated with the start of the drop were identified, and corrected.

The stirred constant volume combustor was first tested while stationary. Two-dimensional LDV carried out within the first couple of seconds after the fan was turned off showed turbulence with an rms velocity of 6 to 7 cm/sec. The reactor was then filled with a methane-air mixture, stirred and ignited at 1g. A typical sequence of images from these tests is shown in Fig. 3. The wrinkles of the flame are clearly identifiable. Flame speeds can be determined from the sequence of images. Most importantly, it can be clearly seen that this flame ball is raising with time, its upper flame front having traveled 10% farther than the lower one. This clearly demonstrates the effect of gravity.

Figure 4 shows a typical sequence of images of a turbulent premixed methane-air flame obtained while the stirred constant volume reactor was dropping in the GT drop tower. Here also the wrinkles in the flame front are clearly visible and the flame speed can be determined. Measurements of the location of the flame front clearly indicate that the center of this flame ball remained at the point of ignition. Thus, the effect of gravity on this turbulent flame has been drastically reduced, if not totally eliminated.

Figure 5 shows a plot of normalized turbulent velocity versus turbulent intensity for different stoichiometries, with and without, gravity. Such a plot allows the reader to quickly grasp the effects of turbulence on flame speed. From this specific plot it can be observed that for one stochiometry gravity enhances flame speeds, while for the other it has the opposite effect. In addition the effects of turbulence, quantified as the ratio of turbulent flame speed to laminar flame speed, vary from being higher than found in literature, for the specific range of turbulence intensities, to having no effect. Nevertheless the expected trend of increase turbulent flame speed with increased turbulence intensity was observed. In addition, gravity does appear to have a significant effect on the burning velocity. However, the nature of this effect seems to strongly depend on small changes in equivalence ratio. This led us to suspect the validity of the data.

LDV results had pointed to several problems with our turbulence generating device. Turbulence levels were limited and there was a slight non zero mean flow. In addition, the data in Fig. 5 raised a number of questions (see previous paragraph). For this reason it was decided that future studies would use a modified stirring system. The selected system consists of 4 opposing fans rotating continuously at the same speed. This will create a central region in the flow where the turbulence will be quasi-isotropic with little net flow. The advantages of such a setup, in which the fans will no longer be turned off prior to taking data, are the elimination problems in timing that resulted in possibly unpredictable decay rates and thus a lack of repeatability. The new device will also produce a more uniform flow pattern and higher turbulent levels. Similar facilities have been used by at least four research teams going as far back as 1975, and possibly earlier[1-7]. Efforts have already been made to retrofit our existing combustion chamber with four fans. This will be the first of its kind to be tested in microgravity.

1.3 Conclusions

A stirred, constant volume combustion chamber for studying turbulent premixed flames in a microgravity environment was designed and built. A drop tower capable of producing 0.4 seconds of microgravity at a level 10^{-3}g was developed and constructed. A shadow-graph set-up that permits constant observation of the flame front during a drop was integrated into the drop tower. The entire system was checked out. Shadow-graphs of lean, turbulent, premixed methane-air flames were obtained in 1g and microgravity environments. Comparison of the images obtained under the two conditions showed that the effect of gravity was essentially eliminated during the drop. Gravity was shown to have an effect on turbulent flame speed. Analysis of the LDV and the combustion data pointed to some problems with the turbulence generated by a single fan. A four fan system is under construction.

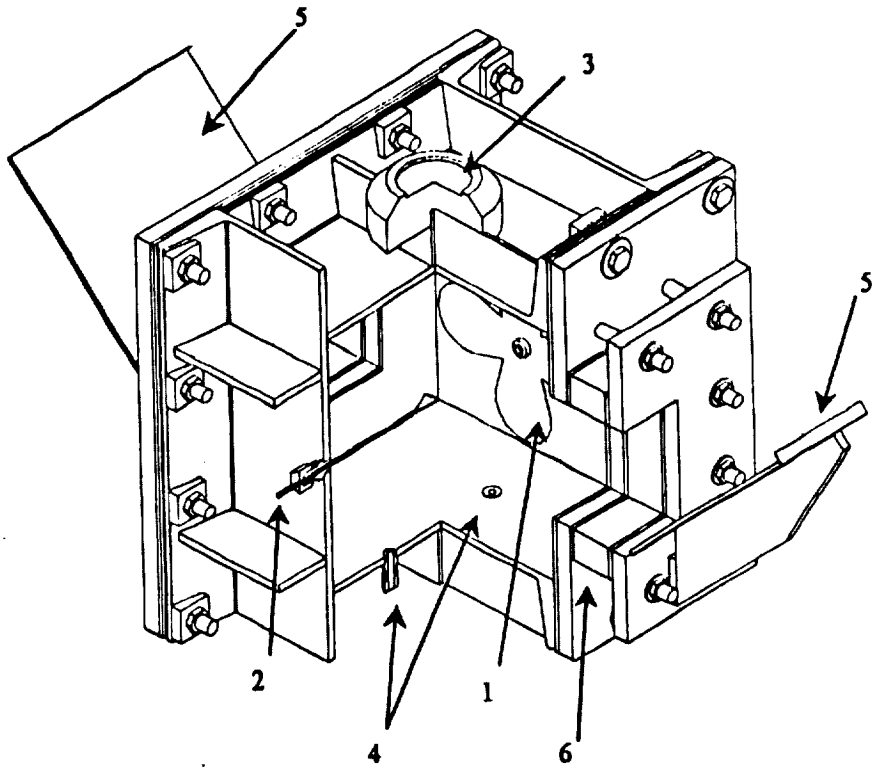

Figure 1. Stirred Constant volume Combustion Chamber. 1) Stirrer; 2) Igniter; 3) Electromagnet Docking guide; 4) Input and output ports; 5) Mirrors; 6) Quartz windows

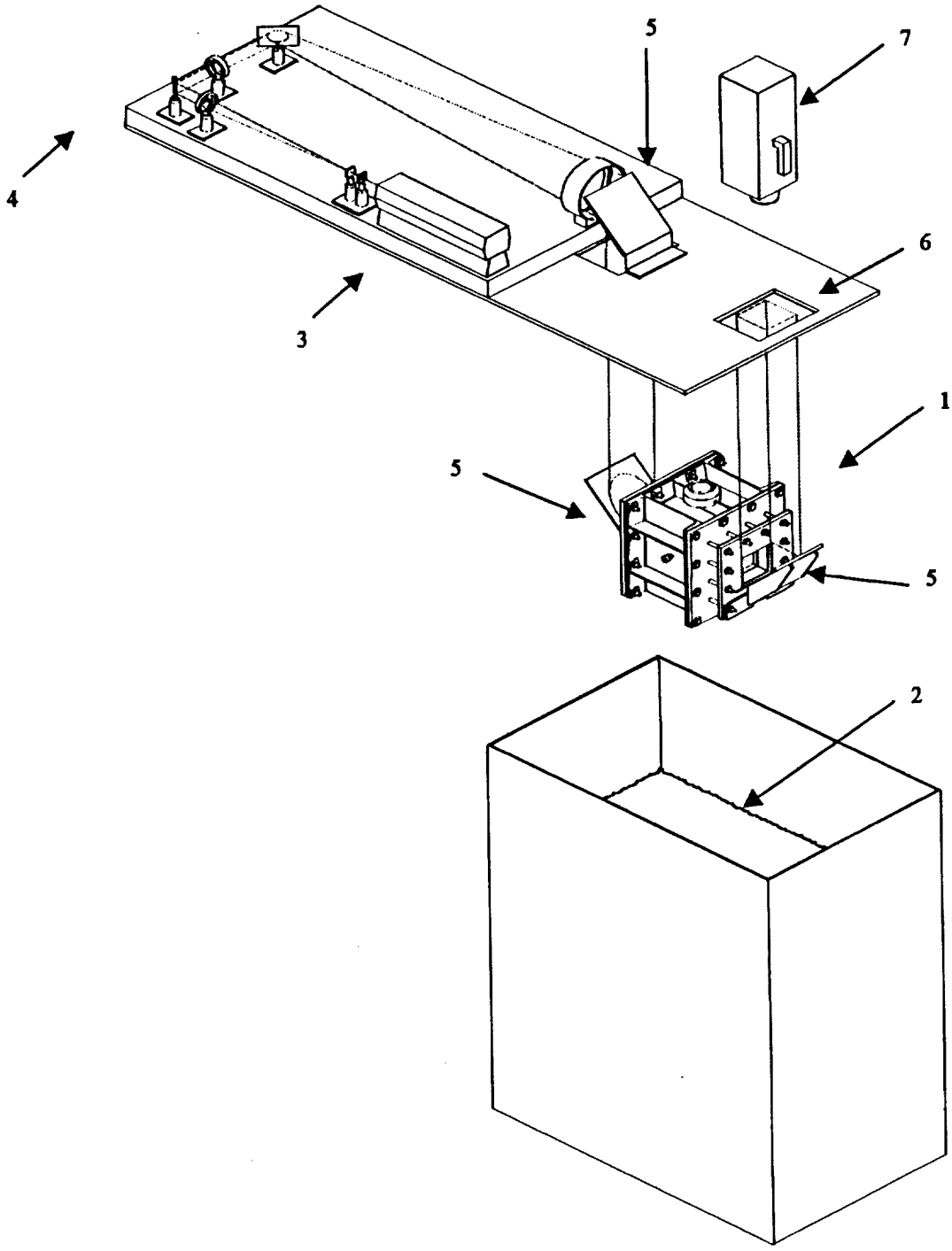

Figure 2. GT Aerospace Engineering Combustion Laboratory's drop tower facility with stirred constant volume combustion chamber. (The lines represent the light path of the shadow-graph system). 1) Stirred constant volume combustion chamber; 2) Expanded polystyrene pellets; 3) HeNe Laser; 4) Expanding and collimating lens set; 5) Mirrors; 6) Screen; 7) High speed intensified camera.

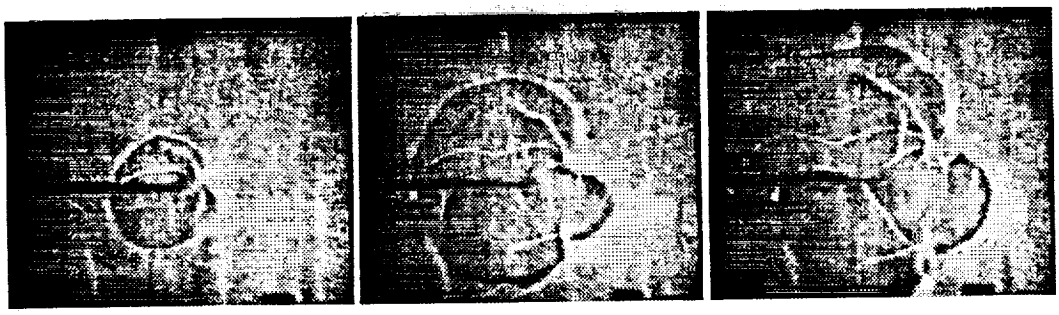

Figure 3. Typical Combustion results in the stirred reactor for the following conditions: 1g; $\phi = 0.90$; turbulence level approximately 7 cm/sec

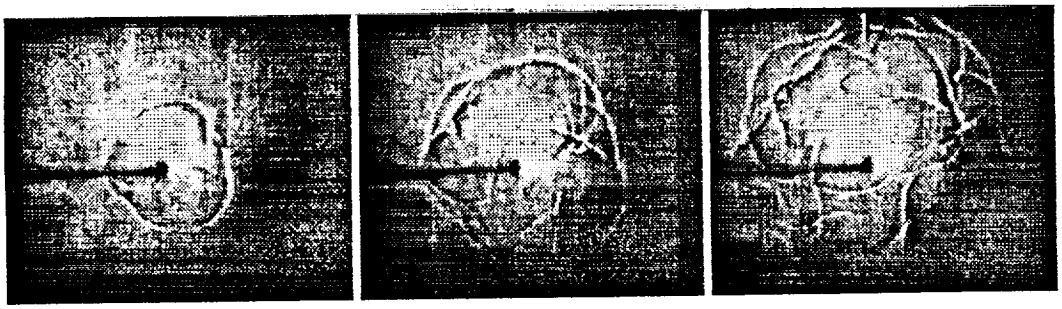

Figure 4. Typical Combustion results in the stirred reactor for the following conditions: ~10^{-3} g or better; $\phi = 0.90$; turbulence level approximately 7 cm/sec

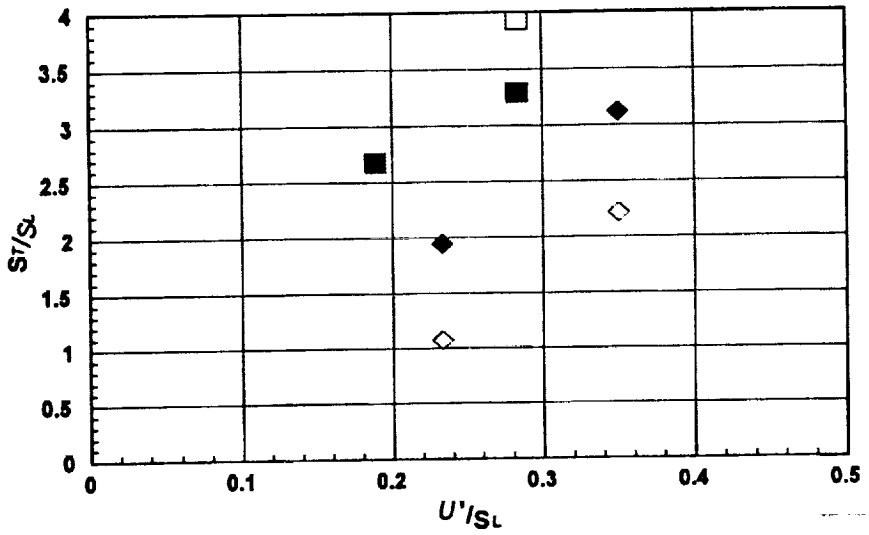

Figure 5. Non-dimensionalized turbulent flame speed verses non-dimensionalized turbulence intensity. Collection of data points from the stirred reactor: rhomboid $\phi = 0.8$; square $\phi = 0.9$; solid = μg; open = 1g

2. Premixed flame studies in the Reacting Couette Flow Facility

2.1 Experimental Facility and Methods

Two Couette devices were designed and built for this research. The first one was used to perform a cold flow study in order to understand, a priori, the turbulent flow field: it is shown in Fig. 6. The device consists of a continuos Mylar belt (1) which provides the "two parallel plates" moving in opposite directions. The belt runs over a series of rollers, two of which drive the belt while four are used to adjust the spacing in the test section. A set of plates (10) is positioned on the outside of the belt to eliminate possible belt vibrations. These vibrations had been found to cause higher levels of turbulence with peaks in the frequency spectrum. An adjustable DC motor (2) connected to the drive roller by a set of pulleys and a v-belt (3) drive the Mylar belt. The rotational speed of the motor is sensed by a magnetic proximity sensor (4). Knowing the pulley ratio and the roller diameter, the speed of the belt can easily be determined. To prevent belt walking and to ease the insertion of a new belt, a set of tensioning screws (5) help position the far roller. The Reynolds number for the device, Re_h, can be changed by either changing the speed of the belt, U_{belt}, or by changing the belt spacing, h. The device is surrounded by a Plexiglas box to prevent any external influence on the flow without disturbing optical access to the experiment.

Acetone PLIF can be performed in the Couette facility using a tunable Lambda Physik excimer laser running with KrF, to produce a laser pulse at a wavelength of 248nm. The beam is used to create a sheet that enters through the quartz window (6). It penetrates in-between the Mylar sheets through a cut in the frame (9), and is turned by a mirror (8), to run along the mean flow direction. A micro-tube 0.254mm in diameter and with a hole cut in its side, is positioned perpendicular to the flow. Liquid acetone is introduced through the tube into the center of the flow. Here a droplet of acetone stays suspended on the tube while it vaporizes. When the excimer beam encounters the acetone vapor the latter fluoresces broadband in the blue (350-550nm), with peaks at 445nm and 480nm. The fluorescence is tracked with a Princeton Instruments Inc. intensified camera with a resolution of 384x576 pixels. At this resolution the camera can operate at a rate of two frames per second. The rate can be increased by decreasing the resolution, yielding 10 frames per seconds with a resolution of 192x288 pixels, and 20 frames per second with a resolution of 96x144 pixels. A 55mm macro glass lens is used on the camera in order to absorb any scattered UV light from the beam. Images are background corrected to remove noise created by fluorescence due to UV scattering off parts of the chamber. This fluorescence is very prominent close to the belt and close to the needle. Therefore, these regions were not imaged.

Before the Couette flow could be used to study turbulent flame propagation under microgravity it had to be established that the effect of gravity would be noticeable in this turbulent flow field. To this end a gas of lower density was introduced into the flow and its interface with heavier air was tracked using shadowgraphy as it progressed though the flow. Helium was injected through a hypodermic needle along the centerline of the Couette flow. The needle was equipped with micro-machined holes on four sides to limit the directional biasing associated with one hole injection. However the strong shear of the Couette flow, along with the high diffusivity of the helium caused the gas to mix with air almost instantaneously. No clearly visible helium-air interface could, therefore, be observed in these test.

Better results were obtained when a density gradient was produced by focusing a laser beam into a small volume at a point located along the centerline between the two belts. The energy furnished by the laser was sufficient to ionize the air and thus form a spark. The propagation of this point source of hot gases was then tracked with the help of a high speed Schlieren system. The laser used to generate the spark is a 300mJ per pulse tunable Lambda Physik excimer laser running with KrF, to produce a laser pulse at a wavelength of 248nm. This laser was chosen because it not only offered enough power per pulse to ionize the air, but being in the UV, scattered light did not affect the Schlieren. The Schlieren light source was a .95 mW HeNe laser. The beam stop was an opaque dot, 1mm in diameter, to avoid directional biasing. Schlieren images were captured using a Kodak Ektapro intensified digital camera running at 1000 frames per second.

To identify the center of the hot gas volume the Schlieren images were first of all processed. Each captured image was turned into its negative and the background was then subtracted from both the positive and negative images. This was done to accurately catch both the above background and the below background structures. The resulting

images were then adjusted for contrast. Because of the zero mean flow that this Couette facility provides along its centerline, the mid-section of the kernel remains stationary in the horizontal direction. This means that for late images the vertical instantaneous location of the bottom and top edges of the kernel can be used to locate the position of the center of the hot gas products. At first, the location of the edges were identified visually and the results used to calculate the position of the center for both the positive and negative images. The data were then averaged over multiple runs.

Later, a more quantitative method was adopted. The pixel intensities were plotted along a vertical axis through the point of origin of the kernel. Such a plot and the image used to obtain it are shown in Fig. 7. In these plots the dark and bright regions corresponding to the hot gas boundaries are clearly defined. The mid-level noise regions, corresponding to the background, are also clearly identifiable. Thus, the edge of the kernel was defined as the point where these two regions met. Here again, centers were determined (by the method described above) for both the positive and negative images and the results were then averaged.

The second Couette device was used to perform combustion experiments. Technical design details on this facility have been reviewed by the 2.2 second drop tower staff. Michael Dobbs furnished us with some good recommendation on possible changes and improvements. These have been considered and the necessary ones have been adapted. Figure 8 shows schematics of the combustion chamber inside the NASA Lewis 2.2 sec drop tower test rig. A combustion proof enclosure now surrounds the Couette device. It is made of 6061-T6 4 in. aluminum channel with a thickness of 0.247 in. The top and bottom plates are made of ½ in. 7075-T651 aluminum. This combination coupled with Aramid/Nitrile gaskets and held together with 104 - ½ in. bolts, allows the chamber to sustain 150 psig. The motor is located outside the combustion chamber, and an o-ring seals the shaft at the wall. Fuel and air are introduced through a fuel port consisting of a stainless NPT swagelock fitting. Two Plexiglas windows positioned on the top plate furnished optical access. Quartz was considered at first, but during the review process with the drop tower staff, it was found that it would not be suitable, due to high stress levels. Some additional modifications had to be made to the original design in order to fit the combustor in the test rig. The belt width was narrowed from 12 in to 8 in, a change that did not affect the two dimensionality of the flow field since the cold flow study had proven that the flow was two dimensional as close as 1.2 cm from the edge of the belt. The four rollers that were used to adjust the spacing of the belt were eliminated since the plates that had been added to eliminate vibrations could do the same job. The new plates were machined out of UHMW Polyethylene to decrease weight and friction. The Mylar was found to be surprisingly resistant to the flame, but its seam did not withstand the thermal shock and broke at the end of every run. Therefore, the Mylar belt was replaced by a continuous urethane coated fabric conveyer belt, with a seamless-z-splice. Possible concerns arose from the change of material, especially with regard to the possible slight increase in surface roughness. However, results by Aydin and Leutheusser showed that even changes of surface roughness produced by 5.8 mm bumps, produced relatively small effects on the Couette flow field [8]. For this reason the difference between the Mylar and the urethane coated belt was deemed not to seriously affect the Couette flow field under investigation.

Light from a 0.95mW HeNe laser, expanded and collimated by a set of lenses into a 4 inch beam, was used as a shadowgraph light source for optical diagnostics. The light is channeled through the combustion chamber with the help of a pair of mirrors and windows onto an image screen. Images are then captured by the Kodak Ektapro intensified digital camera, which runs at 2000 frames per second half screen. Images were downloaded to a PC. A MATLAB code, written in house, extracts a flame contour that can be subsequently used to analyze the combustion flows. The MATLAB code first imports bitmaps into matrix form and prompts the user to input the ignition point. It then proceeds to look at radial light intensity profiles. Based on a user selected light intensity threshold it determines the edge of the flame and moves to the next radial location. Here it repeats the process, but is further constrained by a continuity factor, which prevents the code from picking brighter internal flames. After having processed the whole flame the user is given an opportunity to adjust possible trouble spots. The data can then be exported into a matrix or a bitmap for further processing.

Like in the stirred reactor the equivalence ratio of the mixture was determined by partial pressures. The chamber was evacuated and a predetermined amount of methane was introduced. Air was then added to obtain the desired mixture at the selected initial pressure. The motor was run up to speed to achieve the desired turbulence level. Finally the mixture was ignited using a spark located at the center of the flow field. The ignition source was comprised of the electric circuit from a butane lighter and a home-made spark plug was designed to minimize the

disturbance of the . Runs presented in this report were performed at 1 atm initial pressure, a stoichiometric ratio of approximately 0.87, and a belt speed of 7 m/sec.

2.2 Results

Nomenclature:

x, y, z = axis system
h = height of channel
w = width of channel
L = integral scale
η = Kolmogorov scale
u' = magnitude of large scale turbulent velocity
υ = magnitude of small scale turbulent velocity
U = x component of mean velocity
V = y component of mean velocity
U_i = ith component of mean velocity
$U_{wall} = U_{belt}$ = belt velocity
U_{rms} = x component of root mean square velocity
V_{rms} = y component of root mean square velocity
u_i = ith component of velocity fluctuation
U^* = shear or friction velocity
C_f = coefficient of friction
$Re_h = U_{belt} h / \nu$
$Re_L = u' L / \nu$
τ_{ij} = shear stress
τ_{wall} = wall shear stress
μ = viscosity
ν = kinematic viscosity
ρ = density
k = wave number of spectra
f = frequency of spectra
$\overline{u_i^2(f)}$ = power in frequency space, for the i^{th} velocity component
ϕ_{u_i} = spectral density

2.2.1 Velocity Field Mapping:

Figure 9 shows the velocity distribution and, therefore the two dimentionality of the flow. The z/w = 0 location corresponds to the edge of the belt. It can be seen that the velocity profile is constant for z/w up to 0.04, which corresponds to 1.2cm, from this edge. This yields a usable, two-dimensional test area that is 28.0cm wide. As a result most velocity data were obtained 2cm off-center, which gave better optical access.

Figure 10 shows the velocity distribution across the flow field. Careful inspection of this plot shows that the velocity profile is not totally symmetric. The U component of velocity should go through zero at $y/h = 0.5$, but in reality it does so at $y/h = 0.45$. It was hypothesized that this was due to an asymmetry in the end regions where the driving rollers are located. To prove this the motor was set in reverse and, as expected, the crossing moved to $y/h = 0.55$. This feature does not seem to have any affect on the rms velocity as seen in Fig. 11, and as long as it is kept in mind while analyzing the combustion data, it is not deemed to be a problem.

As mentioned in the experimental section, there was a slight fluttering of the belt during early testing. This flutter was not visible to the naked eye, but was detected by frequency analysis of the velocity spectrum. A non-excited frequency spectrum should decay smoothly. The measured excited frequency spectrum had peaks in the 100 Hz region, as shown in Fig. 12. A microphone placed in the flow showed corresponding pressure oscillations at that frequency. These oscillation were increasing the turbulence intensity, but their frequency was dependent on the belt

tension, which could not be accurately measured or reproduced. Thus this situation was deemed unacceptable. With the plates in position the fluctuation were almost stopped completely. Figure 13 shows the worst case encountered where the oscillations were not fully damped.

To discuss the results further the following quantities have to be introduced. The shear stress τ_{ij} is given by

$$\tau_{ij} = \mu \left(\frac{\partial U_i}{\partial x_j} + \frac{\partial U_j}{\partial x_i} \right) - \rho \left(\overline{u_i u_j} \right) \tag{2}$$

The first term represents the viscous stresses and the second represents the Reynolds stresses. In a pure Couette flow the shear stress is constant; though the Reynolds stresses are mainly concentrated in the center of the flow, and the viscous stresses are mainly present near the wall. Another useful quantity is the shear velocity U^*

$$U^* = \left(\frac{\tau_{wall}}{\rho} \right)^{1/2} \tag{3}$$

The velocity and positions in the flow field are commonly non-dimesionalized as follows:

$$U^+ = \frac{U}{U^*} \quad V^+ = \frac{V}{U^*} \tag{4}$$

$$U^+_{rms} = \frac{U_{rms}}{U^*} \quad V^+_{rms} = \frac{V_{rms}}{U^*} \tag{5}$$

$$y^+ = \frac{yU^*}{\nu} \tag{6}$$

Figure 14 shows U^+ as a function of y^+. The data clearly show the expected behavior for a wall bounded shear flow. The flow can be divided into two regions[10], the viscous sublayer ($y^+<5$), and the inertial sublayer ($30<y^+<1000$). The flow correlates well with the linear behavior at the wall in the viscous sublayer. The logarithmic behavior in the inertial sublayer is also clearly present. However, the data at different Reynolds numbers do not exactly collapse into one single line when non dimesionalized, as predicted by theory and seen by others. This is probably due to the smaller dimensions and re-circulating nature of the present device.

Figure 15 shows U_{rms}^+ and V_{rms}^+ as functions of non-dimensional distance from the belt. As expected, U_{rms}^+ has a turbulence peak close to the wall before it reaches a uniform distribution in the core, and V_{rms}^+ gradually increases to a uniform distribution in the core. Figure 16 shows how velocity fluctuations vary for different devices. Except for Clark's device, which was actually not a Couette, but a channel flow, it would seem that the flow in this device is more turbulent than those in other devices. This feature is also seen by looking at the Reynolds stresses.

It is conventional to non-dimensionalize Reynolds stresses by U^{*2}. Inspection of Equations (2) and (3), and the velocity profile, shows that in theory the non-dimensional Reynolds stress should level out at a value of 1. Figure 17 shows that in this flow the turbulent stresses are higher then expected in a pure Couette flow. This is an advantage in this case since higher turbulence is produced at lower Reynolds numbers. In addition, a peak in Reynolds stress near the wall is seen at the higher Reynolds number. Such a peak has not been reported elsewhere in the literature.

A way of quantifying the shear stresses is by measuring the coefficient of friction.

$$C_f = \frac{\tau_{ij}}{\frac{1}{2}\rho\, U^2_{wall}} \tag{7}$$

In general the coefficient of friction is more meaningful at the wall, and thus usually represents the viscous stresses. Since pure Couette flow has uniform shear, the coefficient of friction measured at the center is supposed to be approximately the same then that at the wall. Figure 18 shows the coefficient of friction measured in this device compared to those in previous investigated Couette flows. C_f calculated from the center measurements of shear stress for this flow field are higher than the ones calculated at the wall. This is due to the higher than expected Reynolds stresses. Deviations from more ideal Couette flow are, once again, probably due to the recirculating nature of the flow in this compact device.

A parallel computational study of this flow assumes the existence of an inertial range in which the flow follow the $k^{-5/3}$ law. The experimental validation of this assumption requires the determination of a wave number spectrum for this flow. Since LDV measurements are single point, wave number spectra can only be obtained from frequency spectra using Taylor's hypothesis[8]. One of the criteria for Taylor's hypothesis to hold is that $U/U_{rms}>>1$. This is clearly not the case, in what can be considered the inertial range of this device. However, it might still be interesting to examine the wavelength spectrum to obtain some qualitative information, while keeping in mind the assumptions made in its calculation.

Following Taylor's hypothesis a wave number can be defined as follows[9]:

$$k_1 = \frac{2\pi f}{U} \tag{8}$$

The absolute value of spectral density in wave number space is given as:

$$\phi_{u_i} = \frac{f}{k_1 y}\frac{\overline{u_i^2(f)}}{U^*} \tag{9}$$

If one now plots ϕ_{u_i} versus $k_1 y$, where y is the position from the wall, one can look at spectra for different regions in the flow and note which ones follow the $k^{-5/3}$ law.

Figure 19 shows $\phi_{u_{11}}(k_1)$ and $\phi_{u_{22}}(k_1)$ versus ky for different regions in the flow. These velocity spectra are for the case of Re_h=10,091. The U, and V spectra for the y^+= 207 location follow the inertial layer law, but those for the y^+ = 10.5 location do not. As a matter of fact the inertial behavior can only be seen in spectra for the $y^+ > 60$ locations, which correspond to the region of constant U_{rms}. Thus the assumption of the existence of an inertial layer necessary for the parallel computational study is valid in the region of interest.

2.2.2 Resolution of Scales:

One of the premises of this study was the need to have access to a wide range of scales, to allow a better understanding of the turbulent combustion process. It is, therefore, important to consider the ability of the cold flow study to resolve these scales. L, the integral length scale, can be approximated as the significant length scale in the flow, which, in this case, is the belt spacing, h, and equals 25.4mm. The Kolmogorov scale, η, can be calculated from

$$L / \eta = (Re_L)^{3/4} \tag{10}$$

where the Reynolds number is determined from the turbulent velocities measured in the core of the flow. They were found to be 0.23mm for the Re_h = 4,366 case and 0.13mm for the Re_h = 10,091 case.

For to the LDV measurements, the integral length scale can definitively be resolved by traversing the measurement volume though the test section. The Kolmogorov scale, on the other hand needs to be more carefully considered. The seed particle size is sub-micron, much smaller than η, while the LDV probe volume is of the order of η. This implies that the scale can just be spacially resolved during two point correlation measurements. However smaller scales may be temporally resolved. Since the scales are moving, residence time inside the probe volume is a more accurate measurement of scale resolution. The velocity of the scale can be estimated by using the relation between the Kolmogorov velocity scale and the magnitude of turbulent velocity:

$$u' / v = (Re_L)^{1/4} \tag{11}$$

Based on the probe volume dimensions and Equation (10) a residence time and, therefore, a frequency can be calculated to be 590Hz for the Re_h = 4,366 case and 1,030Hz for the Re_h = 10,091 case. This means that the data rate for the LDV should be grater than 2,060Hz to resolve Kolmogorov scales temporally. Because of the high noise levels in the system, this is difficult to achieve. It thus requires considerable attention to alignment and seeding to obtain information on the smallest scales in the flow.

For scalar measurements using imaging techniques the integral length scale again can be resolved without problem. However, the full resolution of the camera combined with the macro lens used yields a pixel dimension of 0.05 mm

squared. This results in approximately 3 x 3 pixels per Kolmogorov scale, for Re_h= 10,091, and 5 x 5 pixels per Kolmogorov scale for Re_h = 4,366. Decreased resolution to achieve higher frame rates would of course decrease these estimates. However, reduced areas of interest can be viewed with higher magnification lenses, which would increase the resolution significantly.

2.2.3 Visualization of Turbulent Diffusion:

The hypodermic needle carrying the acetone drop was placed below the centerline where the flow runs from right to left. The fluorescence of the acetone in the region to the left of the needle was recorded. Flow in the lower half of the picture is expected to be acetone laden, while flow in the upper half of the picture is expected to be free of acetone. Figure 20 shows a snapshot of the resulting turbulent diffusion process. The light marking correspond to the presence of acetone. As expected high concentration of acetone is seen in the lower half of the image. Some large scales structures can be seen in this picture. It is not certain whether these are Couette flow structures or whether vortices are shed off the acetone supply line. The Reynolds number based on the diameter of the needle is of the order of 10, thus it is safe to assume that the needle does not produce structures. However the Reynolds number associated with the droplet is of the order of 150, thus making it very possible for it to shed vortices.

For the feasibility study reported here, the fluorescence measurements of acetone were carried out under steady conditions. In order to better determine the influence of turbulent passive scalar diffusion processes, it will be necessary to observe the leading edge of the acetone as it begins to diffuse into the flow. This will require a higher framing rate and a more sophisticated timing of the injector and camera. However, the test reported here did show that it is possible to visualize diffusion in this flow using acetone PLIF.

2.2.4 Density Gradient Study:

As mentioned earlier, test were run to determine whether the effect of gravity persist in this turbulent (Re_h = 10,000) environment by tracking a pocket of hot gasses as it was convected through the flow field. A spark generated by an Excimer laser created a kernel of hot gasses which during the first two milliseconds after its generation expanded to 50% of the belt spacing. This initial expansion was so fast that it was not affected by gravity. However, it was also too fast to be considered a good representation of what would happen to a methane-air flame. After this period, however, the remains of the hot kernel of gasses were left to move and mix with the flow. When these hot gasses were further tracked they were seen to interact with the turbulent mean flow which strongly deformed the shape of the kernel. At the same time it was noted that the center of the hot gas volume rose about 5% of the total belt spacing above the centerline of the flow, in a period of 20 msec, indicating that buoyancy persists even in this turbulent flow.

2.2.5 Combustion Study:

Figure 21 shows a typical series of images of ignition followed by the propagation of a turbulent, premixed flame through the Couette flow under conditions of 1 g. The initial flame kernel grows relatively unaffected by the flow field, but then rapidly develops into a lightly wrinkled turbulent flame. Both the effects of the flow field (upon the left and down or the right) and that of gravity are clearly noticeable.

By analyzing a number of runs at different equivalence ratios and turbulence levels, it was determined that the initial flame kernel remains completely smooth before it starts to develop wrinkles. This transition occured a given time (6 msec) rather than once the kernel has grown to a given diameter. This suggests that the initial smoothness is caused by the unsteady ignition process.

An image analysis software package (described earlier)was written in house, which is able to isolate the outermost flame front with very little input from the operator. Examples of the results are shown in Fig. 22. From these traces it is clearly possible to determine flame properties, such as flame speed, thickness and wrinkledness.

It is interesting to note that some runs produced images that seem to point to possible local extinction of the flame. It has not yet been determined if this is just an optical anomaly of the shadow-graph system or if it is real. Additional experimental runs are currently planned to obtain a statistically significant set of data from which flame properties

and how they are affected by gravity, can be determined. These will then be compared with results obtained from the parallel computational studies. Drop tower experiments can currently not be carried out using this facility since we are not under contract with NASA.

2.3 Conclusions:

The need for a cold flow study in the Couette reactor was two fold. Of first and foremost importance was the validation of the nature of the flow in this new facility. Thus the flow field was thoroughly investigated using laser Doppler velocimetry. The flow was found to be largely two dimensional with constant turbulence intensities near the core. Slight flow asymmetries were introduced by the non symmetric re-circulation of the fluid outside the test region. Belt flutter problems were remedied by adding a pair of guide plates to the belt. In general, the flow field was found to be quite similar to previously investigated Couette flows. However, turbulence levels and associated shear stresses were higher. This is probably due to the confined re-circulation zone reintroducing turbulence into the test section. Turbulence scales were compared with the spatial and temporal resolution of the experimental techniques and it was determined that for Reynolds numbers of about 10,000 structures down to the Kolmogorov scale could be resolved.

Having resolved the resolution issues, the next step was to verify the need for microgravity. The wrinkledness of a turbulent premixed flame depends upon the ratio between the turbulent velocity fluctuation and the laminar flame speed. In the Re_λ = 10,091 flow the core has a U_{rms} of 0.75 m/sec, which is 4 times bigger than the laminar flame speed for lean limit methane air combustion. Since this Reynolds number also lies at the limit of the Kolmogorov scale resolution, this flow regime was identified as the region of interest. For this reason tests were also carried out to determine whether the effect of gravity could influence the turbulent reacting flow under investigation in the Couette facility. When a low density plasma was introduced into the cold Couette flow tracking its interface with the cold air showed that even at the relatively high turbulence intensity present in a Couette flow at Reynolds number of 10,000 buoyancy, and thus, the effect of gravity persists.

Ignition and flame spread in the turbulent Couette flow was visualized using Schlieren. An in-house developed analysis program was used to identify the flame front in the images. This capability permitted us to follow the progress of the flame front as it spread through the turbulent Couette flow. An initial smooth kernel was formed by the ignition process, which then changed into a wrinkled turbulent flame front. The effect of the flow field and that of gravity was clearly noted. Additional results continue to be obtained to demonstrate that meaningful results can be obtained for a flame propagation in this turbulent flow field. These results will then be compared with those obtained from the computational work reported herein.

References

1. Fansler, T.D., Groff, E.G., "Turbulence Characteristics of a Fan-Stirred Combustion Vessel," *Combustion and Flame*, Vol. 80, pp. 350-354, 1990.

2. Andrews, G.E., Bradley, D., and Lwakabamba, S.B., "Measurements of Turbulent Burning Velocity for Large Turbulent Reynolds Numbers," *15th Symposium on Combustion*, pp.655-664, 1975.

3. Al-Khishali, K.J., Bradley, D., Hall, S.F., "Turbulent Combustion of Near-Limit Hydrogen-Air Mixtures," *Combustion and Flame*, Vol. 54, pp. 61-70, 1983.

4. Al-Khishali, K.J., Boston, P.M., Bradley, D., Lawes, M., "The Influence of Fluctuations in Turbulence upon Fluctuations in Turbulent Burning Velocity," *International Conference on Combustion in Engineering*, Vol. 1, pp. 175-180, 1983.

5. Kido, H. Wakuri, Y., Nakashima, K. "Experiments and a Correlation of Turbulent Burning Velocities," Source unknown, pp. 183-190, post 1979.

6. Kido, H., Nakashime, K., Huang, S., Kitano, K., "A Study on the Fine Structure of Propagating Turbulent Flames in Premixed Mixtures," *JSME International Journal*, Series II, Vol. 33, No. 2, pp. 362-369, 1990.

7. Aydin, E. M., and Leutheusser, H. J., "Plane-Couette flow between smooth and rough walls," *Experiments in Fluids,* Vol. 11, 1991, pp. 302-312

8. Hinze, J.O., *Turbulence*, 2nd edition, McGraw-Hill, New York, 1987, pp.44-48.

9. Clark, J.A., "A Study of Incompressible Turbulent Boundary Layers in Channel Flow," ASME *Journal of Basic Engineering*, Vol. 90, 1968, pp.455-468.

10. El Telbany, M.M.M., Reynolds, A.J., "The Structure of Turbulent Plane Couette Flow," *Journal of Fluids Engineering*, Vol. 104, 1982, pp. 367-372.

11. Robertson, J. M., and Johnson, H. F. (1970), "Turbulence Structure in Plane Couette Flow," *J. Eng, Mech.*, Proc. of Am. Soc. of Civil Engg., Vol. 6, pp. 1171-1182.

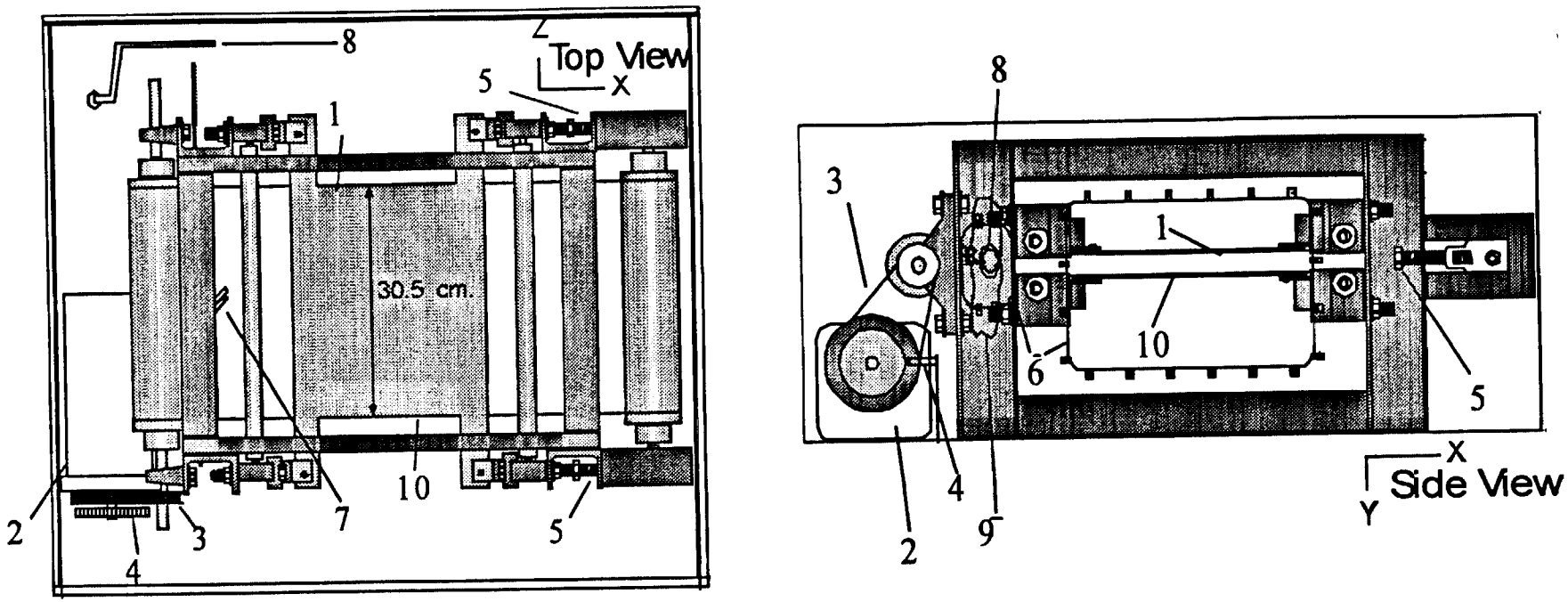

Figure 6. Couette device used for the cold flow study. 1) Mylar belts; 2) DC motor; 3) Pulley system; 4) RPM sensor; 5) Tensioning screws; 6) Windows for optical diagnostics; 7) LDV seeder; 8) Mirror used for acetone PLIF; 9) Input port for UV beams; 10) Vibration plates.

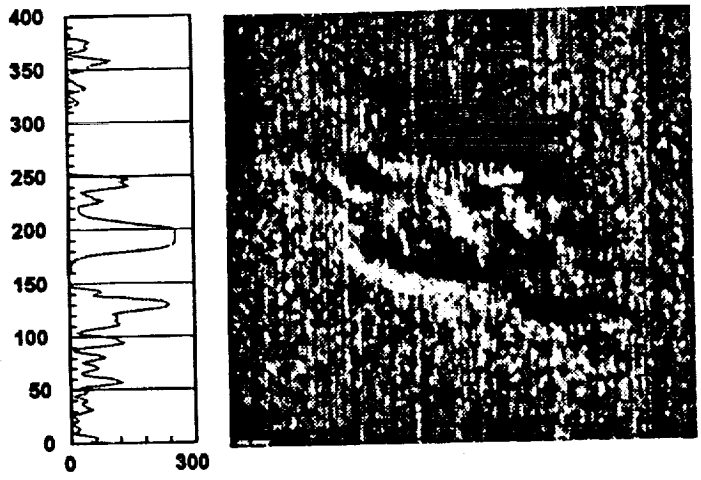

Figure 7. Hot kernel of gasses propagating in Couette facility - corresponding pixel intensity plot.

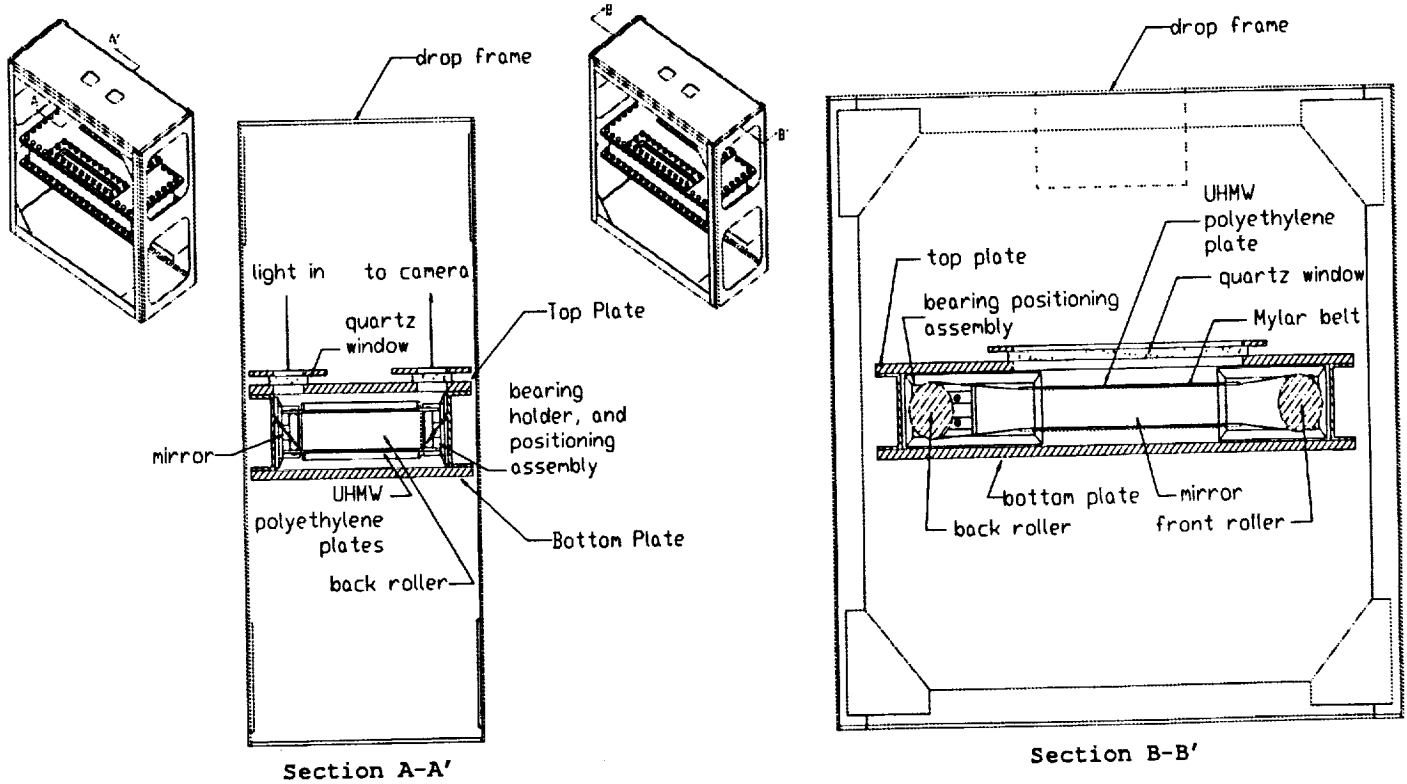

Figure 8. Schematics of the Couette reactor inside the NASA Lewis drop tower rig.

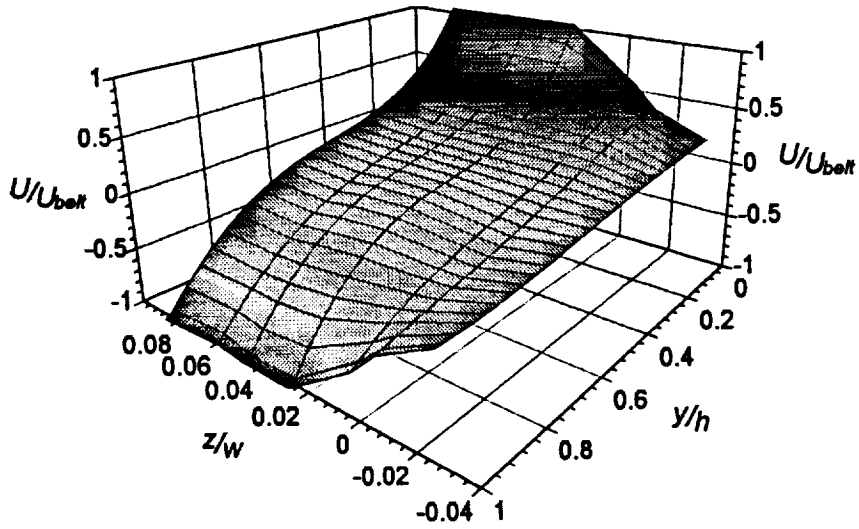

Figure 9. Velocity distribution showing two dimesionality of the flow in the Couette device, $Re_h = 2100$.

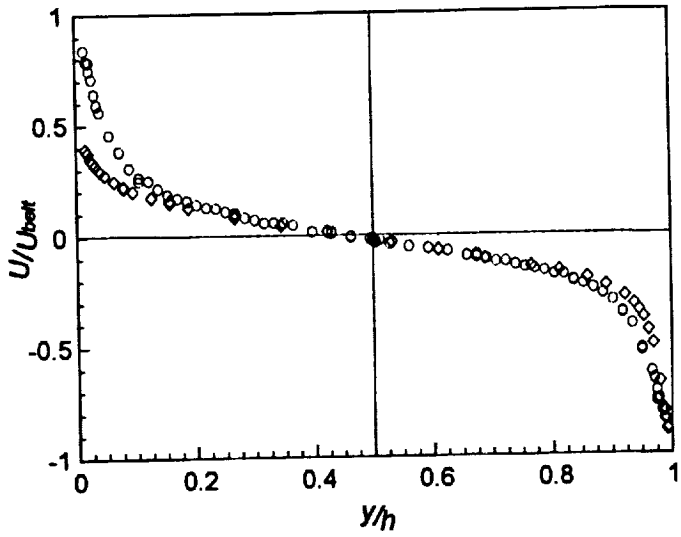

Figure 10. Velocity distribution across the flow in the Couette device ◇Re_h = 10,091, ○ Re_h = 4,366.

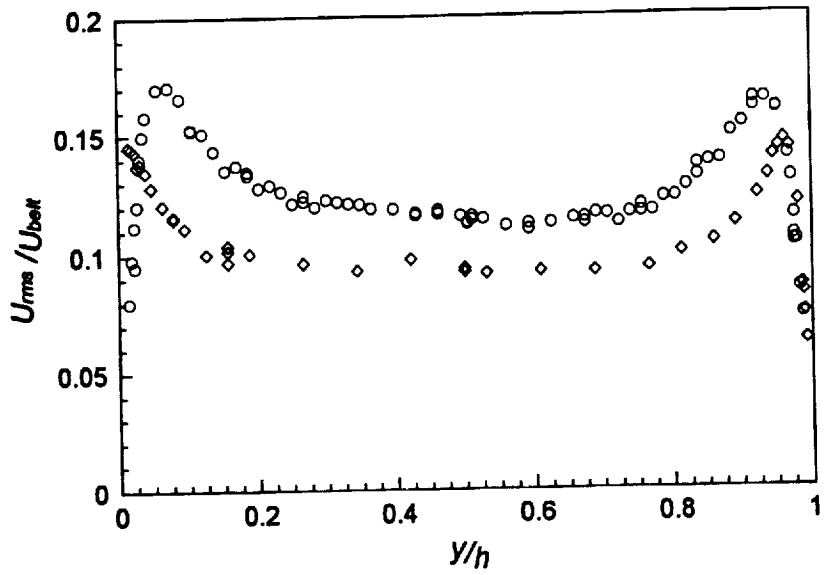

Figure 11. Turbulent velocity fluctuation distribution across the flow in the Couette device: ◇Re_h = 10,091, ○ Re_h = 4,366.

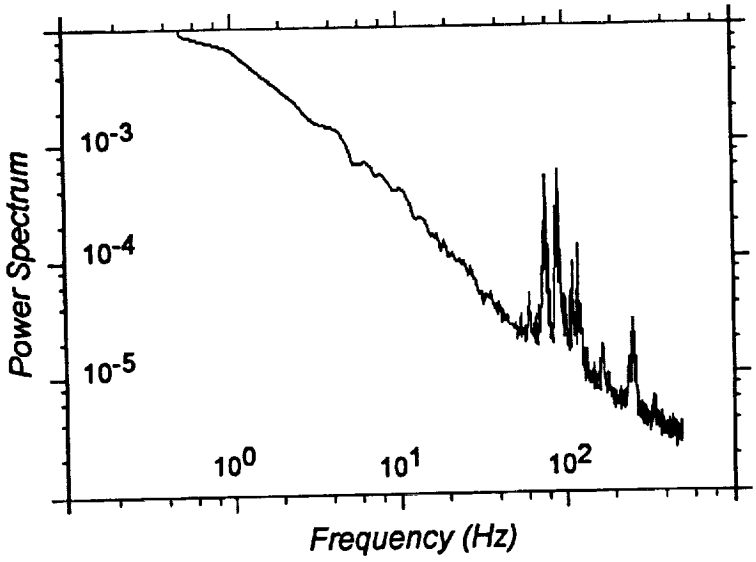

Figure 12. Frequency spectrum of velocity fluctuations in the Couette flow for the case without plates.

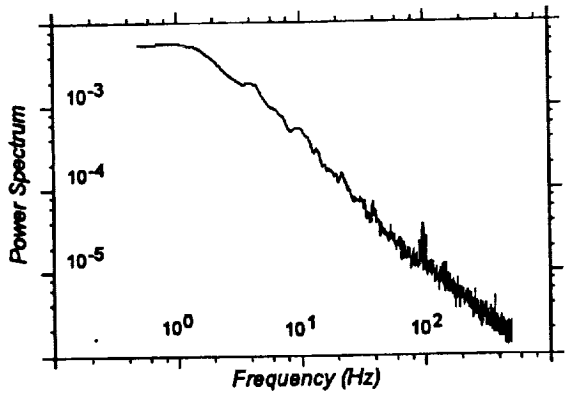

Figure 13. Frequency spectrum of velocity fluctuations in the Couette flow for worst case with plates.

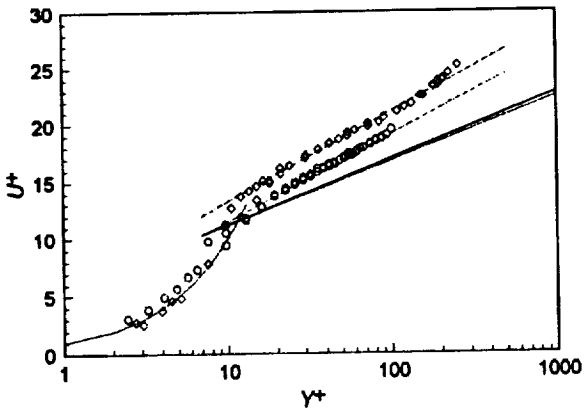

Figure 14. Non-dimensionalized mean flow velocities in a Couette flow and their curve fits: ◇Re_h = 10,091, ○ Re_h = 4,366, $Y^+ = U^+$, U^+=5.4+ 3.4lnY^+ and ·· U^+=3.9+ 3.3lnY^+ for present study; U^+=5.2+ 2.55lnY^+ for El Telbany *et al.*[10]; U^+=5.6+ 2.43lnY^+ for Robertson *et al.*[11]; and — U^+=5.5+ 2.5lnY^+ for Aydin *et al.*[7].

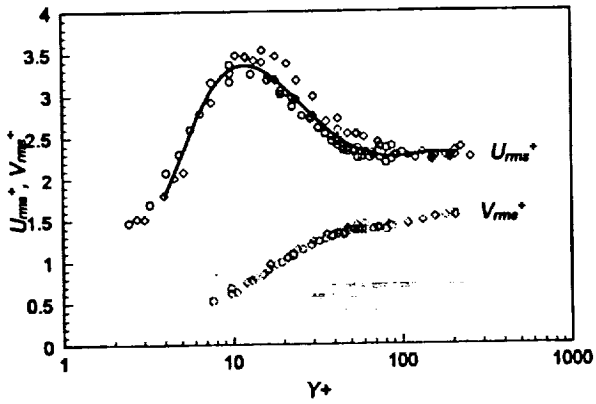

Figure 15. Non- dimensionalized turbulent velocity fluctuation in the Couette flow for present study: ◇Re_h = 10,091, ○ Re_h = 4,366.

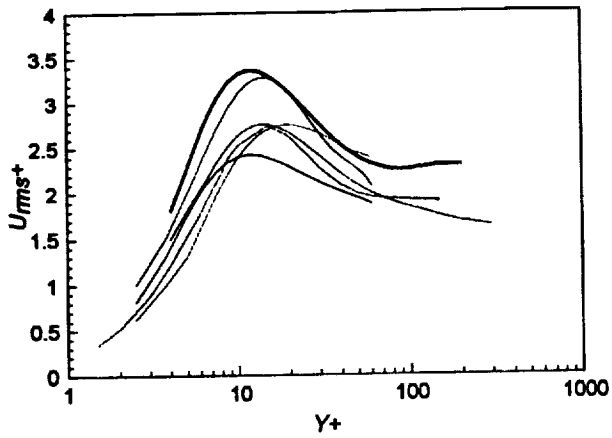

Figure 16. Non-dimensionalized turbulent velocity fluctuation in the Couette flow: Aydin *et al.*[7]; Clark[9]; El Telbany *et al.*[10]; Hussain *et al.*[6]; Robertson *et al.*[11]; present study.

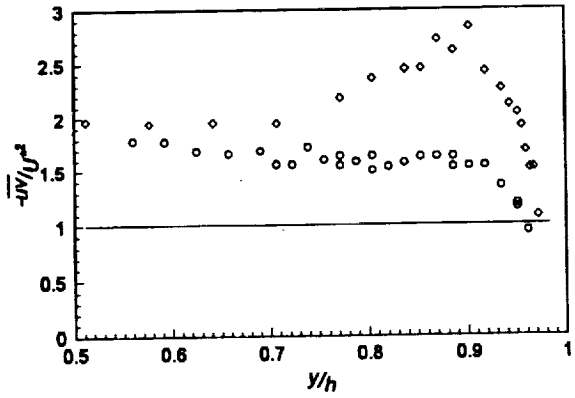

Figure 17. Non-dimensionalized Reynolds stresses in the Couette flow for present study: ◇ Re_h = 10,091,and ○ Re_h = 4,366.

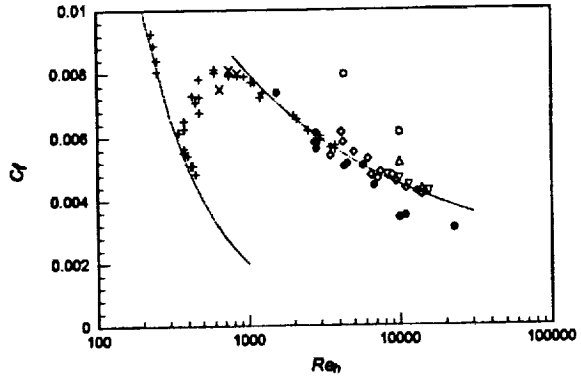

Figure 18. Coefficient of Friction distribution for experimental Couette flows: + Couette in water[11], × Couette in air[11], △ Robertson in air (center)[11], ▽ Robertson in air (wall)[11], ◇ Robertson and Johnson in air[11], ● present study in air (wall), and ○ present study in air (center).

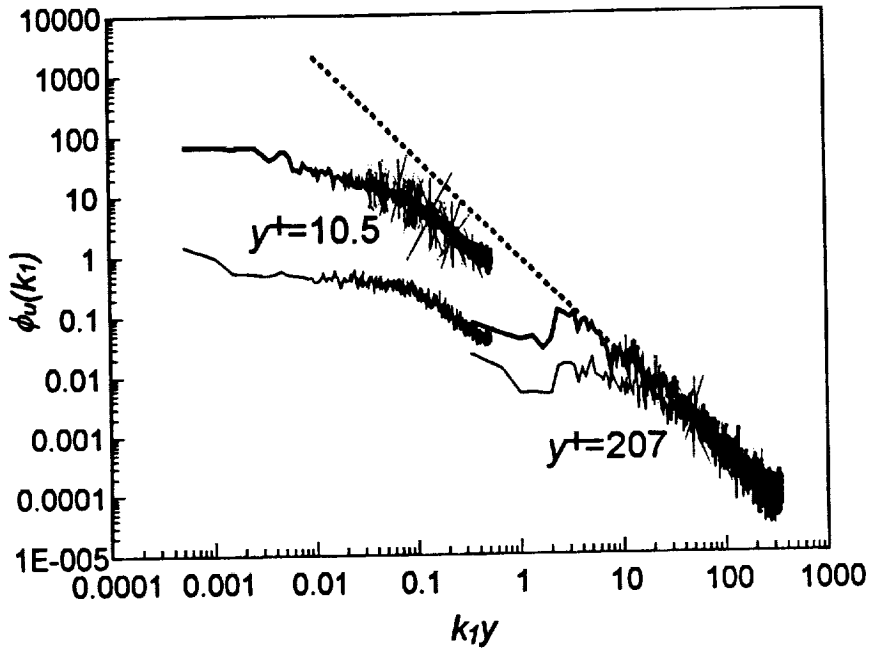

Figure 19. Wave number spectral analysis for the Couette flow: $-\ \phi_{u_{11}}(k_1)\ -\ \phi_{u_{22}}(k_1), \cdot\cdot\ k^{-5/3}$.

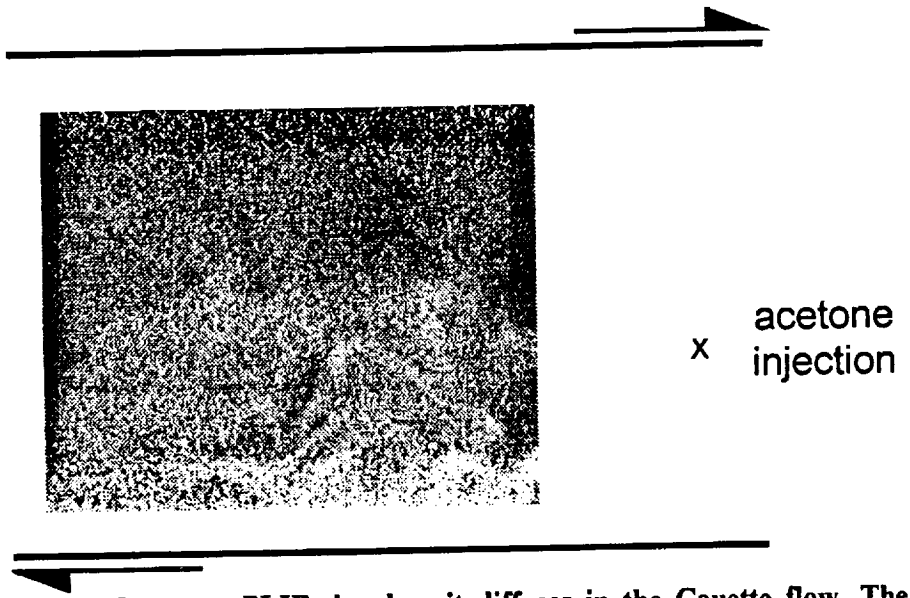

Figure 20. Picture of acetone PLIF signal as it diffuses in the Couette flow. The light regions correspond to the presence of acetone in the flow. To the right of the picture is acetone injection system. The arrows correspond to directions the belt is moving.

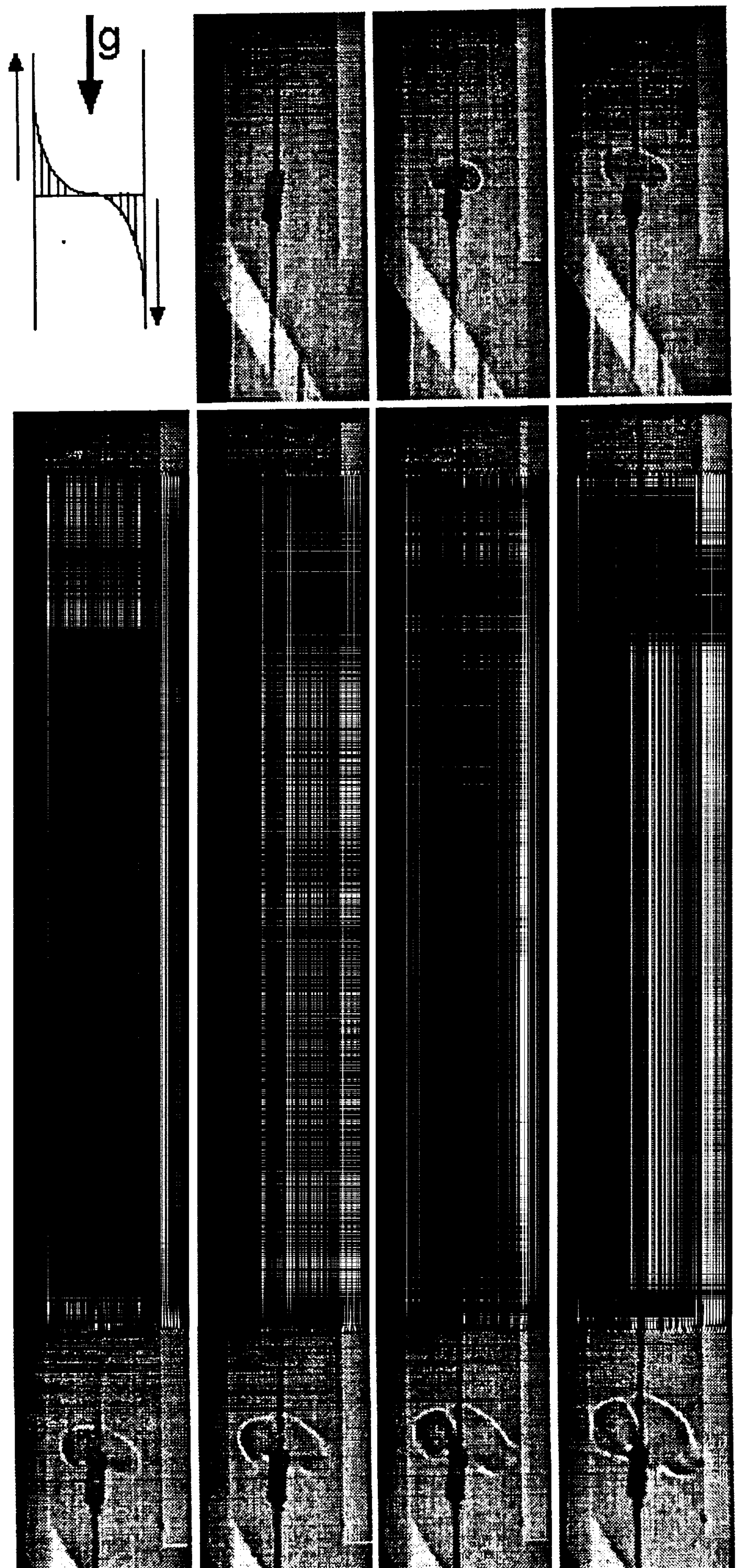
g

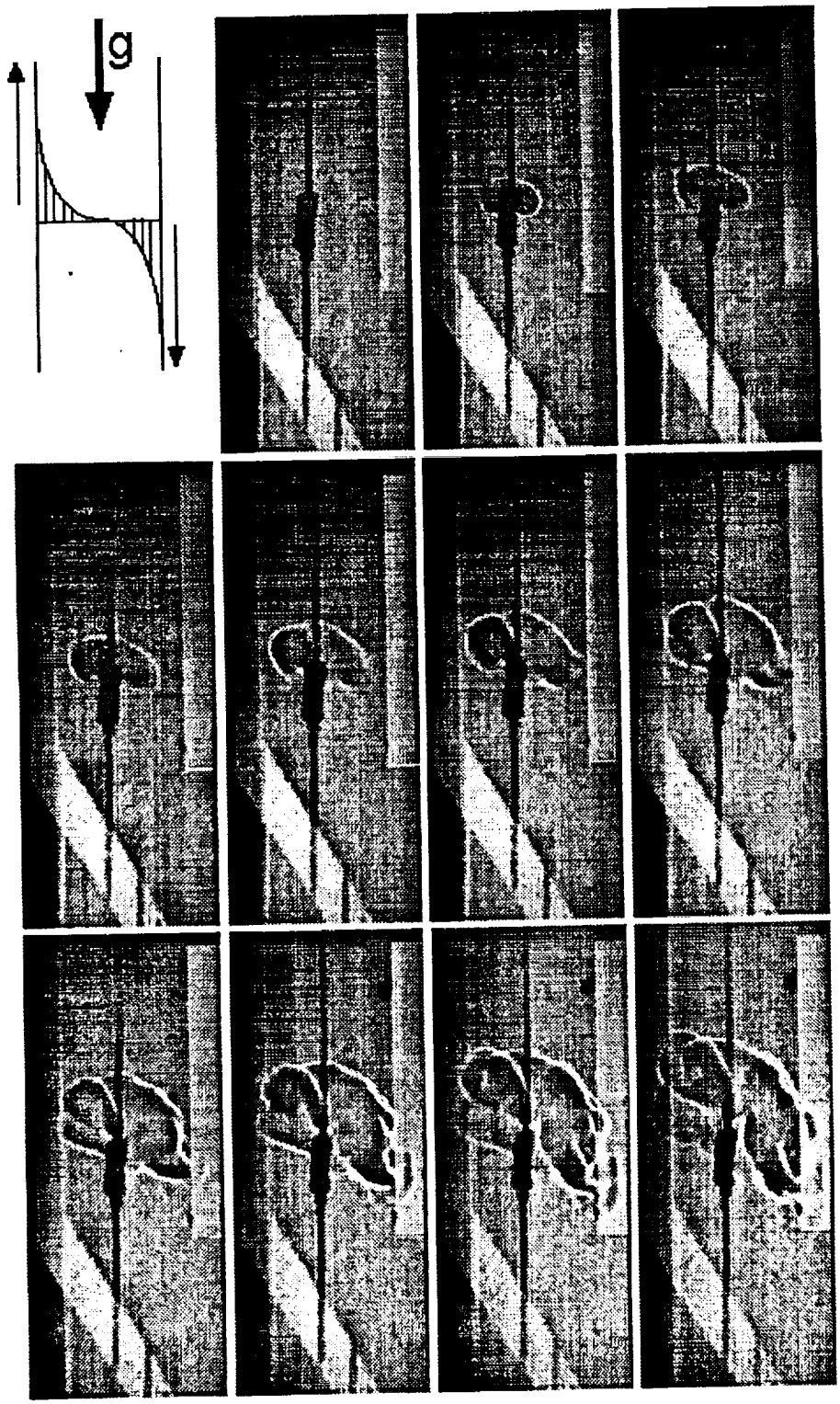

Figure 21. Typical Couette combustion images. Flow conditions: 1g; 1 atm initial pressure; stoichiometric ratio of approximately 0.87; belt speed of 7 m/sec and belt spacing 1". Images are displayed 1.5 msec apart.

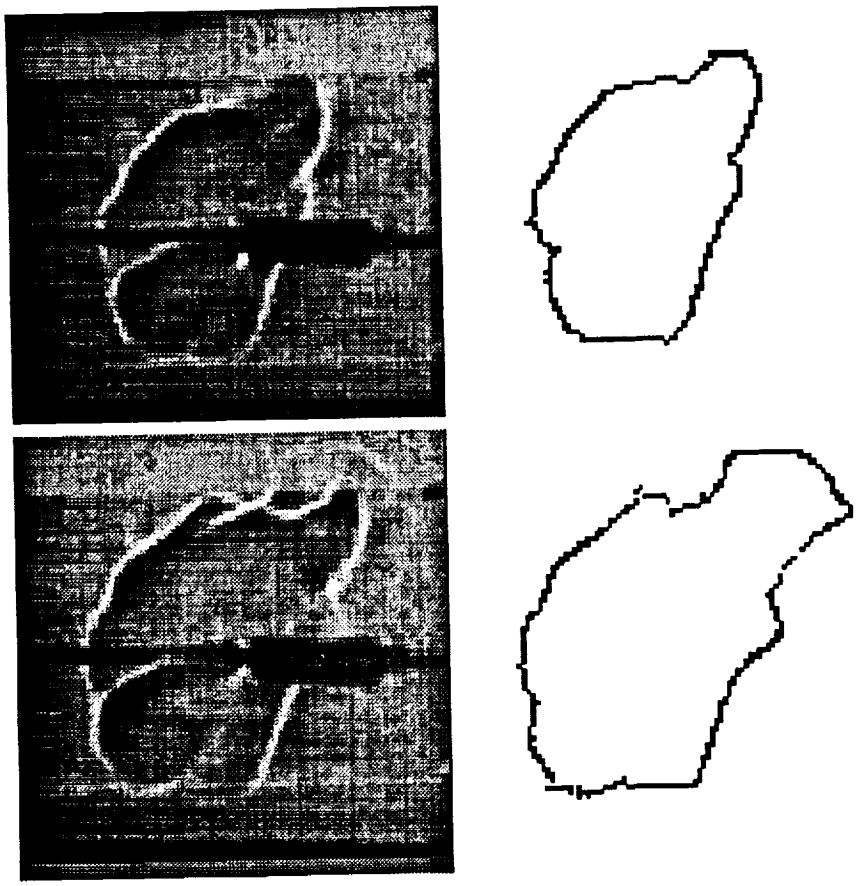

Figure 22. Raw and processed pictures of flame fronts in the Couette combustor. Top is 9 msec after ignition; bottom is 11 msec after ignition.

"Under preparation to be submitted to the *Journal of Combustion Science & Technolog*

Heat Release and Buoyancy Effects on Turbulent Premixed Flames

By

V. K. Chakravarthy and S. Menon
School of Aerospace Engineering
Georgia Institute of Technology
Atlanta, Georgia 30332-0150

Abstract

A modified version of the Linear Eddy model within a large eddy simulation that accounts for non-uniform grid spacing and non-unity grid aspect ratios is presented. This model is used to analyze the structure and evolution of a premixed flame in the core region of a low speed turbulent Couette flow in the presence and absence of gravity. It is seen that heat release significantly changes the flame-vortex interaction process. These findings provide a perspective on how close simulation of passive scalar flamelet modeling is to the real flames. The buoyancy effects are found to depend strongly on the direction of propagation relative to the direction of gravity. Overall, buoyancy increases the tangential strain in the plane of the flame. The overall consumption of the fuel in decreased but the contribution of the subgrid scales towards creation of the turbulent flame area is more in the presence of buoyancy.

1. Introduction

A premixed flame in turbulent flow where the flame thickness (δ) and laminar propagation speed (S_l) are smaller than the smallest significant fluid dynamic length and velocity scales (Kolmogorov scales η and v_η respectively), offers a simplification that can be utilized for computational modeling. The region in the parameter space characterized by the above stated properties is termed as the flamelet regime. In this regime, the turbulence wrinkles the flame producing a turbulent flame brush which is an ensemble of locally laminar flamelets. For flames that are chemically stable (i.e., mixture properties within the flammability limits) and have no differential diffusion effects, one can approximate laminar flame propagation at a constant speed using a Huygen's propagation based equation called the G-equation (Kerstein *et al.* 1988). This model equation is used within a subgrid approach in this study. The subgrid implementation (Menon *et al.* 1993, 1994; Smith and Menon 1998; Chakravarthy and Menon 1997) is based on the linear eddy model (Kerstein 1988, 1989, 1990) and is a method of multiple scales (two scales) for spatio-temporal integration. The large scale equations are integrated using a finite difference or finite volume numerical scheme and constitute the large-eddy simulation (LES) equations. The small scales (separated from large scales by a scale that equals grid spacing) are integrated locally using an Eulerian-Lagrangian algorithm based on the linear eddy mixing model (LEM). The form of this model is briefly explained in the next section since more details are available elsewhere (Menon *et al.* 1993; Calhoon and Menon 1997; Smith and Menon 1998).

The effects of heat release on turbulent premixed flames is one of the primary concerns in this study. In the past, considerable amount of work has been done in flamelet modeling using passive scalar models (Ashurst and Shepherd 1997). The present study attempts to identify the similarities (or dissimilarities) between real flames (i.e., with heat release) and these earlier passive scalar studies.

The effect of turbulence on the flame structure and propagation is another focus of this study. It is difficult to resolve this issue in typical high Reynolds number (Re) flows since it is nearly impossible to resolve (experimentally and numerically), all the turbulent scales at which the flame is being wrinkled. A device in which all the length scales in a turbulent flow can be resolved is the Couette flow facility. In such a facility, fully developed turbulence can be attained at relatively low Re and especially, in the core region, the turbulence fluctuations are nearly gradient free (when compared to configurations such as channel flow, flows in ducts and most free shear layer). However, due to the low flow speed, the turbulent stresses will become overwhelmed by the buoyant stresses in normal gravity. Experimentally, a resolution to this problem is to study this flow in microgravity and is the focus of a current study. Numerically, this issue can be addressed by choosing appropriate parameters so that the gravity effects become noticeable. The present study also addresses the impact of gravity on the flame structure in a Couette flow configuration.

2. Subgrid model

Simulations are carried out using Navier Stokes equations under zero Mach number approximation, formulated using a second order finite difference scheme on a non-staggered grid. The momentum equations are closed using a localized, dynamic, variable density subgrid kinetic energy model [10] which solves a transport equation for the subgrid kinetic energy (a quantity that is also needed for the subgrid LEM closure) along with the LES equations.

The scalar evolution is simulated within the subgrid using LEM (Menon *et al.* 1993; Menon and Calhoon 1996; Smith and Menon 1998) In this approach, the turbulent stirring of the scalar field and laminar propagation are accounted for distinctly in an one-dimensional (1D) domain within each LES cell. This 1D domain represents a ray in the direction of maximum scalar gradient across the turbulent flame brush and is discretized into cells each representing a fraction of the total volume of the LES cell. The present study extends the earlier model employed on uniform grid (Chakravarthy and Menon 1997) to arbitrary cartesian grids. This involves a redefinition of the subgrid domain length and is determined as follows. Consider a planar flame propagating at a arbitrary angle and at a constant speed on a cartesian grid. Without loss of generality, it is assumed that the flame is moving in the direction of increasing computational coordinates. The distance the flame propagates normal to itself in the time it takes to consume the volume of a cell whose diagonal is given by a line connecting computational nodes (i,j,k) and (i+1,j+1,k+1) is given by the projection of the diagonal vector onto the flame normal. Thus, the length of the subgrid domain is given by absolute value of the scalar product of the diagonal vector and the unit flame normal. Tests showed that this ensures planar laminar flame propagation at any angle with the correct speed. Furthermore, the interpretation of the subgrid domain as the direction of maximum scalar gradient is still retained. This prescription is termed the aspect ratio correction. It is found that significant errors occur in flame propagation if this correction is not used.

The scalar G here, is a representation of the rate of advancement in a premixed reaction. It has a binary representation on the subgrid one-dimensional domain with G

= 1 representing an unburnt state and $G = 0$ representing a burnt state. The interface between two dissimilar adjacent cells is considered to be an infinitely thin flame that propagates into the unburnt zone at a specified flame speed. The temperature rise due to the reaction is modeled by assuming that the temperature is a linear function of G and density is an inverse function of T (since the thermodynamic pressure is constant in the present formulation). Thus, the G-equation replaces the reaction-diffusion equations for both species and temperature.

The effect of subgrid velocity (turbulence) is modeled separately using a stochastic process. A Lagrangian rearrangement process (termed stirring) is used to model the effect of turbulent eddies on the scalar field. The length scale of the eddy (segment size on which this rearrangement process is to be conducted) and the frequency of stirring at that length scale are determined using isotropic inertial range (assumed to exist in the subgrid scales of the LES) scaling laws. The details of this stirring process have been reported earlier and therefore, are omitted here for brevity. A key point to emphasize is that, turbulent stirring is implemented based 3D inertial range scaling laws and therefore mimics the effect of 3D turbulence on the scalar field even though the domain is one-dimensional.

Advection due to the supergrid velocity transports the scalar field from a LES cell into it's neighboring cells using a using a procedure termed "splicing" (Menon *et al.* 1993; Smith and Menon 1998) The scalar flux across each LES cell face is computed using the filtered velocity on the cell face. The number of subgrid cells corresponding to the scalar flux are transfered from one cell to it's neighbor in accordance with the direction of the scalar flux.

The splicing algorithm models advection and should not create artificial flames in the subgrid (this is possible whenever a $G = 0$ cell is placed adjacent to a $G = 1$ cell). So whenever such an artificial flame is created, the present algorithm rearranges the spliced-in cells to remove the extra flame. The only exception to this procedure is the case of burning initiation in a fully unburnt cell in which case one flame caused at the interface is retained (this is necessary to initiate flame propagation into a completely unburnt mixture). This approach ensures that the correct laminar flame speed is obtained on the supergrid especially in case of curved flames (cylindrical and spherical). In the turbulent case, the stirring causes multiple flames to exist in the same subgrid domain. There is no restriction on this occurrence and is considered a stochastic representation of flame brush in each cell.

3. Results and analysis

A 129x65x65 grid is used for LES of the Couette flow simulations. Two simulations, with two different values of the body force (per unit mass) but otherwise identical are conducted. The two cases correspond, respectively, to a zero body force case () and a $(+g)$ case with earth's gravity acting in the wall normal direction. The Reynolds number of these simulations is chosen to be 5000 based on distance between the walls and their relative speed.

A LEM resolution of 100 cells (corresponding to volume of LES cell at the center of the domain) is used and this adequately provides for implementation of stirring process at the Kolmogorov length scale. The wall normal grid spacing at the wall (to resolve the wall layer) is set at $0.3y^+$. Grid is then stretched out using a hyperbolic tangent function.

In planar Couette flow, the turbulence intensities are nearly gradient free. Flame propagation in this region has approximately the same characteristics of a flame kernel in homogeneous turbulence. The intensity of turbulence in the core region can be used as

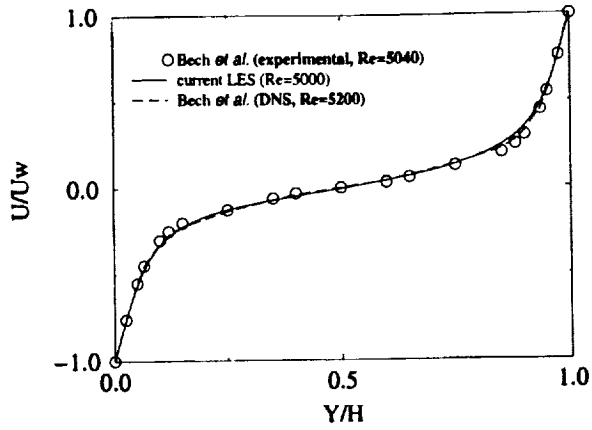

FIGURE 1. Mean velocity in Couette flow

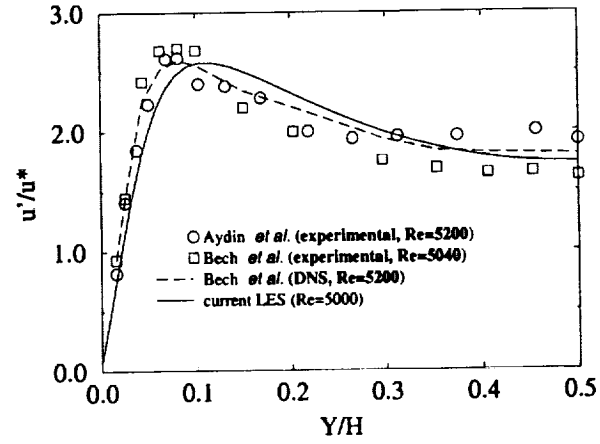

FIGURE 2. Axial velocity fluctuations in Couette flow

a reference (incident turbulence) in order to characterize the effects of turbulence on the flame kernel evolution. The simulations are stopped once the flame reaches out of mid 60% of the domain. Flame growth beyond this region is affected strongly by the higher turbulence intensity (in the vicinity of the wall) and the flame wall interactions (which can not be modeled using the G equation).

Figure 1 shows the prediction of axial velocity profile (non-dimensionalized using the wall speed) along with corresponding results from earlier studies (Bech *et al.* 1995; Aydin and Leutheusser 1987). Shown in Fig 2 are the axial *rms* velocity fluctuations non-dimensionalized using the wall friction velocity. The predictions compare favorably with earlier results to within relatively small errors which indicates that the flow is adequately resolved on the grid used.

For the stagnation point simulations, a jet of 50mm diameter is used to supply the premixed reactants. This jet is surrounded by coflowing laminar stream at the same speed. A planar plate is placed at a distance of 100mm from the jet. The stagnation point flow thus created anchors a planar turbulent flame brush. A uniform and isotropic grid (with grid spacing of 0.8mm) is used in the core region of the flow where the flame is anchored. In other regions, the grid is stretched out to provide problem free boundary conditions to the simulations.

The configuration used here is similar to those used in the experiments by Cho *et al.* (Cho *et al.* 1986, 1988), Cheng *et al.* Cheng and Shepherd (1991). Grid turbulence is used for the inflow in these experiments. In this study, velocity fluctuations that have a von-Karman energy spectrum (k^4 at small wavenumbers and $k^{-\frac{5}{3}}$ at large wavenumbers) are added to the mean inflow velocity using Taylor's hypothesis. A rapid decay is seen in the turbulence intensity close to the inflow. This can be attributed to the fact that the component of specified inflow turbulence that is incompatible with the finite difference equations describing the interior of the computational domain gets filtered out. After this decay, a gradient free turbulent stream is established. This value of turbulence intensity is used as reference turbulence level that the flame encounters. Five different simulations, each corresponding to a different parameter set, are conducted. The conditions/parameter sets for these simulations are shown in Table 1.

There are some measures that are conventionally used to characterize the geometry and dynamics of turbulent premixed flames. The wrinkling of any surface at any given point is characterized by the local curvature which is obtained mathematically as follows.

$$h_{ij} = -\frac{\partial^2 G}{\partial x_i \partial x_j}\frac{1}{|\nabla G|} + \frac{1}{|\nabla G|^3}\frac{\partial G}{\partial x_i}\frac{\partial G}{\partial x_k}\frac{\partial^2 G}{\partial x_k \partial x_j} \tag{3.1}$$

The two non-zero eigenvalues of the curvature tensor h_{ij} give the two principle curvatures Ashurst *et al.* (1987). Positive curvature is defined in the present study as concave to the fuel side. The sum of the two eigen values is the mean curvature. The inverses of these eigen values give the two principle radii of curvature. A ratio of the smaller of these two eigen values, magnitude wise, to the other eigen value is called the shape factor. Given that it is the ratio of principle radii of curvature, it determines the local shape of the surface. A shape factor of 1.0 indicates a spherical shape and 0.0 indicates a cylindrical shape, locally. A negative value of shape factor indicates a saddle structure of the surface. The absolute value of the shape factor, by it's definition, is bounded by 1.0.

The effect of fluid dynamics on the flame structure can be measured in terms of the strain rate on the tangent plane of the flame surface. A positive strain rate on the flame surface is indicative of the tendency of fluid dynamic eddies to wrinkle the flame surface. Also a self propagating surface tends to replanarize if the curvature is positive. These two effects contribute towards the overall change in flame area locally which is measured using flame stretch. The flame surface area is the primary factor in determining the consumption rate in the flamelet regime of combustion. The overall stretch on a self propagating surface is given as follows.

$$\kappa = \frac{\partial u_k}{\partial x_k} - \eta_i S_{ij} \eta_j - \frac{S_L}{R} \tag{3.2}$$

η_i in the above equation, is the flame normal. The first two terms on the right side of the above equation give the local tangential strain rate and the last term is the replanarizing effect of self propagation. Physically, the flame stretch is defined as the rate of change of a Lagrangian flame surface element. Flame stretch has the unit of inverse time and hence in all the illustrations included here, it is non-dimensionalized using the Kolmogorov time scale. In some sense, it represents an inverse time scale characterizing planarization. The flame stretch is found to change the flame speed and thickness of a laminar flame and these are usually accounted for by the famous Markstein correction. The flame stretch is also found to be main reason for local flame extinction observed mostly in lean premixed flames in high intensity turbulence. These two issues are not considered here due to the

limitation imposed by the G equation. These two issues deal with dynamic aspects of the flame structure that cannot be reproduced while using the G equation. Also these issues are only of secondary importance in the flamelet regime. The tangential strain rate depends the interaction of the flame surface with the turbulent structures. Kinematically, this interaction can be quantified in terms of the relative alignment of the surface gradient with the vorticity vector and the principle directions of strain.

The kinematic response of the flame to fluid dynamics plays an important role in determining the flame structure and the tangential strain rates discussed above. In cold premixed flames, it is seen that the flame normal has a tendency to align itself along the direction of most compressive strain rate. The most compressive strain rate is given by the least eigen value of the strain rate tensor. The sum of the eigen values of strain rate is zero due to continuity equation in case of incompressible flows. So atleast one of the eigen values is negative. This need not be the case in real flames with volumetric dilatation in which case the phrase "most compressive" is to be interpreted as "least tensile". The unit eigen vector corresponding to this eigen value gives the direction of most compressive strain (γ). Similarly, the direction of maximum positive strain rate is denoted by α. By aligning itself with the most compressive strain direction, a premixed flame surface is subject predominantly tensile strain rates on it's tangent plane. The consequence of this is a constant tendency to wrinkle.

The amount of heat release and the ratio of turbulence intensity to the laminar flame speed are two factors that effect the turbulent flame structure. The value of $\frac{u'}{S_l}$ in the Couette flow simulations (u' is the axial rms velocity of the core region turbulence) is set at 5.7 (to mimic a typical parameter in the experimental part of the program). $\frac{u'}{S_L}$ values of 1.6 and 0.65 are used for the stagnation flame simulations. The heat release is chosen to give a temperature rise of 7 times which is typical of real flames.

In experiment, the turbulent jet flow that creates the stagnation point flame is moving vertically upwards. The turbulent flame thus creates hot products that are above cold reactants. The buoyancy forces are expected to be stabilizing in this case. The simulations that correspond to this setup are referred to as the "+g" simulations. The simulations that do not have a body force term are called the "μg" simulations. The "+g" and "μg" simulations are conducted at both $\frac{u'}{S_L}$ values. For the case with $\frac{u'}{S_L}$ of 1.6, a "-g" simulation is also conducted. In this case, the direction of gravity and the jet flow direction are both vertically downward. This creates hot products below cold reactants, which, at first glance, is expected to be stabilizing.

Since the characteristizations discussed above are local and vary from one location to another, probability density functions (PDF) of these quantities (as resolved on the LES-grid) over the whole flame surface are constructed for analysis. For presentation, the strain rate (flame stretch) and the mean curvature are non-dimensionalized by the Kolmogorov time and length scales, respectively. Also, to obtain statistical stationary results, 16 Couette flow simulations (using different initial realizations) are used in order to obtain these PDFs. Typically, each realization provides more than 1400 data points on the flame surface. In case of stagnation point flames, 80 to 100 realizations at equally spaced time intervals within 5 flow through times (defined as axial distance from the jet exit to the wall divided by the average velocity) are used. To avoid edge effects (due to reactants-coflow air interface at the sides) on the statistics, only the core region of the flow (75mmx75mm) is used for analysis. This gives a sample space of atleast 400000 for flame analysis.

Each of the turbulent flame characteristics discussed above are difficult to study experimentally. The numerical studies have so far been restricted to flames with no heat

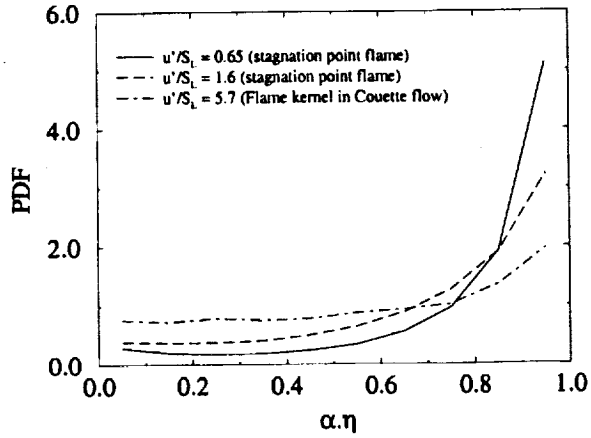

FIGURE 3. Flame normal alignment with direction of maximum strain rate

release. the primary focus here is on the changes brought about by the presence of heat release. Also of importance is the role played by buoyancy forces on premixed flame structure. Each of the flame characteristics is discussed separately in the following.

3.1. Flame alignment

The alignment of the flame normal with the vortical structure of turbulence is found to determine the topological structure of the flame brush. It was shown) that the flame normal tends to align near perfectly with direction of minimum (principle) strain rate in isotropic turbulence. In shear flows, the most likely angle between the flame normal with the most compressive strain direction is found to be 30°. LEM-LES of cold flames in Couette flow) predicted these two features at high and low values of $\frac{u'}{S_L}$ respectively. The PDFs of flame normal (η_j) alignment with maximum strain rate direction are shown in Fig3. In the presence of heat release, it is seen that the flame normal tends to align more with the most tensile strain rate direction. The reason is that there is rapid straining induced due to the steep density drop across the flame in the direction of the flame normal. In the limit of low turbulence, the flame normal aligns more with direction of highest acceleration. As the turbulence is increased relative to S_L, the wrinkling is more three dimensional and fine grained. The local flame orientation is more randomly distributed over all possible directions. Due to fine scale nature of wrinkling, the zone of heat release is also broadened. This smearing is partly numerical. The heat source term computed from subgrid averaged quantities is highly discontinuous due to thin front tracking used here. As explained earlier, this source term is filtered in space to facilitate the convergence of the implicit numerical scheme used here. This filtering renders a finite thermal thickness to the local flamelets. This filtering reduces the correlation between the actual flame normal (computed using ∇G) and the direction of acceleration induced by the flame. These factors lead to a reduced tendency for the flame to align with the direction of most tensile strain rate when the turbulence is high.

The predominant structures in the flow are still cylindrical. This can be ascertained from Ashurst *et al.* (1987) the fact that the vorticity vector is aligned most with the intermediate strain rate direction.

3.2. Flame geometry

A recent study of the flame front curvature distribution suggested that the curvature PDF normalized by it's own variance is fairly independent of volumetric dilatation when the

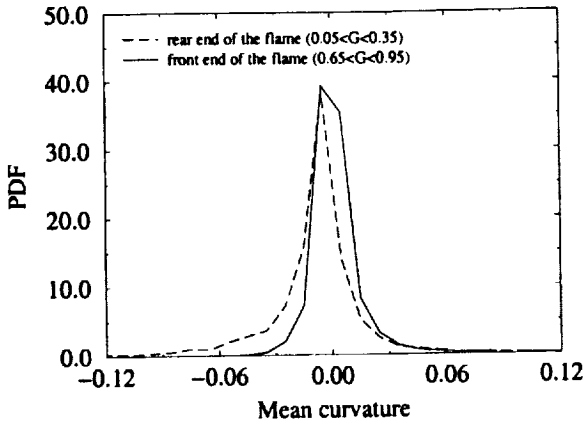

FIGURE 4. Mean curvature PDF in Couette flow

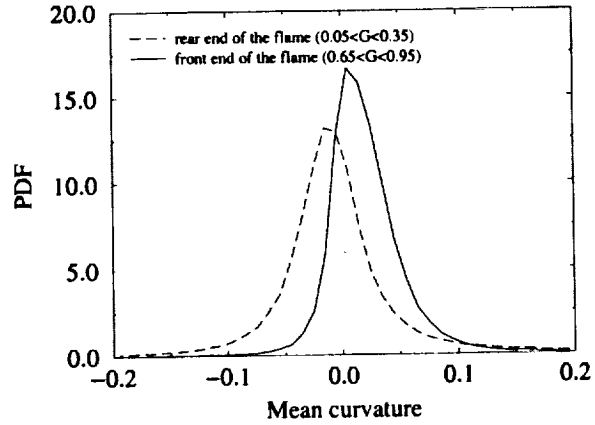

FIGURE 5. Mean curvature PDF in stagnation point flames

overall flame shape is perpendicular to the propagation direction. The LEM predictions from the present and earlier studies are in agreement with this hypothesis. The mean curvature PDF is slightly skewed to the positive side and fairly symmetric about it's mean. However, the distribution of curvature is found to change across the turbulent flame brush. To analyze this, the flame brush is divided into two zones: the front ($0.65 \leqslant G \leqslant 0.95$) and the rear ($0.05 \leqslant G \leqslant 0.35$) ends. The mean curvature PDF for these zones, in Couette flow and stagnation point flow ($\frac{u'}{S_L} = 1.6$), are plotted in Fig4. and Fig5. respectively. It can be seen that the front end of the flame has a higher likelihood of having positive curvatures when compared to the rear end.

The PDFs of the shape factor, defined as the ratio of lower to higher (magnitude only) curvatures are shown in Fig6. Only the results from stagnation point flames with $\frac{u'}{S_L} = 1.6$ are shown here. This is because of better convergence of the PDFs in this case. Locally, the flame structure seems to tend to be cylindrical. However, there is a shift in the most likely value from positive to negative across the flame brush. This indicates that either negative curvature increases across the flame brush or positive curvature decreases or both. These results are consistent with recent results obtained in simulations of passive premixed flames. It is inferred from these results that the flame structure varies within the flame brush. As a result, flame speeds with reference to hot and cold regions cannot be related simply by the expansion ratio as pointed out by Mishra et al. (Mishra *et al.*

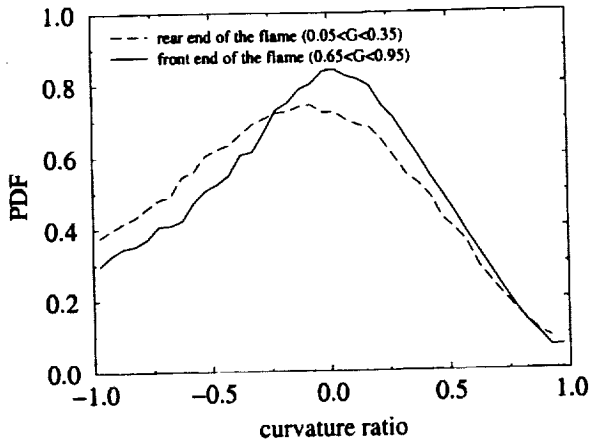

FIGURE 6. PDF of curvature ratio in a stagnation point flame

1997). Hence the velocity at the leading edge of the flame is not a true measure of turbulent flame speed (as assumed by Cho et al.). The flame surface density is found to vary across the turbulent flame brush ,i.e. the projected surface area of the isosurface $G = 0.2$ would be different from that of isosurface $G = 0.8$. The structure of the whole flame brush contributes to the overall burning rate. Some of the flux entering the flame brush does not exit in the normal (to the flame brush) direction, flow divergence causes some transverse exit flux.

Since the gravity is vertically downwards here, the upper portion of the flame in Couette flow is propagating against gravity, while the lower portion is propagating just the opposite. Thus, the effect of gravity is hidden when one constructs a PDF using the whole flame surface. The lower portion has hot products above the cold reactants which corresponds to the "+g" case. The upper portion, under similar arguments, corresponds to a "-g" case. The PDFs for each portion are constructed by dividing the Couette flow domain into two halves in the vertical direction. Since the flame moves up due to buoyancy, the upper region of the flame has more points on it's surface than the flame in the lower half. Also the expected unstable (cold reactants over hot products)state of the upper portion of the flame kernel could lead to faster growth of flame area on the top portions. So the PDFs come out little coarser for the lower region (however, there is sufficient data for reasonable accuracy).

The differences in mean curvature PDFs between the "-g" case and the "+g" case for the Couette flow flame kernels and turbulent stagnation point flames are presented in Fig. 7 and Fig. 8, respectively. The stagnation point flames with low $\frac{u'}{S_L}$ (0.65) are unaffected by gravity as far as the curvature distributions are concerned. It is seen that the "+g" cases have longer tails for PDFs indicating the presence of more small scale wrinkling. The tendency of small scale wrinkling is also seen to increase with turbulence intensity ($\frac{u'}{S_L}$). This means that small eddies, in the presence of gravity, are more successful in wrinkling the flame at the bottom than at the top. This is in contrast to the expectation that stable stratification makes the density interface (flame surface) more stiff and the smaller eddies (that have low energy) may not be able to penetrate it. Previously, it was shown that a stably stratified non-reacting density interface is more penetrable at low Froude numbers. Froude number is defined as follows.

$$Fr = \frac{ga^3}{\Gamma} \tag{3.3}$$

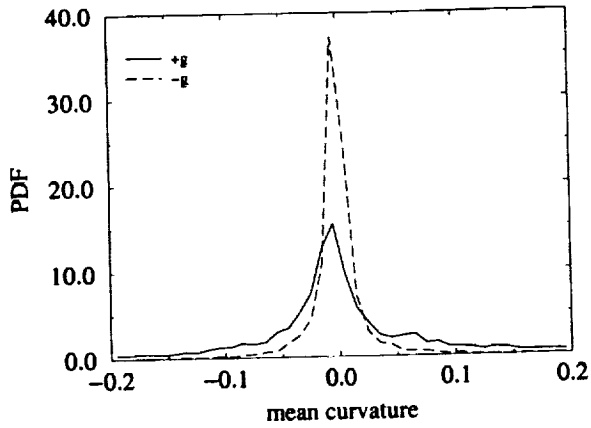

FIGURE 7. Effect of gravity direction on mean curvature PDF in a flame kernel

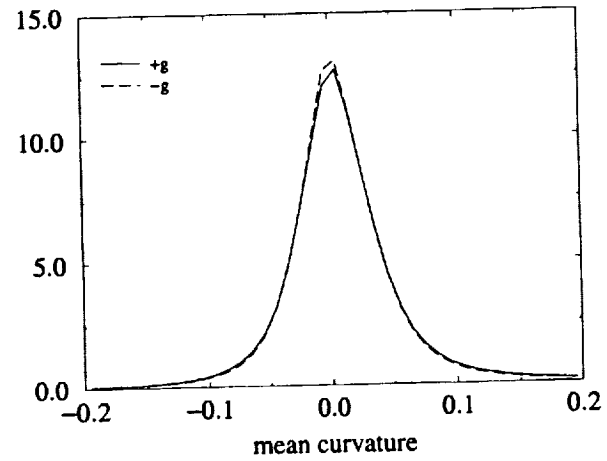

FIGURE 8. Effect of gravity direction on mean curvature PDF in a stagnation point flames

In the above equation, a is the eddy size and Γ, it's circulation. Note that the Froude number is defined for an eddy unlike the Richardson number which is defined using the mass flux. If the incoming turbulence is considered an ensemble of eddies with certain size and energy distributions, the observation of the mean curvature PDF indicates that the Froude number for smaller eddies is smaller than that for larger eddies. It is however to be noted that, the study by Marcus is not fully relevant to the present study. The self propagative nature of premixed flames adds additional stiffness to the density front. Also the entrainment of a lighter fluid into the heavier fluid, as noticed by Marcus, is not possible in premixed flames.

It is conceivable now that a flow with low integral length scale is less effected by stabilizing effects of gravity. This is because the Froude numbers for typical eddies in this flow are low and hence the penetration of a density interface (flame surface) is much easier. Large eddies on the other hand cannot penetrate the flame surface as easily. In the limit of a single isolated eddy in laminar flow ?), the flame generated vorticity acts to hinder penetration of the flame surface. Further study is needed to study the effects of integral length scale on the flame dynamics in the presence of gravity.

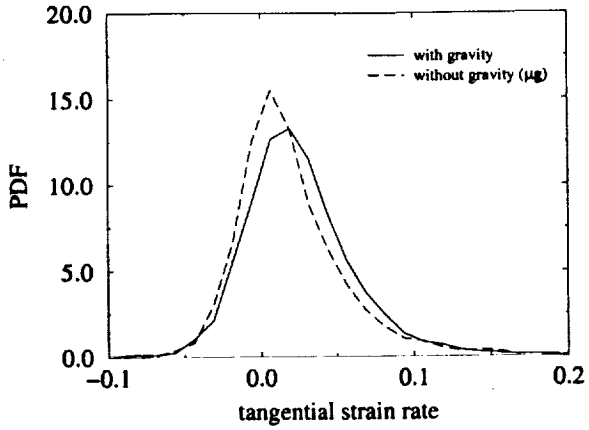

FIGURE 9. Effect of buoyancy on tangential strain rate

3.3. Fluid dynamic effects on flame evolution

The buoyancy effect on the growth of the flame kernel is to be significant. The tangential strain rate PDFs for flame kernels in Couette flow are plotted for the cases with and without gravity in Fig9. As expected (from the mathematical expression), the strain rate is typically positive in the presence of heat release due to non-zero volumetric dilatation. It is seen that buoyancy induces increased postive strain rates on the flame surface. The mean curvature PDF is changed by the presence of gravity, but due to the near symmetric nature of the mean curvature PDFs, the contribution of self propagation towards flame stretch is negligible. So the rate of change of flame area is primarily determined by the tangential strain rate.

The bottom portion of the flame kernel can be thought of to be stably stratified due to the presence of hot products above cold reactants. Stable stratification is expected to reduce the flame wrinkling. Since the upper portion has has cold reactants above hot products, it could be under unstable stratification with high wrinkling. If this is the case, there is faster growth of flame area on the top portion of the flame than at the bottom. As a consequence, all PDFs characterizing the overall flame surface would likely be skewed more towards the corresponding PDF constructed for the top portion of the flame kernel. This however is not the case for the tangential strain rate PDF. The overall PDF is skewed to the right in the presence of gravity. This means that a flame brush with reactants above hot products does not necessarily experience a (statistically) reduced strain rates on the surface. It is perhaps relevant at this point to note the fact that, in case of laminar flows with vertical variations of density, the Richardson number (a stratification parameter that weighs buoyancy force against the inertial forces) of 0.0 is not an absolute stability limit (Taylor and Schlitchting). Hence, one cannot judge the effects of gravity on stability (or instability), consumption rate and tangential strain rates of the flame brush based on the alignment of mean density gradient and direction of gravity.

The tangential strain rate and flame stretch PDFs for the case of $S_L = 0.76$ seem to be independent of gravity. The simulations with $(+g)$ and without gravity (μg)produce virtually indistinguishable results. The tangential strain rate PDFs for the turbulent flames with $S_L = 0.4m/s$ are shown in Fig. 10. The three simulations, under discussion here, are identical in every aspect except for the values of body force input into the numerical code. So, any small differences that are seen in the results can only be attributed to the differences in buoyancy forces. Buoyancy, in general, seems to increase the tangential

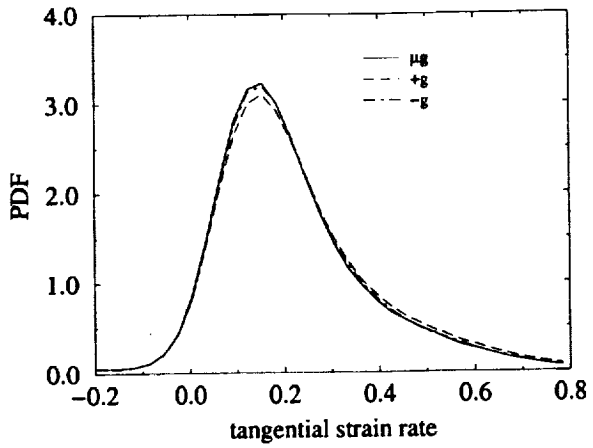

FIGURE 10. Effect of buoyancy on tangential strain rate

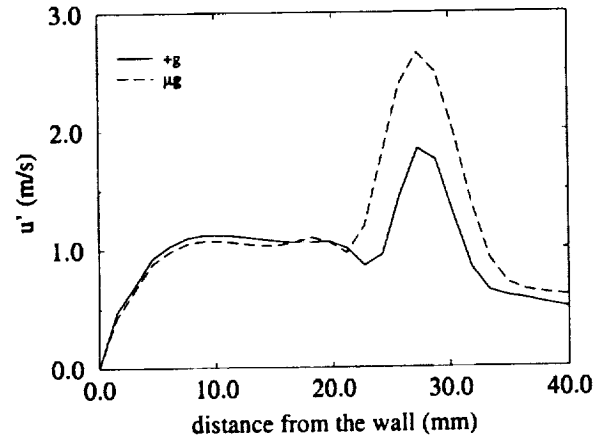

FIGURE 11. Axial velocity fluctuations in the stagnation point flame

strain rate in the presence of gravity. This increase in positive tangential strain rate is more pronounced in the case where the products are on top ($+g$ case). While this could be attributed to possible stable stratification, it is not clear as to why the tangential strain rates are higher also in the "-g" case.

3.4. Heat release and buoyancy effects on turbulence

The stationary nature of turbulent premixed flames aids in calculation of velocity statistics using LES. Steep gradients in density field exist across the flame surface in the flamelet regime of premixed combustion. Mass conservation law then demands a very high velocity rise across the flame front. Unsteady oscillations of flame surface causes high level of velocity intermittency in the flame brush. The *rms* value of axial velocity is increased due to this intermittency (see (Cho *et al.* 1986, 1988; Cheng and Shepherd 1991)). If a finite difference of finite volume scheme is used to model premixed flames (G equation), several grid points are required to resolve the flame profile. The density gradient and the subsequent flow acceleration across the flame are reduced greatly as a consequence. So the correct increase in velocity fluctuations cannot be predicted.

The current LEM-LES predictions of u' and v' along the jet axis, for the case of $\frac{u'}{S_l} = 0.65$, are shown in Fig. 11 and Fig. 12. Like in the experiments Cheng and Shepherd

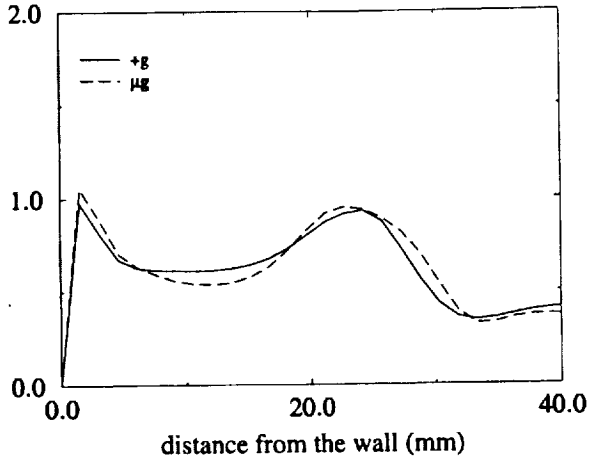

FIGURE 12. Radial velocity fluctuations in the stagnation point flame

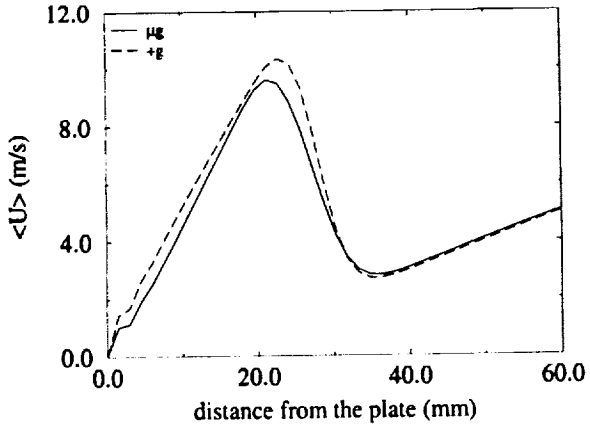

FIGURE 13. Mean velocity along the axis in the stagnation point flame

(1991), the u' is amplified to more than twice it's value within the flame brush. The turbulence level downstream of the flame brush settles down to almost twice the incident value. While the overall turbulence generation by the flame is unaltered in the presence of gravity, it is seen that the peak in u' is reduced significantly by gravity. This is a consequence of the stabilizing effect of gravity due to the fact that products are on top of reactants. This can further be established from the unconditioned mean velocity variation shown in Fig13. The reduced flame oscillations have led to a reduction in the width of the flame brush by about 10%. Gravity seems to make the pockets of product in the flame brush more buoyant thus increasing the peak velocity at the rear end of the flame brush. From this Figure, it might appear that the turbulent flame speed is higher in the case with gravity ("+g"), but the correct evaluation (discussed later) would prove to the contrary.

The effect of gravity on unconditioned mean velocity in case of $\frac{u'}{S_L} = 1.6$ is shown in Fig. 14 . It is seen that the overall axial volume flux across the flame brush is higher in "+g" case. Also, the turbulence levels within the flame brush are slightly higher. The u' and v' predictions along the center line are shown in Fig. 15 and Fig. 16. Although

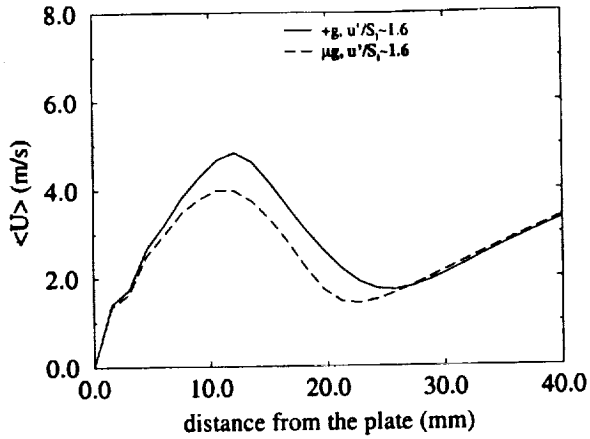

FIGURE 14. Mean velocity along the axis in the stagnation point flame

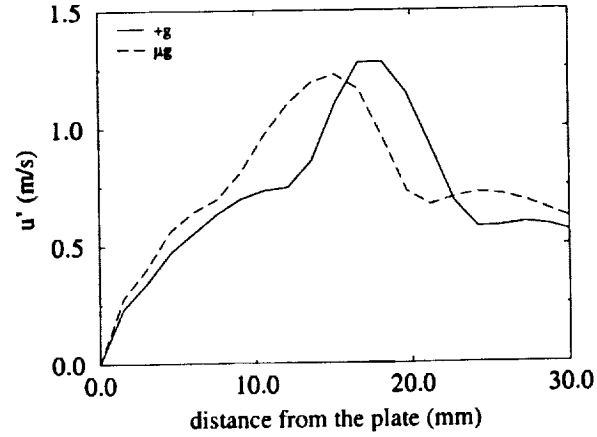

FIGURE 15. Axial velocity fluctuations in the stagnation point flame

hot products are above the cold reactants much like in the earlier case ($\frac{u'}{S_L} = 0.6$), the wrinkling is not reduced by gravity.

The process of flame generating turbulence is associated with two distinct mechansims: distortion of incoming turbulence by velocity strain rate and flame generated vorticity due to flame wrinkles. The vorticity generation mechanisms were discussed earlier in the context of a single (large) eddy interaction with laminar premixed flame by Driscoll et al. While there may be nothing unphysical about visualizing turbulence as an ensemble of eddies of different sizes, the interaction of a premixed flame with turbulence cannot be deduced from the physics of it's interaction with each of those eddies. This is because, an eddy in laminar flow is isolated and hence it's interaction with a flame has some permanence associated with it. In turbulence, there are birth and death rates for each eddy size and so there is a finite time for which an eddy interacts with the flame. Hence the observations made by Driscoll et al. about the effects of gravity on fuel consumption, flame generated turbulence, using a laminar flame vortex interaction study, are not extendable, in general, to all regimes of turbulent premixed combustion. In fact, experiments using turbulent V-flames (Cheng et al.) show that the burning rate increases even when the configuration is supposedly stable (hot products over cold reactants).

The passage of turbulence through a near planar density interface (flame) causes rapid

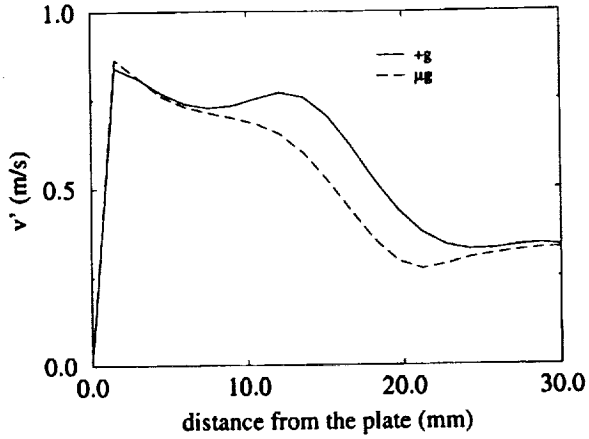

FIGURE 16. Radial velocity fluctuations in the stagnation point flame

distortion of turbulence. This is the first of the mechanisms of turbulence generation by the flame mentioned above. All turbulent eddies have finite time scales associated with them. The time taken for the flow to pass through a very thin flame (that is used here) at any finite speed would be much lower than any of the eddy time scales. The turbulent thus undergoes what is termed as "rapid distortion". The RDT was used to compute the amplification of turbulence intensities across a sharp density interface. It was seen that a thin density interface causes significant amplification of turbulence.

In the wrinkled flamelet regime ($\frac{u'}{S_l} \lesssim 1$), the flame sheet is not highly convoluted. The flame sheet has low wrinkling and is a simply connected surface. In this regime, each vortex structure impinges on a relatively planar flame surface with laminar propagation. The baroclinic torque (due to flame induced vorticity mentioned earlier) generated as a consequence has a preferred direction. It acts to inhibit the impingement and passing through of the eddy. As explained earlier, although the case with continuous impingement (in turbulence) is not topologically similar to the laminar-single eddy interaction, the preferred direction of flame generated vorticity is more likely to be the same. So, at low turbulence levels, the flame wrinkling by turbulence is inhibited by the stabilizing effects of gravity. Since the flame sheet is only slightly curved and near planar, the density gradient is abrupt across a single surface in space. So the turbulence generation is expected due to distortion of turbulence like in []. It can now be concluded that, for the low $\frac{u'}{S_l}$ case, the rapid distortion amplifies turbulence but this is countered to a certain extent by the stabilizing effects of gravity.

When the turbulence is higher (corrugated flamelet regime) the wrinkling is at a finer scales and more three dimensional. The flame, in this regime, can have a multiply connected structure. Large tongues which are thin protrusions of reactants that extend into the product zone are formed. Separated pockets of reactants can be found surrounded by products on all sides. The density, in this case, is more a continuous function in space. The rapid distortion assumption is not valid any more. Thus the largest contributor to flame generated turbulence is missing. Given the higher (than in the wrinkled flamelet regime) turbulence intensity, the eddies in this case could lead to flame generated vorticity of very high magnitudes. But the local flamelets (flame normals) are very randomly oriented in space. So there is no overall preferred direction of the torque. So the gravity effect is not as stabilizing in this case as in the wrinkled flamelet regime. In the current study, the turbulence levels for $\frac{u'}{S_l} = 1.6$ case are increased due to gravity even in the

"+g" case (which was earlier supposed to be stabilizing). As one approaches the distributed reaction zone of premixed combustion, the turbulence generated by the flame may be quite insignificant. Also, the effect of gravity on this generation would be quite negligible.

3.5. Burning rates and turbulent flame speeds

The burning characteristics are also affected by buoyancy. It is not easy to compute the turbulent flame speed for the Couette flow kernels. Hence only qualitative observations are made in this case. The average number of flames in each of the subgrid domains contained in LES cells inside the flame brush is calculated in time for each of the simulations. Starting from the same initial state, LES with buoyancy has more flames per LES cell for the case of Couette flow flame kernel. This number is indicative of burning rate increase caused by subgrid (unresolved curvature) turbulence on the flame. This number times the laminar burning velocity is seen as the effective burning velocity by the supergrid scales. Thus, the effective $\frac{u'}{S_l}$ at the supergrid level which is given by the ratio of rms resolved velocity fluctuations to the effective burning velocity at the supergrid level (velocity based on consumption rate in the subgrid as a consequence of laminar propagation and subgrid stirring) is more with zero gravity. As a result, more flame wrinkling is seen at the supergrid level for this case. This conclusion cannot be made by visualization alone and requires analysis of the subgrid information. For two nearly similar flames (i.e., the same size based on burnt volume), the number of supergrid points in the flame brush are more in case of zero gravity indicating that this flame is more wrinkled at supergrid level. It is seen that small scale wrinkling leads to creation of more flame area in the case of premixed turbulent flame kernels under the influence of gravity.

The mean reaction rate, in the standard Favre-averaging notation, is given as follows.

$$\overline{w} = \frac{\partial}{\partial x_i}\left[\overline{\rho}\tilde{u}_i\tilde{c} + \overline{\rho u_i'' c''}\right] \tag{3.4}$$

Here, c is the progress variable given as $(1 - G)$. The reaction rate computed from the above equation is utilized to define a consistent definition of a turbulent flame speed [] as follows.

$$u_t = \frac{\int_{-\infty}^{\infty} \overline{w} dx}{\rho_r} \tag{3.5}$$

ρ_r is the density of the reactants. From this, the values of $\frac{u_t}{S_L}$ is computed for the five stagnation point simulations.

For stagnation point flame with $S_L = 0.76m/s$, the turbulent flame speed is found to be 2.63m/s. In the presence of gravity, this is reduced to 2.58m/s. This is due to the stabilization mechanisms explained earlier.

At $S_L = 0.4m/s$, the turbulent flame speeds for the "μg" , "+g" and "-g" cases are respectively 2.41m/s, 2.7m/s and 2.53m/s. It is surprising that both directions of gravity lead to an increased burning rate. A similar trend was seen in experiments on V-flames Cheng *et al.* (1999). Further work is necessary to explain this. A general trend, however, emerges for the dependence of burning rate on the body forces. A flux Richardson number needs to be defined to present this trend. In the context of turbulent premixed flames, it should be defined as follows.

$$Ri = \frac{f_b \delta_t}{{u_p}^2 - {u_r}^2} \tag{3.6}$$

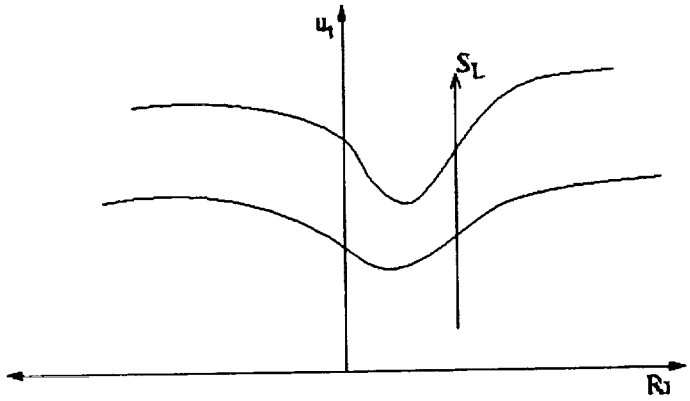

FIGURE 17. Proposed buoyancy effect of the burning rate

Ri is the Richardson number defined for a hot flame. f_b is the body force that can be both postive or negative. δ_t, u_p and u_r are respectively the flame brush width, velocities at the leading and rear edges of the flame brush. In the limit of no turbulence, there is acceleration of the flow across the flame. So the denominator in the above expression is finite. The turbulent flame thickness has to be replaced by the laminar flame thickness which in the flamelet regime is very small. Hence, laminar flames have extremely low Ri, for reasonable values of the body force whether it is positive or negative. It was reported by Cheng et al. Cheng *et al.* (1999) that laminar flames do not seem to be affected by gravity (for both "+g" and "-g" cases). The reason is because, all the laminar cases correspond to Ri near zero. The turbulent case is now discussed by fixing the absolute value of the body force and varying amount of turbulence. As turbulence level increases, the flame brush increases in size and the increase in mean flow velocity across the flame brush is found to drop. This means that Ri goes up as turbulence is increased. As turbulence is increasing from a zero level, first the wrinkled flamelet regime is encountered. In this regime, as explained earlier, the flame generated vorticity mechanisms stabilize the flame surface. The turbulent consumption rate is thus reduced as a consequence. In the corrugated flamelet regime, the fine scale and highly convoluted flame surface does not experience these gravity induced stabilizing mechanisms. So the burning rate starts to increase as Ri increases. For the "-g" cases, the gravity always leads to more wrinkling due to an inherently unstable configuration. The growth in burning rate, however, cannot be indefinite with increasing magnitude of Ri. This is because gravity is seen to increase positive strain rates on the flame surface in both "-g" and "+g" cases. Once the distributed regime in encountered, the strain rates start to affect the propagation speed and internal flame structure. So the burning rate is expected to level off to a certain value. The possible variation is provided in Fig. 17. Increasing strain rates on the flame surface is also given as a possible explanation for the bending of the turbulent flame speed versus the turbulent intensity curve at high intensities. The data from experiments Cheng *et al.* (1999) seems to support the current explanation. The data on the negative Ri side of the above curve is reflected laterally to the positive side by Cheng et al. Cheng *et al.* (1999) in their presentation. So far, it is clear that stabilizing mechanisms of gravity

are reduced as turbulence intensity is increased. Further research is still required at this point to explain why the burning is increased.

Acknowledgment

This research was supported in part by the NASA Lewis Research Center and the AFOSR Focussed Research Initiative. The computer time was provided by the High Performance Computing Center, ARL at the Aberdeen Proving Ground, Maryland. The authors would like to thank these organizations for the support.

References

Ashurst, W., Kerstein, A., Kerr, R. and Gibson, C. (1987) Alignment of vorticity and scalar gradient with strain rate in simulated navier stokes turbulence. *The Physics of Fluids* **30** (8), 2343–2353.

Ashurst, W. and Shepherd, I. (1997) *Combustion Science and Technology* **124**, 115–144.

Aydin, E. M. and Leutheusser, H. J. (1987) *ASME Forum on Turbulent Flows, ASME-FED* **51**, 51–.

Bech, K. H., Tillmark, N., Alfredsson, P. H. and Andersson, H. I. (1995) *J. of Fluid Mech.* **286**, 291–325.

Calhoon, W. and Menon, S. (1997) Linear eddy subgrid model for reacting large eddy simulations: Heat release effects. *AIAA-97-0368* .

Chakravarthy, V. and Menon, S. (1997) Characteristics of a subgrid model for turbulent premixed combustion. *AIAA-97-3331* .

Cheng, R., Begat, B. and Kostiuk, L. W. (1999) Effects of buoyancy on lean premixed v-flames part i: Laminar and turbulent flame structures. *Combustion and Flame* **116**, 360–375.

Cheng, R. and Shepherd, I. (1991) The influence of burner geometry on premixed turbulent flame propagation. *Combustion and Flame* **85**, 7–26.

Cho, P., Law, C., Cheng, R. and Shepherd, I. (1988) Velocity and scalar fields of a turbulent premixed flame in a stagnation flow. In *Twenty-second Symposium (International) on Combustion*, pp. 739–745.

Cho, P., Law, C., Hertzberg, J. and Cheng, R. (1986) Structure and propagation of turbulent premixed flame stabilized in a stagnation flow. In *Twenty-first Symposium (International) on Combustion*, pp. 1493–1499.

Kerstein, A. R. (1988) Linear-eddy model of turbulent scalar transport and mixing. *Combustion Science and Technology* **60**, 391–421.

Kerstein, A. R. (1989) Linear-eddy model of turbulent transport ii. *Combustion and Flame* **75**, 397–413.

Kerstein, A. R. (1990) Linear-eddy model of turbulent transport iii. *Journal of Fluid Mechanics* **216**, 411–435.

Kerstein, A. R., Ashurst, W. and Williams, F. (1988) Field equation for interface propagation in an unsteady homogeneous flow field. *Physical Review A* **37**, 2728–2731.

Menon, S. and Calhoon, W. H. (1996) Subgrid mixing and molecular transport modeling in reacting shear layers. In *Twenty-sixth Symposium (International) on Combustion*, pp. 59–66.

Menon, S., McMurtry, P. and Kerstein, A. (1993) A linear eddy mixing model for les of turbulent combustion. In *LES of Complex Engineering and Geophysical flows* (ed. B. Galerpin and S. Orszag). Cambridge Univ. Press.

Menon, S., McMurtry, P. and Kerstein, A. (1994) A linear eddy subgrid model for turbulent combustion : Application to premixed combustion .

Mishra, D. P., Paul, P. J. and Mukunda, H. S. (1997) *Combustion and Flame* **99**, 379–386.

Smith, T. and Menon, S. (1998) Subgrid combustion modeling for premixed turbulent reacting flows. *AIAA-98-0242* .

"The Effect of Gravity on Turbulent, Premixed Flame Propagation,"

M. Disseau, S. Menon, M. Lal and J. Jagoda
Georgia Institute of Technology
School of Aerospace Engineering
Atlanta, GA 30332

Poster Presentation:

AIAA 36th Aerospace Sciences Meeting and Exhibit

Reno, NV.

January 12-15, 1998.

Overall Objective

improve understanding of turbulent premixed combustion as found in practical combustors

Requirements

generate a turbulent reacting flow in which one can:

- measure flame wrinkles, speed, thickness
- resolve complete range of turbulent scales

without the effect of buoyancy

Approaches

- Couette flow combustor in μg environment
- stirred combustor in μg environment

Couette Combustor

Belts create sustained high levels of turbulence

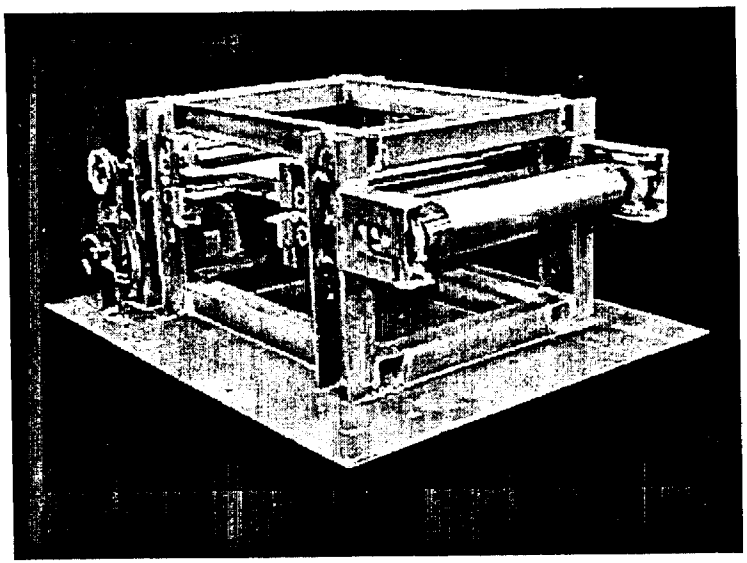

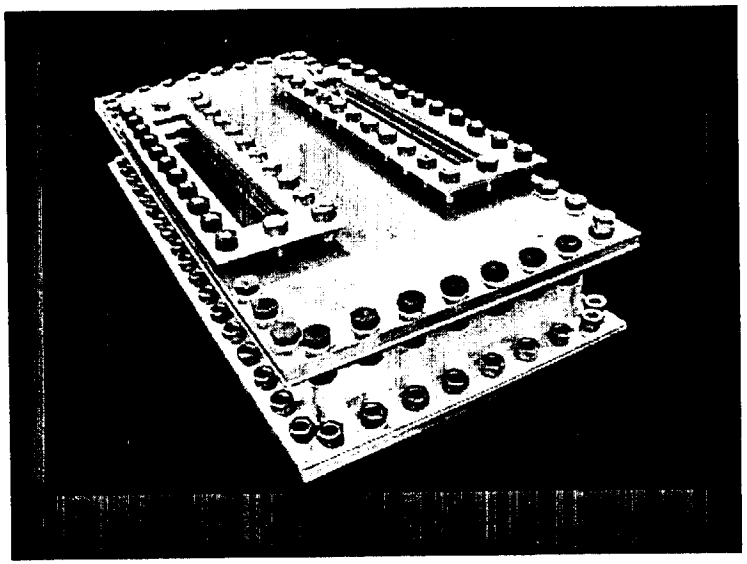

☹ complex

😐 NASA LeRC drop tower

☺ high levels of turbulence

fluctuations ~ 70 cm/sec

☺ sustained constant turbulence

Needs & Approaches

- ➢ practical combustion systems are highly turbulent
- ➢ high turbulence increases wrinkledness
- ➢ high Re_h decrease turbulent scale size - difficult to resolve
- ✓ Couette flow produces high turbulence at relatively low Re_h
- ➢ buoyancy affects low Re_h reacting flows
- ✓ microgravity eliminates buoyancy - requires drop tower

Cold Flow Study Experimental Considerations

- ➢ Compact facility to fit drop tower: is it really Couette Flow?
- ✓ In depth velocity characterization using LDV
- ➢ Identify best regime for hot flow testing:
  - Turbulence level required for wrinkling
  - Associated scales of turbulence
- ✓ Identify best turbulence condition using LDV
- ✓ Determine scale resolution capabilities using PLIF of vapors from acetone drop suspended in Couette flow
- ➢ Is μg still needed ?
- ✓ Track laser generated hot kernel of gas in Couette flow using high speed Schlieren to identify gravity effects

Cold Flow Experimental Setup

$$600 < \mathrm{Re}_h < 30{,}000 \qquad \left(\begin{matrix} 1\,m/sec < U_{belt} < 8\,m/sec \\ 0.01m < h < 0.076m \end{matrix}\right)$$

$$0.15 < \frac{U_{rms}}{S_L} < 3.5 \qquad \left(\begin{matrix} 0.07\,m/sec < U_{rms} < 0.76\,m/sec \\ 0.2\,m/sec < S_L < 0.4\,m/sec \end{matrix}\right)$$

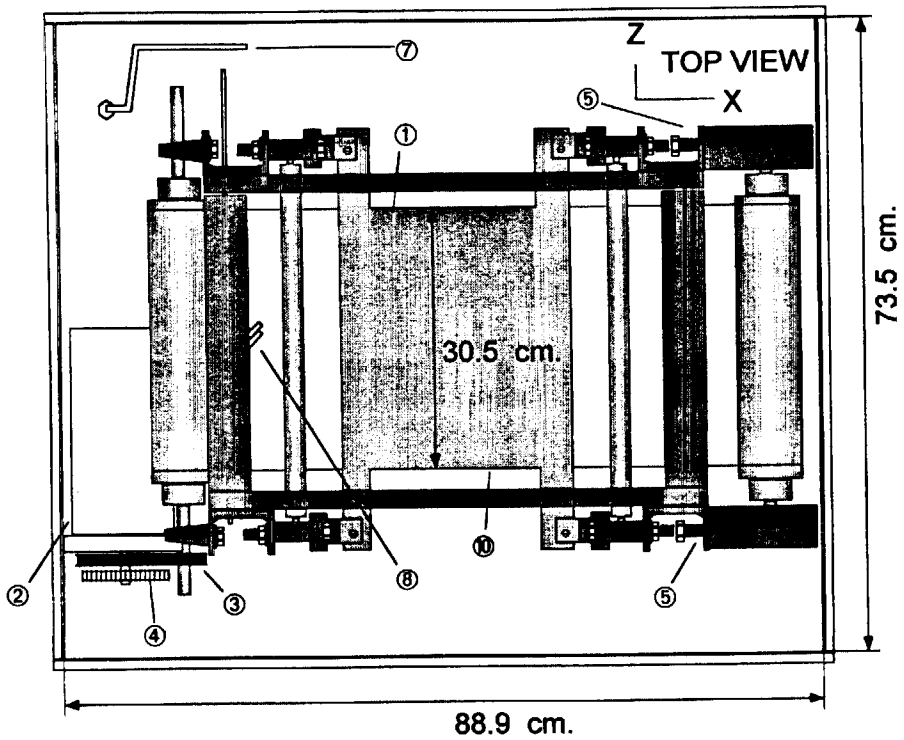

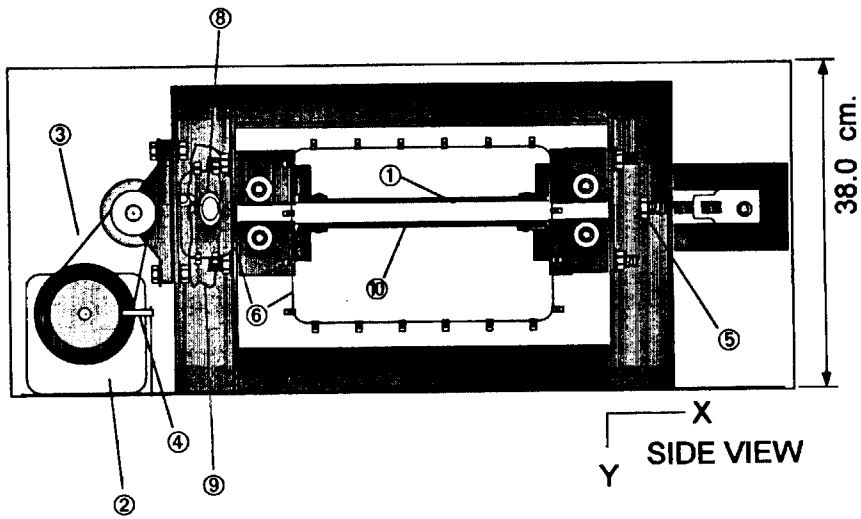

① Mylar belt
② Adjustable DC motor
③ Drive system
④ Magnetic proximity sensor
⑤ Tensioning screws
⑥ Optical access windows
⑦ LDV seeding injection system
⑧ UV Mirror for acetone PLIF
⑨ Optical port for acetone PLIF
⑩ Vibration dampening plates

Cold Flow Results

- velocity field shown to be largely two dimensional

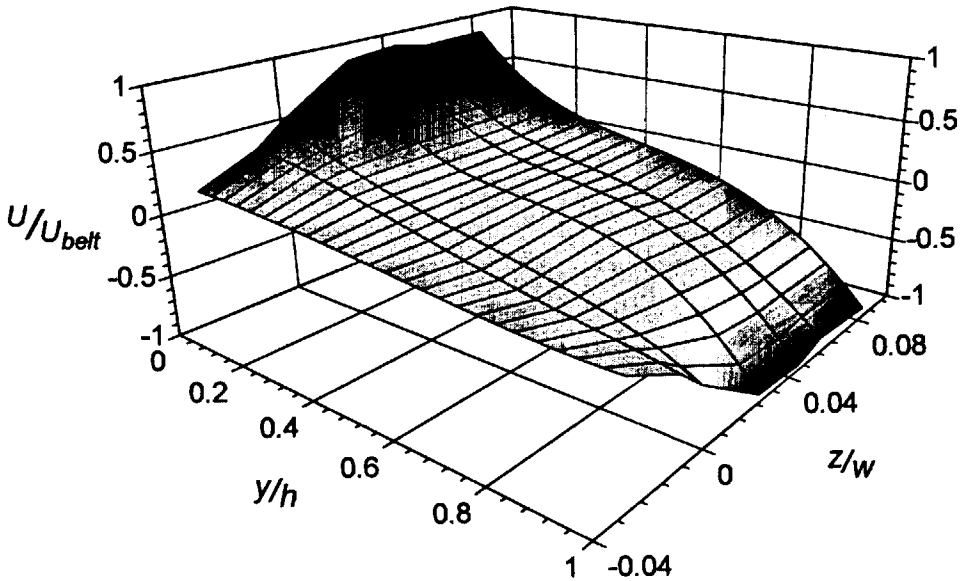

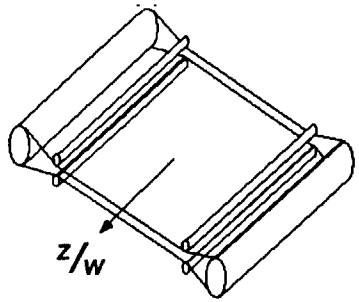

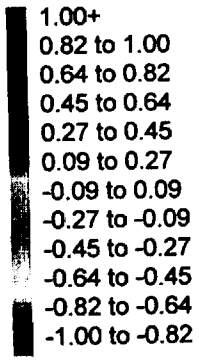

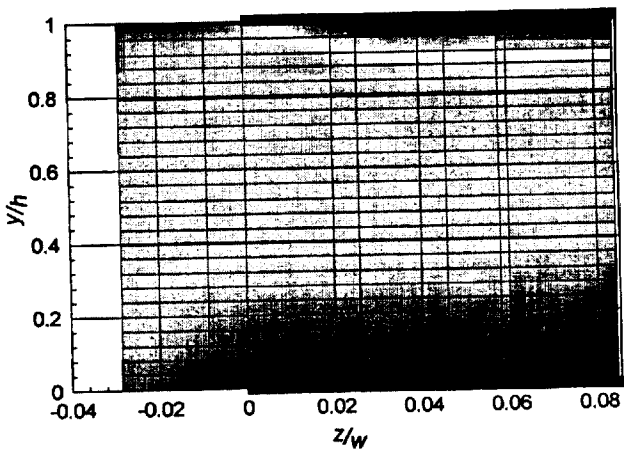

- flow field, fully mapped for different conditions, shows distinctive Couette properties

◇ Re_h = 10,091 , ○ Re_h = 4,366

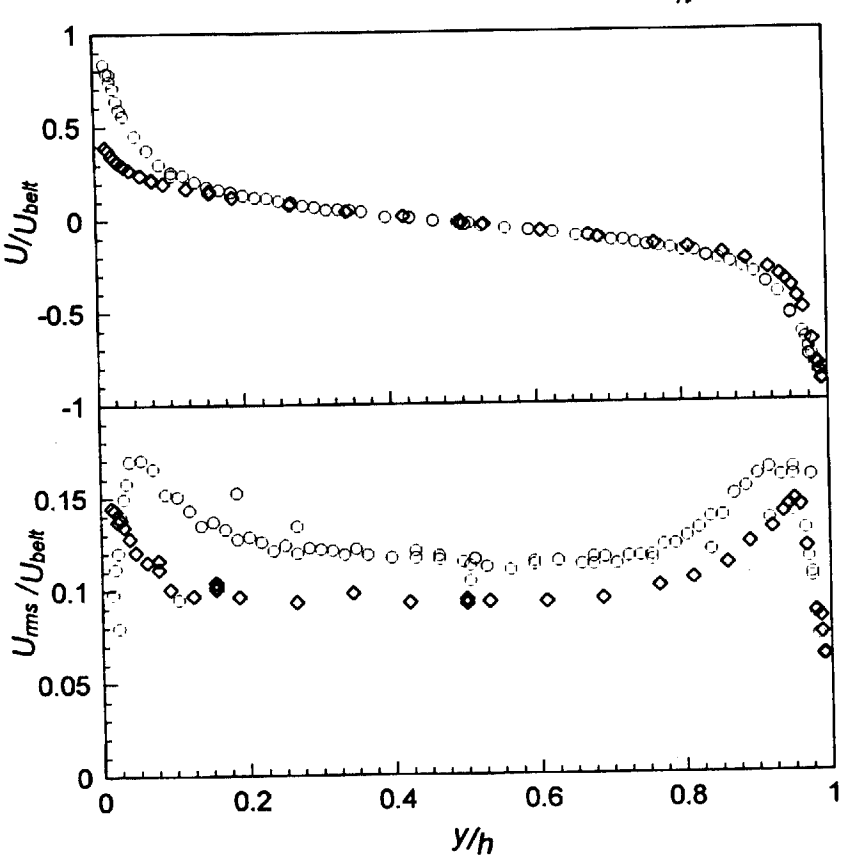

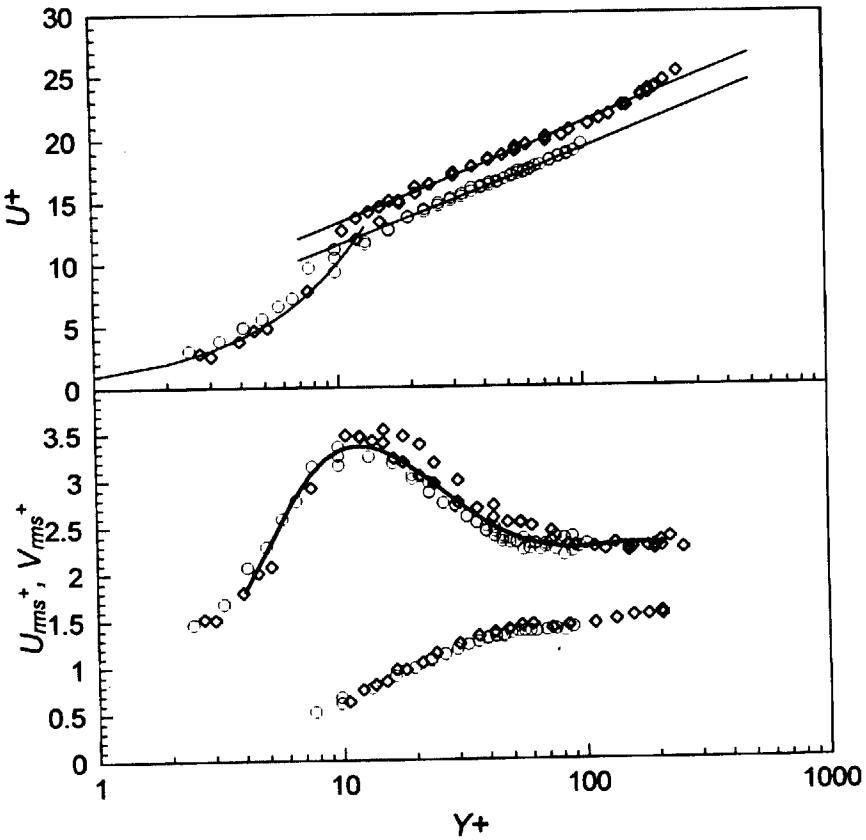

➢2D scalar imaging proven feasible in Couette Flow

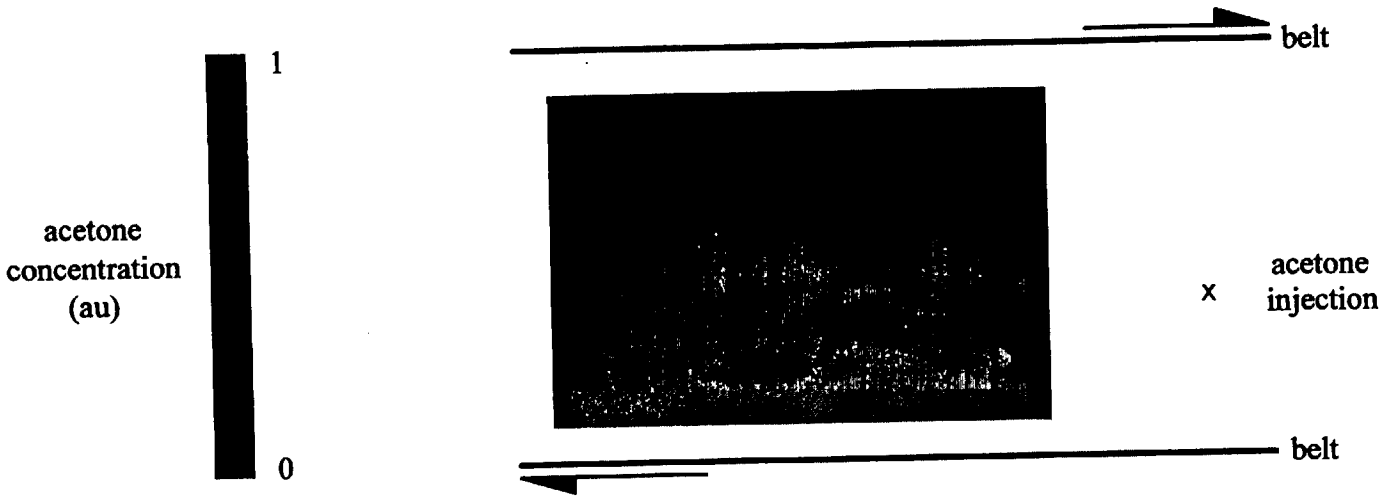

- determined that μ-gravity was still needed
  - Center of hot air kernel, identified by both visually tracing edges on Schlieren image and correlating with intensity profile, shown to rise 5% of *h* in a period of 20 msec

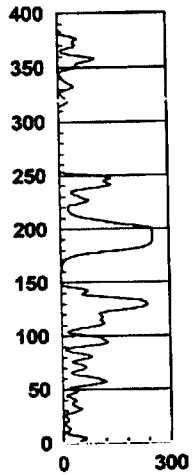

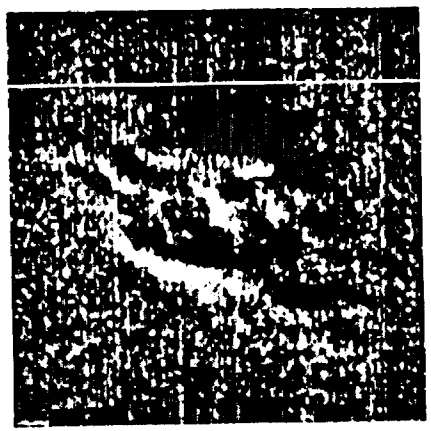

t = 2 ms

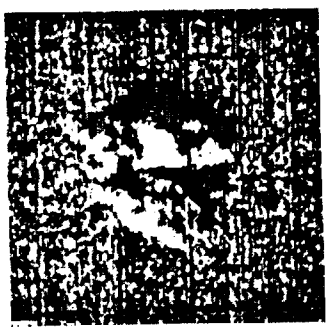

t = 6 ms

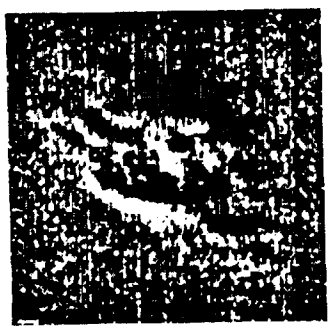

t = 12 ms

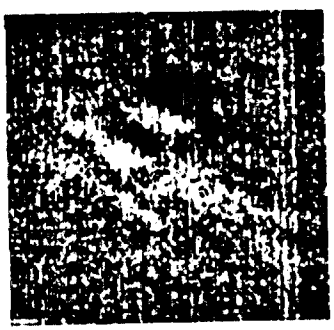

t = 16 ms

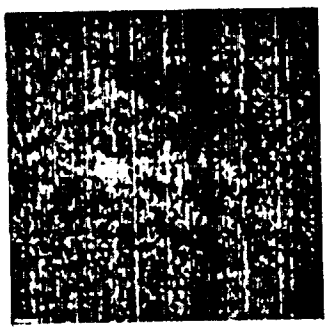

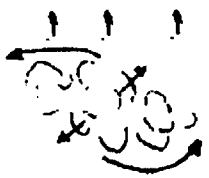

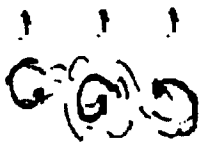

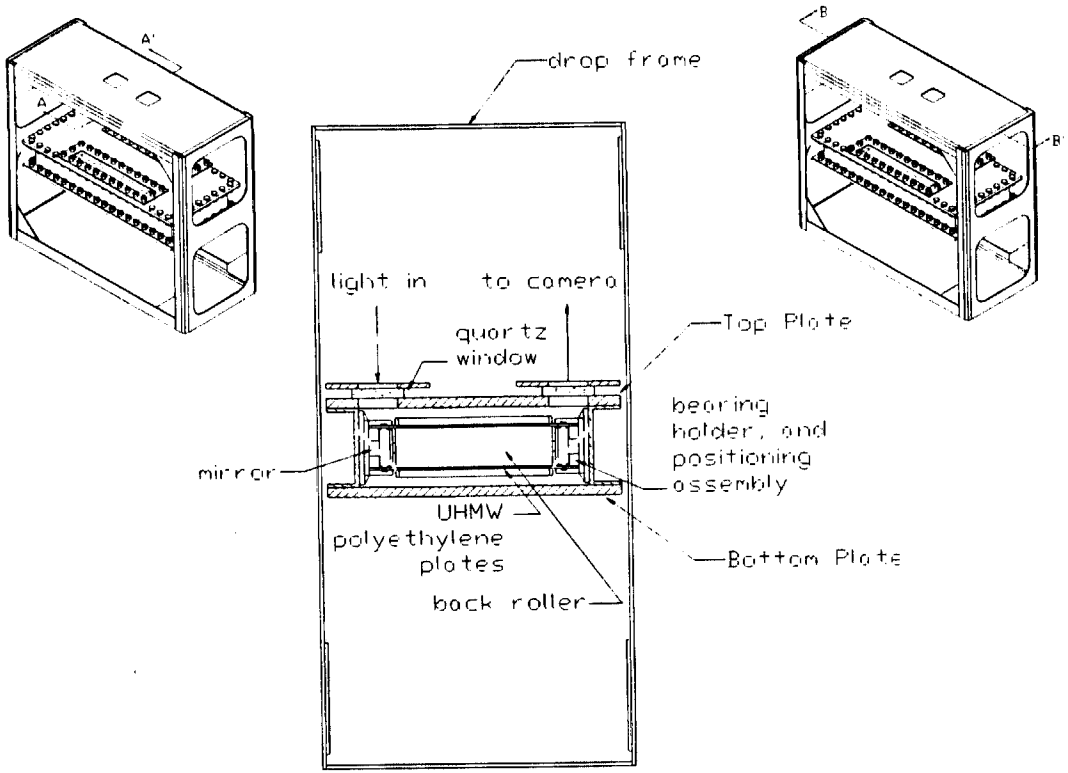

Section A-A'

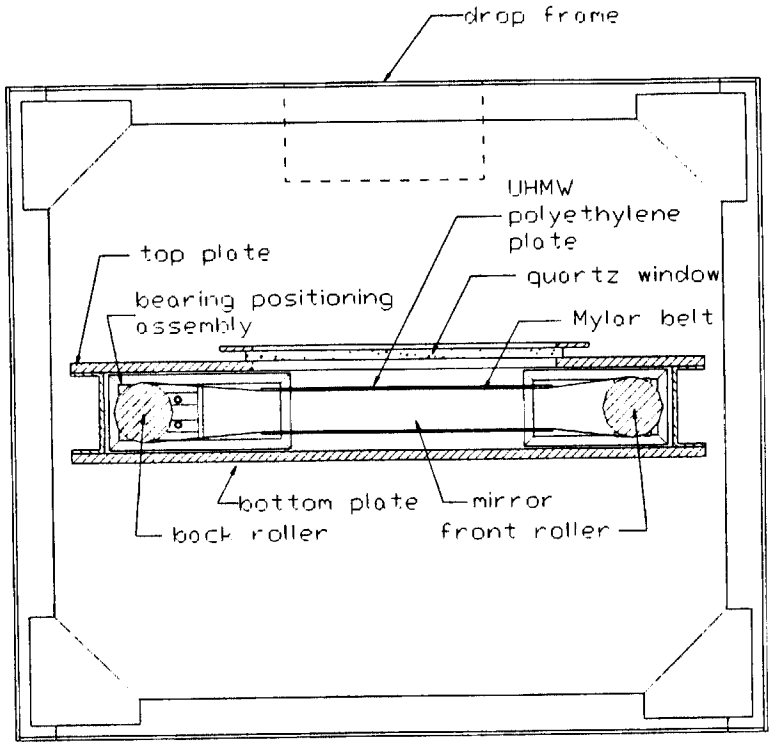

Section B-B'

- Schlieren diagnostics
  - High temporal and spatial resolution 16mm camera
  - Fiberoptic light source on top of tower for space and weight constraints

Stirred Combustor

Stirrer creates isotropically decaying turbulence

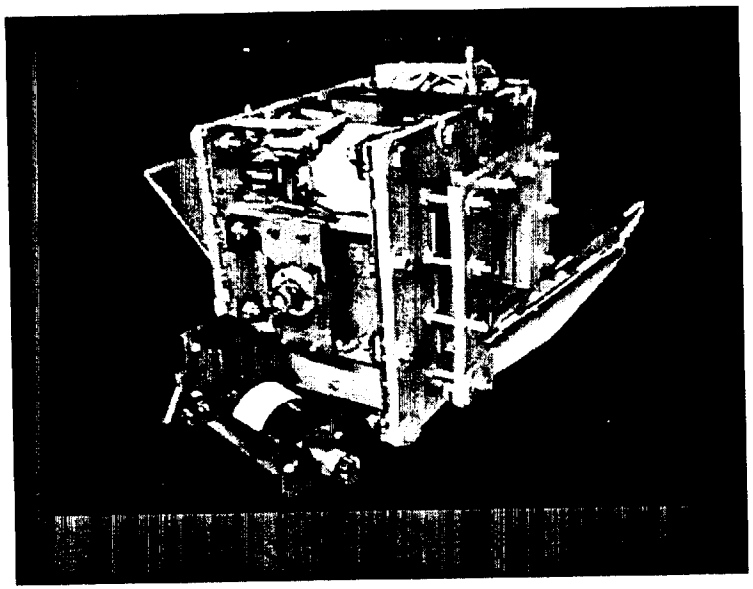

☺ simple

☺ dropped in house

☹ low levels of turbulence

fluctuations ~ 7 cm/sec

☹ decaying turbulence

Needs & Approaches

- ➢ need for facility with short turnaround time
- ✓ simple in-house reduced gravity facility 0.4 sec of ~10^{-3} g or better capability
- ➢ dropped package to be small with minimum umbilicals
- ✓ combustion facility small and light weight
- ✓ stirrer detached before drop
- ✓ diagnostic instrumentation off-board
- ✓ ignition with timing circuit on-board

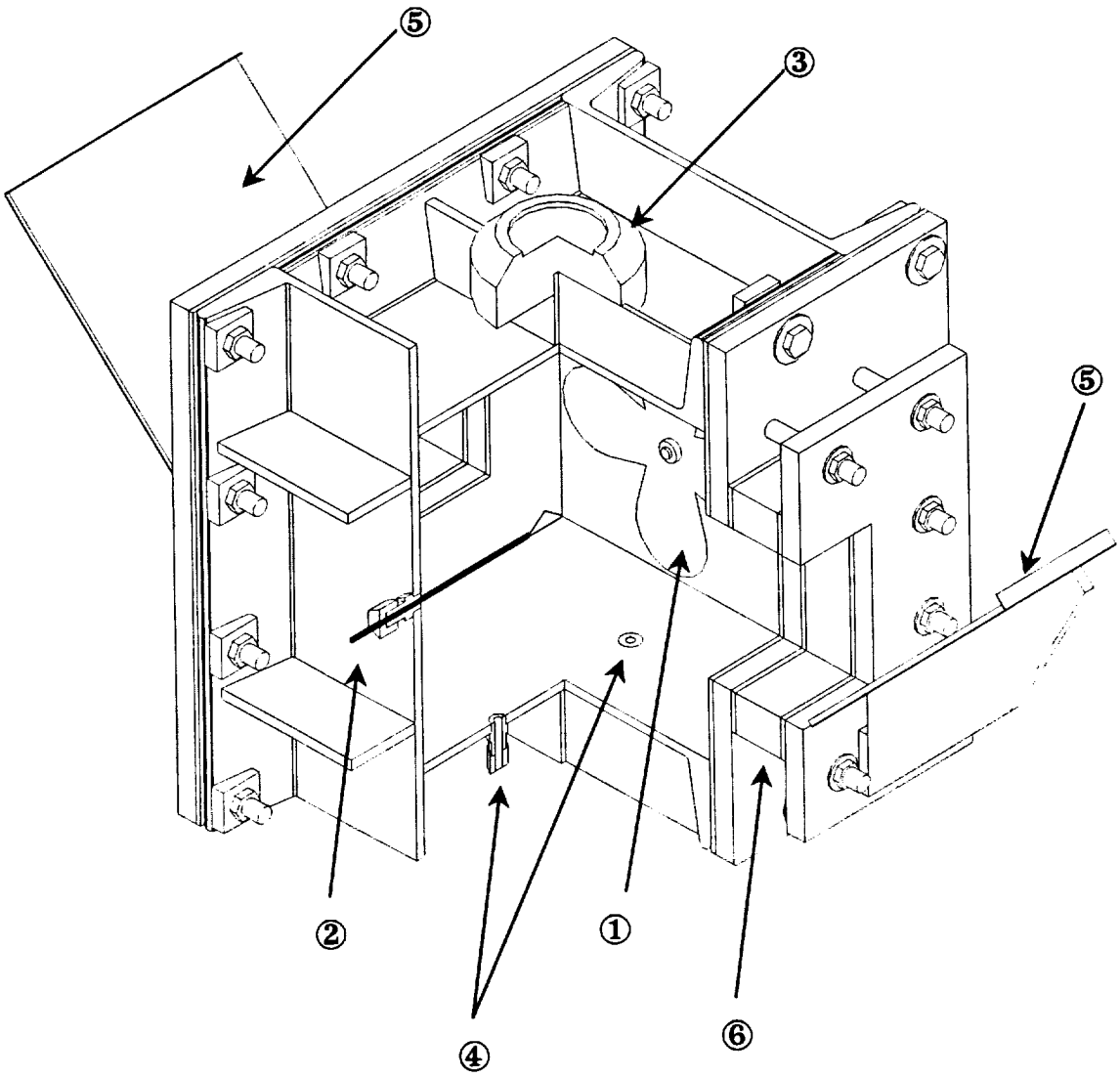

Stirred Combustor

① Stirrer
② Igniter
③ Magnet docking guide
④ Fuel input ports
⑤ Mirrors
⑥ Quartz window

Experimental Setup

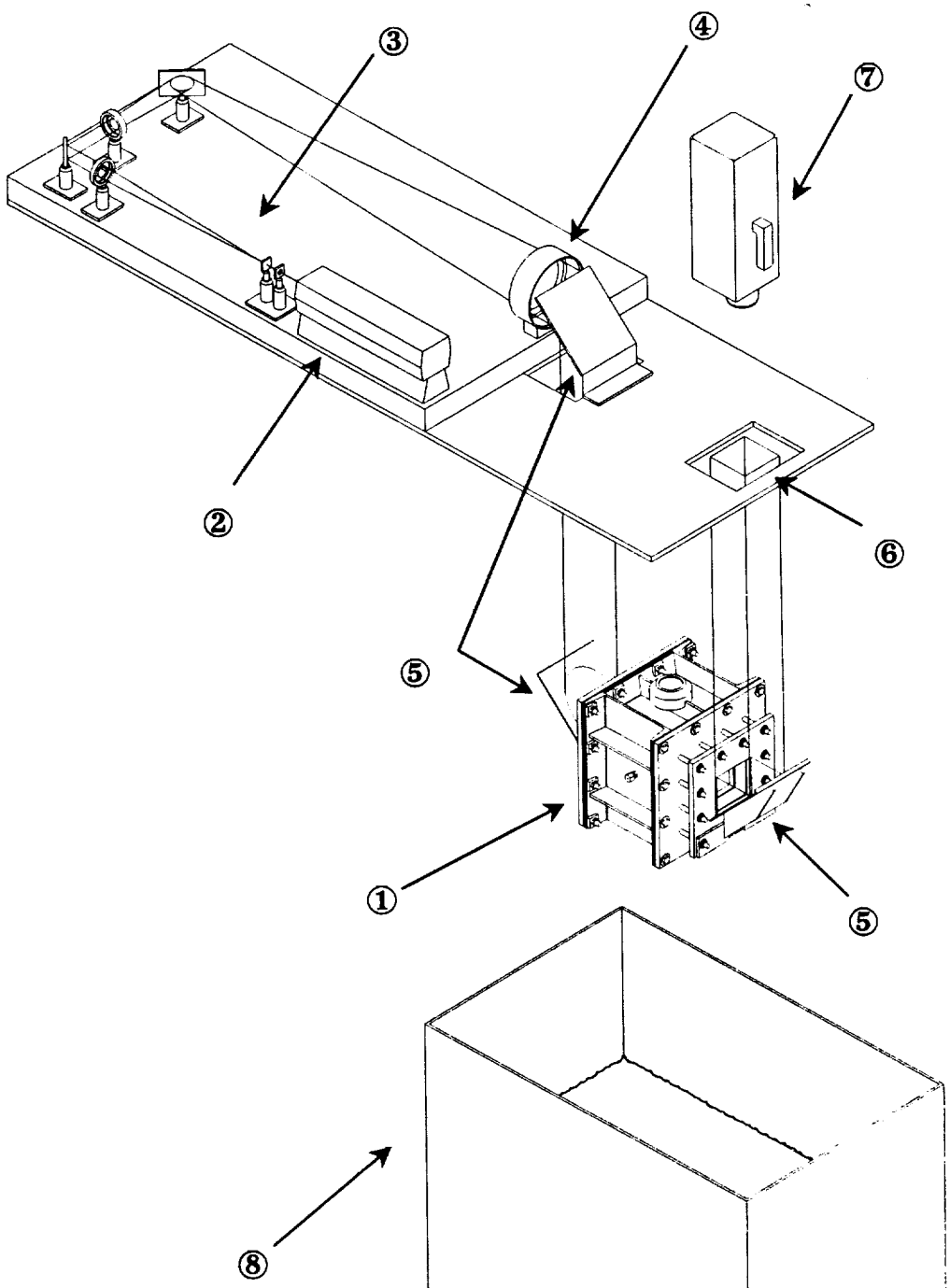

Drop Facilty

① Stirred combustor
② HeNe Laser
③ Expanding optics
④ Collumating lens
⑤ Mirrors
⑥ Screen
⑦ High speed intensified digital camera
⑧ Deceleration box - filled with expanded polystyrene pellets

Typical 1g and μg Results

1g - $\phi = 0.90$ - turbulence level $\cong$ 7 cm/sec

× Denotes ignition location

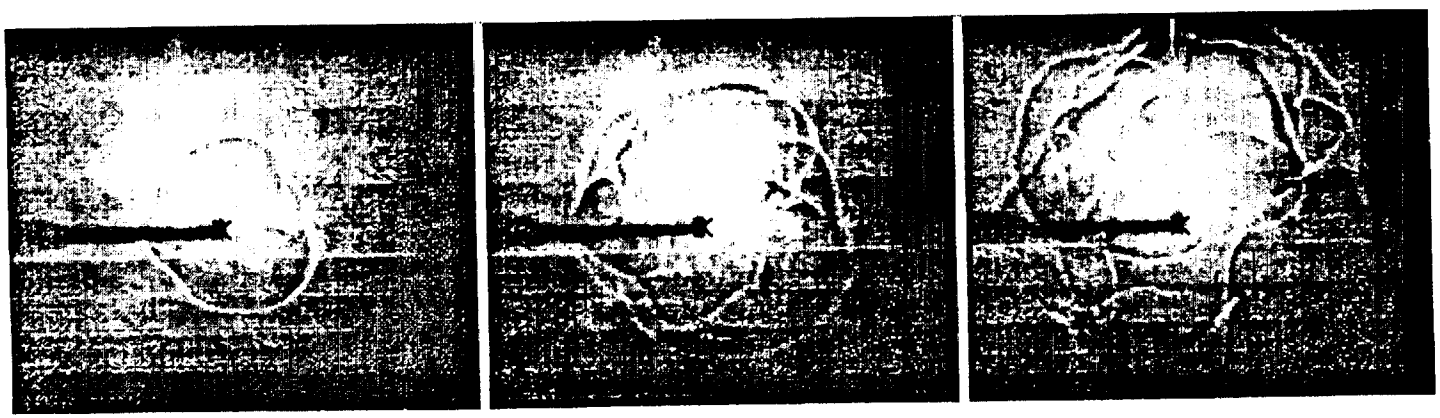

~10^{-3} g or better - $\phi = 0.90$ - turbulence level $\cong$ 7 cm/sec

Preliminary Results

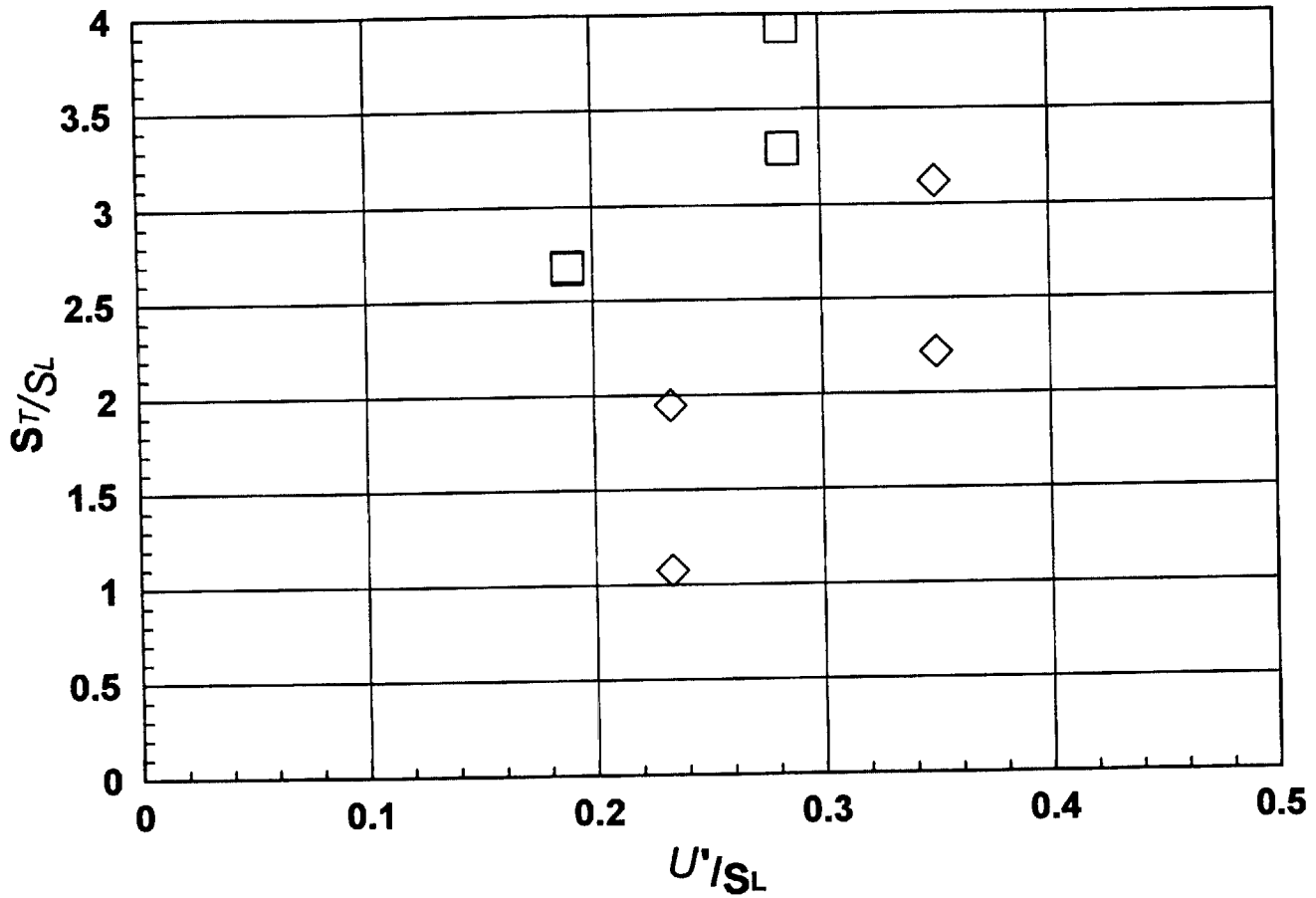

◇ $\phi = 0.8$ □ $\phi = 0.9$ blue = μg red = 1g

Note: The authors would like to warn the readers that these results have yet to be validated.

Current Accomplishments

- Couette Combustor
  - cold flow study completed
  - hot flow facility built and being assembled and tested

- Stirred Combustor
  - 1g and μg results obtained
  - two parameter have been varied in both 1g and μg
    - turbulence intensity
    - stoichiometric ratio
  - initial results show right trend, but further investigation needed for validation of magnitudes

Future Work Plans

- Stirred Combustor
  - acquiring and processing flame velocity, thickness, and wrinkledness data for full test matrix varying:
    - stoichiometry
    - turbulence levels
    - fuel types

    during 1g and μg combustion
- Couette Combustor
  - thoroughly test reacting flow facility and associated diagnostics
  - complete approval process for drops at NASA LeRC
  - acquiring and processing flame velocity, thickness, and wrinkledness data for full test matrix varying:
    - stoichiometry
    - turbulence levels
    - fuel types

    during 1g and μg combustion

AIAA 98-0566

The Effect of Gravity on Turbulent Premixed Flame Propagation

M. Disseau, D. McElhannon, M. Lal,
S. Menon, and J. Jagoda
Georgia Institute of Technology
School of Aerospace Engineering
Atlanta, GA

36th Aerospace Sciences Meeting & Exhibit
January 12–15, 1998 / Reno, NV

AIAA-98-0566

THE EFFECT OF GRAVITY ON TURBULENT, PREMIXED FLAME PROPAGATION

M. Disseau*, D. McElhannon†, M. Lal‡, S. Menon§, and J. Jagoda¶
Georgia Institute of Technology
School of Aerospace Engineering
Atlanta, Georgia

Nomenclature

x, y, z = axis system (see Fig.3)
h = height of channel
L = integral scale
η = Kolmogorov scale
τ_{wall} = wall shear stress
u' = magnitude of large scale turbulent velocity
U_i = ith component of mean velocity
U = x component of mean velocity (i=1)
V = y component of mean velocity (i=2)
$U_{wall} = U_{belt}$ = belt velocity
U_{rms} = x component of root mean square velocity
V_{rms} = y component of root mean square velocity
$U^* = \left(\frac{\tau_{wall}}{\rho}\right)^{1/2}$ = shear or friction velocity
$U_i^+ = \frac{U_i}{U^*}$ = non-dimensional U_i
$y^+ = \frac{yU^*}{\nu}$ = non-dimensional y
$Re_h = U_{belt} h / \nu$
$Re_L = u' L / \nu$
ν = kinematic viscosity
ρ = density

Abstract

Turbulent premixed combustion, while of increased practical importance, is still not fully understood. A serious barrier to further progress in this area lies in the fact that at the high Reynolds numbers encountered in most turbulent reacting flows the Kolmogorov scale is too small to resolve experimentally. When tests at lower Reynolds number are run, the effects of buoyancy become important. The goal of the present study is to remove the effect of buoyancy from two different turbulent combustion facilities by testing them under microgravity condition. One facility uses a stirrer to create isotropic turbulence in a constant volume combustor. I has been dropped in house. The other uses a Couette flow to create sustained turbulence and will be dropped at NASA Lewis. In the work reported here, the isotropic turbulence facility was tested in the GT Aerospace Combustion Laboratory drop tower. Shadowgraph images were obtained under 1g and μg conditions. The effect of buoyancy was seen to essentially disappear under microgravity conditions. Additional test were carried out to determine whether the turbulent flow under investigation in the Couette facility could be influenced by gravity. Such an effect was clearly observed emphasizing the need for future microgravity tests.

Introduction

Recently there has been a rising interest in premixed combustion because of the ability to control local temperatures and thus reduce NO_x emissions. Practical premixed combustors are turbulent, however, and there are still a number of unresolved issues related to turbulent premixed combustion. This means that these types of reacting flows are not accurately predictable[1]. The overall objective of this study is to increase our understanding of turbulent premixed flames by characterizing their behavior. Particular attention is

* Graduate Research Assistant - AIAA Student Member
† Graduate Research Assistant - AIAA Student Member
‡ Post-Doctorate Fellow - AIAA Member
§ Associate Professor - AIAA Member
¶ Professor and Associate Chair for Research and Graduate Studies - AIAA Member

being paid to flame speeds, flame wrinkles, and flame thickness.

A number of important factors have to be considered when studying turbulent reacting flows. First of all it is important to have access to all the scales involved: from L, the integral length scale, to η, the Kolmogorov scale. Their relative magnitudes change with Re_L by the relation

$$L / \eta = (Re_L)^{3/4} \quad (1)$$

For a given experimental flow field the integral length scale is fixed. At the same time experimental resolution considerations limit the smallest Kolmogorov scales that can be measured. As a result only relatively low Reynolds number flows can be fully investigated. However, turbulence in practical devices is usually associated with high Reynolds numbers. An additional problem is encountered when trying to simulate a high Reynolds number reacting flow by one with low Reynolds number. At high Reynolds numbers large scale turbulent stresses are responsible for momentum transport. These stresses, however, can be overwhelmed by buoyancy forces in lower Reynolds number flows.

To remove the effect of buoyancy in a low Reynolds number turbulent reacting flow field a microgravity environment is required. As stated by King[2] microgravity has numerous benefits in combustion science including, but not limited to: increased scalar resolution by allowing the use of larger scales, truly one dimensional geometries, or at least geometries not deformed by buoyancy, and more uniform flames, since buoyancy is temperature dependent, and thus affects different areas of the flame differently. This enables a more accurate study of the combustion processes, which leads to an increased understanding of turbulent combustion.

In this study two approaches where taken to investigate turbulent premixed flames. The first more simple approach, involved using a stirred constant volume combustion vessel. Prior to combustion the stirrer was stopped leaving decaying isotropic turbulence for the flame to propagate in. A high speed shadow-graph was used to visualize the propagating flame front, and these images where subsequently analyzed to obtain flame properties.

This facility, being of moderate size and requiring less than half a second of microgravity, was dropped at the Georgia Tech Aerospace Engineering Combustion Lab in a drop tower facility especially developed for these tests. This drop facility allows continuos high speed shadowgraph images of the experiment to be taken during the drop.

Since this setup can not produce sustained high levels of turbulence a second, more elaborate facility was developed. A Couette flow configuration was selected since it generates a sustained turbulent flow at relatively low Reynolds numbers. A Couette flow is a classical shear layer flow produced between two parallel plates moving in opposite directions, each at a fixed velocity U_{wall}. This flow has the benefit that the shear stress is constant though-out the cross-section, and that the intensity of turbulent fluctuation is constant for most of the cross-section. In addition, such a flow can be generated in the confined space available in the drop tower facility at the NASA Lewis Research Center.

The NASA Lewis 2.2 Second Drop tower was chosen as the site for the microgravity experiments using the Couette facility. This drop tower facility allows a 40.64cm by 96.52cm by 83.82cm experimental rig to experience 2.2 seconds of $\sim 10^{-4}$g followed by 0.2 sec deceleration (at 15 to 30 g). Due to the spatial and temporal restriction imposed by this experimental facility[4] many diagnostic techniques, like laser Doppler velocimetry (LDV) or OH fluorescence, cannot be used to study the flow field. To interpret the results from more basic diagnostic techniques, like Schlieren imaging, it is essential to first understand the non-reacting flow field. Velocity and shear distribution in the cold flow field measured by LDV were previously mapped for different flow conditions[3]. The feasibility of carrying out 2D image mapping of a spreading scalar in the flow was tested by injecting acetone at a point into the flow field and visualizing its spread using passive species planar laser induced fluorescence. In addition, the effect of gravity at the Reynolds numbers under investigation were evaluated by generating a low density plasma in the flow and tracking the resulting density gradient using high speed Schlieren.

This paper will report the capabilities of the new facilities and preliminary microgravity combustion results obtained in the GT drop tower. It will also present the continuing cold flow study results of the Couette facility.

Experimental Facility and Methods

A small drop tower facility was designed and constructed in the Aerospace Engineering Combustion Laboratory on the Georgia Tech campus, see Fig. 1. The experimental device to be dropped is raised to it's starting position using a winch ①. Here it is lined up with an electromagnet ②. Once the magnet is powered, its 175 lbs. lifting capacity, holds the device tightly in place. The lifting cables are then disconnected. Turning off the power to the magnet results in a clean release. At the end of the free-falling drop the device is decelerated in a box filled with expanded polystyrene pellets ③, kindly donated by TechPak, Inc. Also shown in Fig. 1 is the shadowgraph system that is used to track the flame front during the drop. Light from a 0.95mW HeNe laser ④ is expanded and collimated by a set of lenses ⑤, into a 4 inch beam. This beam is sent down, through the box, and then back up, using 3 mirrors ⑥, one fixed on the drop tower and two attached to the dropping facility. The beam is then imaged onto a screen ⑦. A Kodak Ektapro intensified digital camera ⑧ running at 1000 frames per seconds records the images. These images can then be downloaded to a PC where they are enhanced and processed to obtain flame speeds, shapes, and thickness.

A stirred constant volume combustion chamber, which is used in the GT drop tower, is shown in Fig. 2. It is

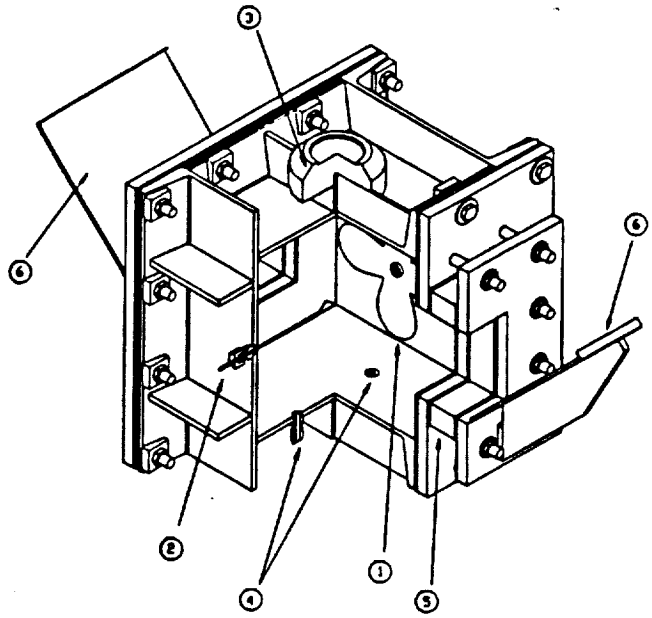

Figure 2 - Stirred Constant Volume Combustion Chamber

fabricated out of steel and designed to withstand pressures up to 150 psi. A stirrer ①, which consists of a 6 inch in diameter 4 blade fan, is mounted on one side. It is supported by two bearings, and sealed with an o-ring. A Lovejoy connector is attached to the end of the drive shaft to allow, not only easy alignment with the motor, but also a quick disconnect. Two quartz windows ⑤ allow optical access to the turbulent flame in the chamber. The two mirror ⑥ attached to the device are part of the aforementioned shadow-

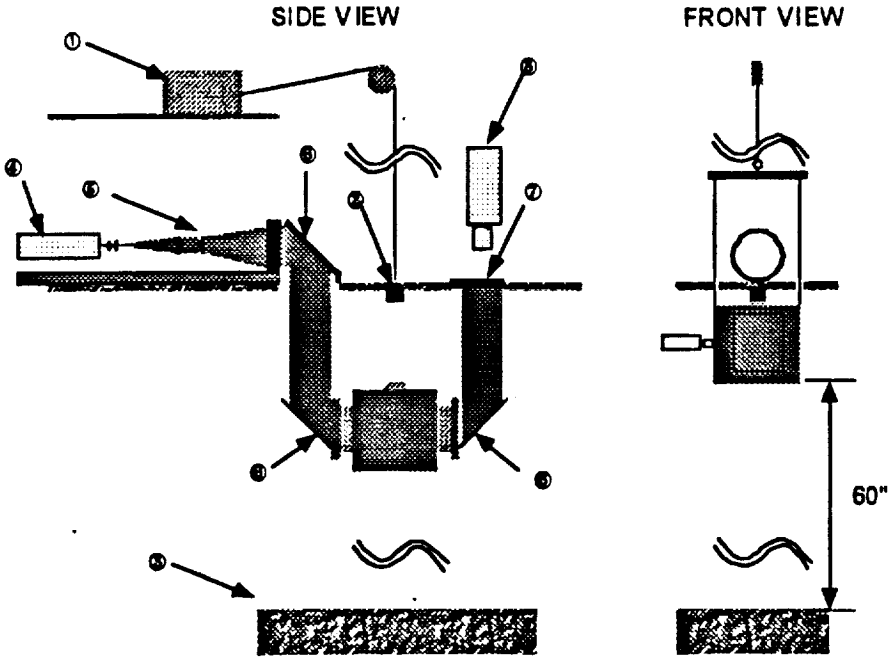

Figure 1 - GT Aerospace Engineering Combustion Laboratory's Drop Tower Facility

graph system. The stirred reactor is filled with a combustible mixture through a port located at the bottom ④. The partial pressure method was used to calculate the stoichiometry of the mixture. A home made spark plug ⑦ and its ignition system are located on the side opposite the stirrer.

Because the electromagnet does not release the experiment immediately after its power has been turned off, switching off the magnet could not be used to trigger the igniter. Instead, a hall effect sensor, positioned on the magnet docking guide ⑧, senses the instant the experiment is separated from the electromagnet, and triggers a pulse. After a 50 msec delay, during which the dropping experiment has ample time to stabilize, a pulse triggers the ignition transformer. A small neon light DC transformer connected to the home made spark plug is used to ignite the flammable mixture. It is powered by two 9 volts DC batteries and provides 1500 volts AC at 20KHz and 5 mA, more than enough to created an ignition spark.

A Kistler K-BEAM capacitive accelerometer is attached to the device to be able to monitor the degree of microgravity experienced by the combustion process. This accelerometer has a range of ± 1g with a sensitivity of 1959 $^{mV}/_{g}$ and can survive a maximum of ± 40g. The manufacturer's guaranteed precision, around 0 g, is $\pm 3 \times 10^{-2} g$.

Once the device is in position the overall drop procedure consist of turning on the ignition circuit first. This prevents a spark generated by turning on the circuit from igniting the flammable mixture prematurely. Next the methane is injected in the chamber, and the gasses are given time to mix. The pressure in the reactor is monitored by a pressure gauge and excess pressure is relieved. The external piping are then disconnected. The motor is connected to the shaft and turned on to the desired speed. After the flammable mixture has been stirred for about one minute the motor is disconnected. Then the camera is turned on, and the power to the electromagnet is turned off. The ignition circuit ignites the mixture as discussed above. After the run the combustion device is retrieved, purged, checked for possible problems, hoisted back up in position, and prepared for a new run.

The Couette device used in this study is shown in Fig. 3. The device consists of a continuos Mylar belt ① which provides the "two parallel plates" moving in opposite directions. The belt runs over a series of rollers, two of which drive the belt while four are used to adjust the spacing in the test section. A set of plates is positioned on the outside of the belt to eliminate possible vibration of the belt. These vibrations had been found to cause higher levels of turbulence with peaks in the frequency spectrum. The belt is driven by an adjustable DC motor ② connected to the drive roller by a set of pulleys and a v-belt ③. The rotational speed of the motor is sensed by a magnetic proximity sensor ④. Knowing the pulley ratio and the roller diameter, the speed of the belt can easily be determined. To prevent belt walking and to ease the insertion of a new belt, a set of tensioning screws ⑤ help position the far roller. The Reynolds number for the device, Re_h, can be changed by either changing the speed of the belt, U_{belt}, or by changing the belt spacing, h. The device is surrounded by a Plexiglas box to prevent any external influence on the flow without disturbing optical access to the experiment.

Before the Couette flow could be used to study turbulent flame propagation under microgravity it had to be established that the effects of gravity could survive in this turbulent flow field. To this end a gas

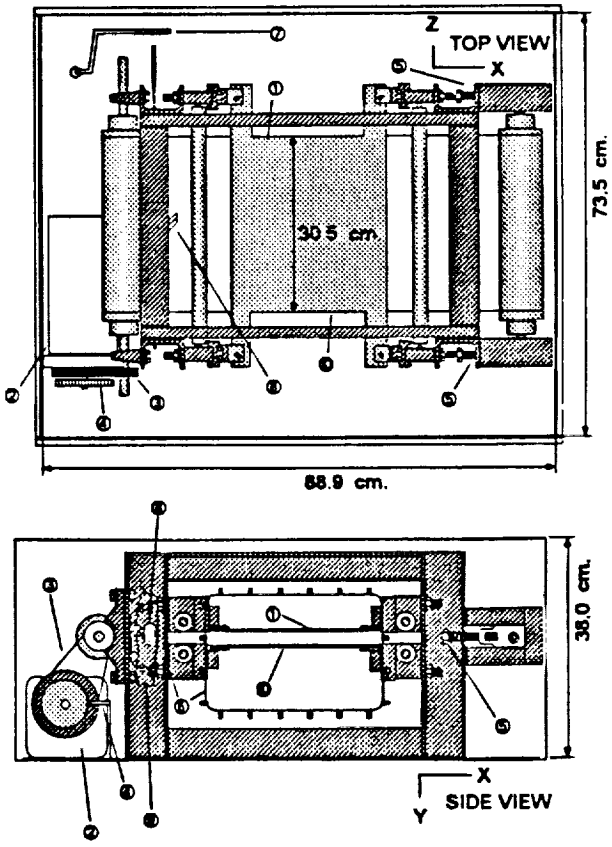

Figure 3- Current setup of the experimental device. Call-outs described in the text.

of lower density was introduced into the flow and its interface with heavier air was tracked as it progressed though the flow. Helium was injected through a hypodermic needle along the centerline of the Couette flow. The needle was equipped with micro-machined holes on four sides to limit the directional biasing associated with one hole injection. However the strong shear of the Couette flow, along with the high diffusivity of the helium caused the gas to mix with air almost instantaneously. No clearly visible helium-air interface could, therefore, be observed in these test.

Better results were obtained when a density gradient was produced by focusing a laser beam into a small volume at a point located along the centerline between the two belts. The energy furnished by the laser was sufficient to ionize the air and thus form a spark. The propagation of this point source of hot gases was then tracked with the help of a high speed Schlieren system. The laser used to generate the spark is a 300mJ per pulse tunable Lambda Physik excimer laser running with KrF, to produce a laser pulse at a wavelength of 248nm. This laser was chosen because it not only offered enough power per pulse to ionize the air, but being in the UV, scattered light did not affect the Schlieren. The Schlieren light source was a .95 mW HeNe laser. The beam stop was an opaque dot, 1mm in diameter, to avoid directional biasing. Schlieren images were captured using a Kodak Ektapro intensified digital camera running at 1000 frames per second.

Results and Discussion

Previously Reported Results

Previously reported data for this facility have proven the velocity flow field to be two dimensional[3]. Therefore, the analysis of subsequent data is performed using centerline profiles. Figures 4 and 5 show dimensional and non-dimensional mean and turbulent profiles at two different Reynolds numbers, respectively. Figure 4 clearly indicates constant levels of turbulence throughout most of the flow field, while the data in Fig. 5 clearly shows the expected behavior for a wall bounded shear flow. The flow can be divided into two regions[5], the viscous sublayer ($y^+<5$), and the inertial sublayer ($30<y^+<1000$). The flow correlates well with the linear behavior at the wall in the viscous sublayer. The logarithmic behavior in the inertial sublayer is also clearly present. However the data at different Reynolds numbers do not exactly collapse into one single line when non dimensionalized, as predicted by theory and seen by others. This is probably due to the smaller dimensions and re-circulating nature of the present device. Figure 5 also shows U_{rms}^+ and V_{rms}^+ as functions of non-dimensional distance from the belt. As expected, U_{rms}^+ has a turbulence peak close to the wall before it reaches a uniform distribution in the core, and V_{rms}^+ gradually increases to a uniform distribution in the core. Most of this information was presented in the reference[3].

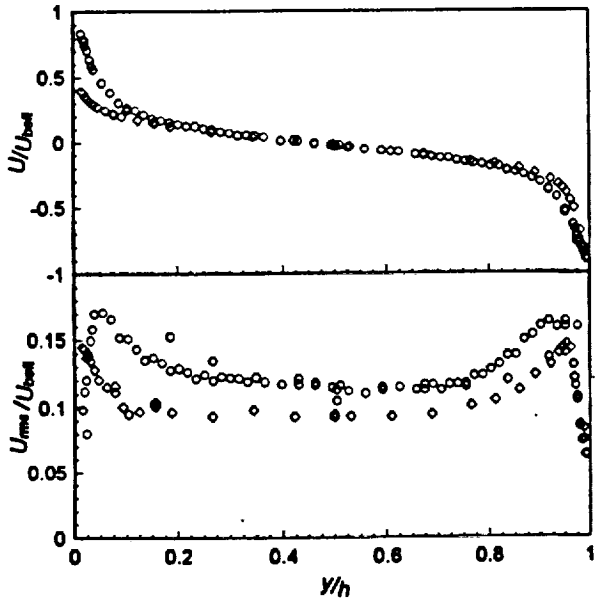

Figure 4 - Velocity distribution across the flow ◇ Re_h = 10,091, ○ Re_h = 4,366.

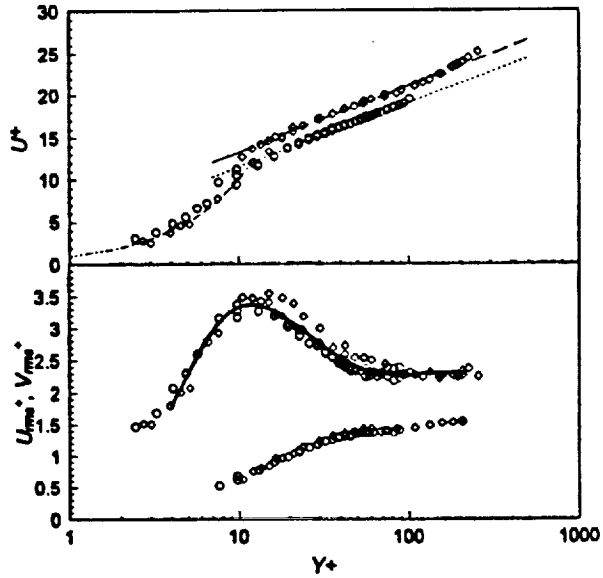

Figure 5 - Non-dimensionalized velocity distribution across the flow ◇ Re_h = 10,091, ○ Re_h = 4,366.

NASA Conference Publication 10194

Fourth International Microgravity Combustion Workshop

Proceedings of a workshop sponsored by
NASA Headquarters
Microgravity Science and Applications Division;
organized by the Microgravity Combustion Discipline Working Group;
and hosted by NASA Lewis Research Center,
Microgravity Science Division;
held at the Cleveland Sheraton City Centre Hotel
May 19–21, 1997

National Aeronautics and
Space Administration

Office of Management

**Scientific and Technical
Information Program**

1997

TURBULENT PREMIXED FLAME PROPAGATION IN MICROGRAVITY

S. MENON*, M. Dissean+, V. K. Chakravarthy+, and J. Jagoda*
Georgia Institute of Technology
School of Aerospace Engineering
Atlanta, Georgia

Introduction

The structure and propagation characteristics of turbulent premixed flames have been investigated for some time. For example, the turbulent flame speed has been typically estimated in terms of the laminar flame speed S_L and the local turbulence intensity u'. However, the exact form of the functional relation: $u_T/S_L = f(S_L, u')$ has not yet been determined although various models have been proposed (ref. 1). A key reason for this uncertainty is the inability to experimentally resolve all scales of motion that could contribute to the wrinkling of the premixed flame and hence, to an increase the effective burn speed. In a typical high Reynolds number flow, the small scales are impossible to resolve in an experiment (e.g., using LDV). However, turbulent fluctuations at the small scales (e.g., Kolmogorov scale) could be resolved if the Reynolds number is reduced (for example, by reducing the flow velocity). A flow field that provides sustained turbulent flow in a relatively low Reynolds number is Couette flow. It has been shown in past studies that stationary turbulent Couette flow could be achieved at Reynolds number as low as 1800. Once combustion is included, however, the large-scale turbulent stresses responsible for momentum transport can be overwhelmed by the buoyant stresses in 1g. Since this phenomenon is not present in realistic high Reynolds number devices, a microgravity environment is required to suppress the buoyancy effects while still maintaining reasonable operating pressure, temperature and observable scales at all sizes.

This paper summarizes the results obtained so far in this study. Both experimental and numerical studies are being performed to investigate turbulent premixed flames. The experiments so far have focused on characterizing the turbulent flow field in this new Couette flow facility. A major reason is that the current device has been designed to fit inside the NASA Lewis 2.2 s drop tower rig (ref. 2). As a result, this facility is much smaller than the facilities used in the past (ref. 1-3). For example, the current length to gap ratio is 14 compared to 30-158 of the earlier devices (refs. 3-7). In addition, the current device operates in a closed loop, i.e. turbulent flow is forced to reenter the test section whereas earlier devices transition the flow from laminar to turbulent. Thus, it is essential to quantify the turbulence properties of this device.

The numerical study employs large-eddy simulation (LES) technique. In this approach, all scales of motion larger than the grid resolution is captured in the simulation without modeling and only scales smaller than the grid are modeled. A localized dynamic subgrid model for the subgrid kinetic energy is used in this study to model the subgrid stresses. However, since the flame thickness is much smaller than the typical grid resolution employed in LES, conventional LES of species equations will not capture the true features of the flame. Here, a new subgrid combustion methodology has been developed to simulate the burning process within the small scales (refs. 8,9). In this approach, the local laminar burning, wrinkling due to the local subgrid turbulence and volumetric expansion due to heat release are explicitly included within the subgrid scales. This approach also predicts the local (turbulent) burn speed provided the local turbulent field is known. The experimental data on the turbulence provides the required information to (hopefully) accurately evaluate the propagation characteristics of turbulent premixed flames using this simulation approach. Thus, the present study combines the capabilities of both experimental and numerical methods to investigate premixed flames.

Experimental Facility

The experimental device shown in Fig. 1 consists of a continuos Mylar belt moving in opposite directions over a series of rollers, two of which drive the belt while four are used to adjust the spacing in the test section. It is driven by an adjustable DC motor connected to the drive roller by a set of pulleys and a v-belt. To prevent belt walking and to ease the insertion of a new

Work funded by NASA Grant NAG3-1610
* Professor
+ Graduate Research Assistant

belt, a set of tensioning screws help position the far roller. Two plates are placed on the outside of the belt to reduce belt vibration. The Reynolds number for the device, Re_h, can be changed by either changing the speed of the belt, U_{belt}, or by changing the belt spacing, h. The device is surrounded by a Plexiglas box to prevent any external influence on the flow without disturbing optical access to the experiment.

The velocity flow field was mapped with a TSI 9100-7 two component laser Doppler velocimeter, which uses the 514.5 nm and 488 nm wavelengths of an 5 watt Ar^+ laser. After going through an expander and focusing using a 14 mm aperture lens, with a 750 mm focus, the probe volume was 0.13 mm in diameter and 1.3 mm long. The system was used in back scatter mode. The output signals were analyzed by a TSI IFA656 digital burst correlator, which can cope with lower signal to noise ratios than a traditional counter. One beam of each pair was frequency shifted by a Bragg cell to allow for measurement of negative velocities. Sub-micron TiO_2 particles were used to seed the flow. After passing though a fluidized bed, TiO_2 laden air is inserted into the device through a tube which produces a cloud of seed around the moving belts that is then entrained into the flow. This eliminates the possibility of biasing the data with artificial seeding velocities. FIND software, from TSI, was then used to statistically process the 50,000 samples obtained at each location. Data was velocity bias corrected according to the algorithm provided in FIND.

Numerical Method

A modified version of a subgrid model proposed earlier (refs. 8,9) is used in the present LES. The kinematic structure of premixed flames was investigated earlier (ref. 9). The model is extended here to include heat release. Within each LES cell, a representative one-dimensional domain is used to stochastically represent a local ray through the flame brush. The G-equation flame propagation model (refs. 9,10) is solved on this 1D line. The G-equation allows for propagation of the flame as a sharp front (negligible flame thickness) corresponding to a case of fast chemical kinetics (ref. 10). The effect of turbulent eddies on the species field is modeled stochastically using a scalar rearrangement process on segments chosen on the one-dimensional domain. More details is given elsewhere (refs. 9-12).

For heat release, the temperature is assumed to be a linear function of G. The obvious implication is that the transport and diffusive properties of the reactive scalar and the thermal energy are closely correlated (corresponding to a often used physical assumption of a constant Lewis number) in the subgrid domain. Transport of species and heat across LES cells is modeled using a "splicing" procedure (refs. 11,12). The thermodynamic pressure in each of the LES cells is assumed to be constant since it is well known that the second order reaction mechanisms do not cause a change in thermodynamic pressure across the flame. It is further assumed that the thermodynamic pressure is gradient free through out the physical domain. Any acoustic disturbance created by the flame is assumed at have small amplitude (zero Mach number approximation) and is communicated at infinite speed through out the domain. The LES-resolved temperature field can be obtained by filtering the local subgrid temperature fields. However, this procedure can lead to sharp discontinuity and hence, to numerical instability. Therefore, to locally smooth the LES-resolved temperature field (which is needed to close the LES equations), a diffusion equation for temperature is solved on the LES-grid at each LES time step using the subgrid-aveeraged field as an initial condition.

The numerical method is a fourth-order accurate finite-difference scheme in space and second order accurate in time. Since the thermodynamic pressure is constant, a zero Mach number version of the fractional step method (ref. 13) is used to integrate the LES equations.

Results and Discussion

Experimental Results: Figures 2a and 2b shows respectively, the mean and rms velocity distribution in the flow field. It can be seen that the profiles are not totally anti-symmetric. It was determined that this was due to an asymmetry in the end regions where the drive rollers are located and could not be avoided. However, this asymmetry did not appear to have any significant effect on the rms velocity. More importantly, the data shows a nearly constant rms fluctuations in the core which is of interest here. Figure 3 shows U^+ as a function of y^+. The data shows the expected behavior for a wall bounded shear flow. Both the viscous sublayer ($y^+ < 5$) and the inertial sublayer ($30 < y^+ < 1000$) can be clearly observed. However, due to the noted asymmetry, the data at different Reynolds numbers do not exactly collapse as predicted by theory.

Figure 4 compares the measured streamwise fluctuations in various devices. The peak location in the present facility is in good agreement with earlier data but turbulence intensity magnitude is somewhat higher. This is probably due to the continuous nature of the flow and the compact nature of the device and is unavoidable here. Figure 5 compares the skin friction coefficient measured in this device to those in earlier devices. Deviations from the more ideal Couette flow are, once again, probably due to the recirculating nature of the flow in this compact device.

However, these results clearly establish that stationary turbulence with nearly constant turbulent fluctuations in the core of the flow exists in the present facility. Furthermore, the overall nature of the flow is in good agreement with theory and past studies in similar devices.

The experimental data can be utilized to estimate the resolved scales of motion. Using the belt spacing, h = 2.54 cm as the typical integral length, the Kolmogorov scale, η, is estimated in the core to be 0.23 mm for the Re_h = 4,366 case and 0.13 mm for the Re_h = 10,091 case. For the LDV system, the seed particle size is sub-micron, much smaller than η, while the LDV probe volume is of the order of η. This implies that the smallest scale can be nearly resolved. However, due to flow motion, the residence time inside the probe volume is a more accurate measure of the resolution. The velocity of the scale can be estimated by using the relation between Kolmogorov velocity scale and the magnitude of turbulent velocity: $u'/v = (Re_L)^{1/4}$. Based on the probe volume, a residence time and, therefore, a frequency 590Hz for the Re_h = 4,366 case and 1,030Hz for the Re_h = 10,091 case is estimated. This means that the data rate for the LDV should be greater than 2,060Hz to resolve Kolmogorov scales temporally. Because of the high noise levels in the system, this is difficult to achieve. Therefore, the best estimate is that the resolution is of the order of η. or larger.

These studies have clearly established the turbulent flow properties in this facility. Although hot flow studies cannot be carried out using this device (an identical hot flow facility is currently under construction), a preliminary study of buoyancy was carried out by using an excimer laser to ionize a small region of air in the flow. This produced a hot gas kernel that propagated into the flow. Using high speed Schlieren imaging, it was possible to observe the effects of shear caused by the Couette flow and the apparent distortion caused by buoyant stresses. This preliminary study suggested that buoyant effects should be observed in the actual reacting flow case. This is the focus of current study and the results will be reported in the near future.

Numerical Results: LES of non-reacting and reacting Couette flow corresponding to a Reynolds number (as defined earlier) of 10,000 have been conducted on a 49x49x33 grid. The mean velocity profile is compared with the corresponding result from the experiment in Fig 6. The LES profile is anti symmetric about the centerline whereas (as noted) there is some asymmetry in the experimental data. The rms velocity in the streamwise direction is compared to the experimental data in Fig. 7. The experiment indicates a peak in urms more closer to the wall than obtained in the LES. Assuming that the experimental results in such close vicinity of the moving belt are free of any error, one might be able to capture the peak in urms by increasing the near wall resolution. However, some uncertainty in the rms estimate is inevitable in the LES, since, the unresolved part of the turbulent kinetic energy (grid dependent) is captured only approximately as the subgrid kinetic energy. In any event, the propagation of the flame in the central core region with constant rms fluctuations is of interest in this study and this feature is captured here. Increase in the resolution in the core region captures the constant rms region more accurately, as shown earlier (ref. 9).

For reacting flows, the grid is rapidly stretched out from the wall but in the core region (mid 78%) a uniform grid is used to allow proper resolution of the propagating flame ball. The grid width is 10η in the core region and the simulation is stopped once the flame crosses this region All simulations described here are for a reference u'/S_L of 4.0. Temperature rise factors of 4 and 7 were studied. Comparison with a model simulation using Yakhot's model for the turbulent flame speed (ref. 9) were also carried out to evaluate the predictions by the new subgrid LES method. Some representative results are reported below.

Five contours corresponding to equally spaced values of G between 0 and 1 are shown for each case in Fig. 8. As can be seen, the subgrid approach tends to capture the thin premixed flame quite well (usually within 2-3 grid points) when compared to conventional LES (i.e., solving the G-equation with the LES equations). As seen earlier (ref. 9), in the conventional approach significant numerical diffusion of the scalar gradients in G occurs and overwhelms the burning rate. This error is expected in all simulations that evolve the species equations on the LES grid using finite difference or finite volume schemes. Flame surface tracking methods can be implemented for cold flames but cause problems when heat release is added. The flame generates velocities normal to the flame surface because of the expansion behind it. The vertical currents are however curtailed by the presence of the wall, so the flow velocity tends to increase greatly in the streamwise and spanwise directions leading to flattening of the flame. A iso-level of G-surface corresponding to a value of 0.5 predicted by the subgrid approach is shown in Fig. 9. This figure shows visually an approximate shape of the wrinkled flame front.

To investigate the effect of gravity, two simulations (using the subgrid model) were conducted with heat release corresponding to a temperature ratio of 7.0. The first case is run with conditions corresponding to gravity on earth, the second with zero gravity. The density gradients caused due to heat release tend to compress the flame in the upper region and diffuse the flame in the lower regions in the presence of gravity. This is not very noticeable in the present simulations because of very high burning rate causing the flame to reach the wall very quickly. In Fig. 10, ten equally spaced contours of G at the same cross plane location are plotted for the cases with and without buoyancy. The whole flame tries to lift up in the presence of gravity due to buoyancy, although it is not very noticeable in the figure. However, it can be seen that the two simulations diverge in time indicating an observable buoyancy effect on premixed flames.

There are many structural and propagation properties of premixed flames that can be analyzed to characterize the flame structure. Figure 11 shows the pdf of the stretch in the plane of the flame (caused by flame curvature and rate-of-strain effects) for the two cases. Clearly, the flame structure under 1g exhibits increased positive stretch compared to the 0g case. Further study using finite-rate kinetics model is underway to understand the effect of buoyancy on such low Re turbulent premixed flames.

Conclusions

A facility in which turbulent Couette flow could be generated in a microgravity environment was designed and built. To fit into the NASA Lewis drop tower the device had to be very compact. This means that edge effects and flow re-circulation were expected to affect the flow. The flow was thoroughly investigated using LDV and was found to be largely two dimensional away from the edges with constant turbulence intensities in the core. Slight flow asymmetries are introduced by the non symmetric re-circulation of the fluid outside the test region. Belt flutter problems were remedied by adding a pair of guide plates to the belt. In general, the flow field was found to be quite similar to previously investigated Couette flows. However, turbulence levels and associated shear stresses were higher. This is probably due to the confined re-circulation zone reintroducing turbulence into the test section. An estimate of the length scales in the flow showed that the measurements were able to resolve nearly all the length scales of interest.

Using a new LES method for subgrid combustion it has been demonstrated that the new procedure is computational feasible even on workstation type environment. It is found that this model is capable of capturing the propagation of the premixed flames by resolving the flame in the LES grid within 2-3 grid points. In contrast, conventional LES results in numerical smearing of the flame and completely inaccurate estimate of the turbulent propagation speed. Preliminary study suggests that there is observable effect of buoyancy in the 1g environment suggesting the need for microgravity experiments of the upcoming experimental combustion studies.

With the cold flow properties characterized, an identical hot flow facility is under construction. It is assumed that the turbulence properties ahead of the flame in this new device will closely match the results obtained here. This is required since the hot facility will not enable LDV measurements. The reacting flow facility is also being constructed with planned drop tower experiments in mind. Therefore, issues related to safety and structural integrity are being take into account. Further development of the numerical model will also be carried out to include finite-rate kinetics for representative premixed cases. More detail analysis of the flame structure and propagation nature will be investigated. Simulations will also be compared to the flame properties observed in the experiments.

References

1. Williams, F. A., *Combustion Theory*, Second Edition., Addison-Wesley, New York, 1985.
2. Lekan, J., Gotti, D. J., Jenkins, A. J., Owens, J. C., Johnston, M. R., "User Guide for the 2.2 Second Drop Tower of the NASA Lewis Research Center," *NASA Technical Memorandum 107090*, 1996.
3. Aydin, E. M., and Leutheusser, H. J., "Plane-Couette flow between smooth and rough walls," *Experiments in Fluids*, Vol. 11, pp. 302-312, 1991.
4. Bech, K. H., Tillmark, N., Alfredsson, P. H., Andersson, H. I., " An Investigation of Turbulent Plane Couette Flow at low Reynolds Numbers," *Journal of Fluid Mechanics*, Vol. 285, pp. 291-325, 1995.
5. El Telbany, M. M. M., Reynolds, A. J., "The Structure of Turbulent Plane Couette Flow," *Journal of Fluids Engineering*, Vol. 104, pp. 367-372, 1982.
6. Robertson, J. M., and Johnson, H. F., "Turbulence Structure in Plane Couette Flow," *J. Eng. Mech.*, Proc. of Am. Soc. of Civil Engg., Vol. 6, pp. 1171-1182, 1970.
7. Clark, J. A., "A Study of Incompressible Turbulent Boundary Layers in Channel Flow," ASME *Journal of Basic Engineering*, Vol. 90, pp. 455-468, 1968.
8. Menon, S., McMurtry, P. A., and Kerstein, A. R., "A Linear Eddy Mixing Model for LES of Turbulent Combustion," in *LES of Complex Engineering and Geophysical Flows*, Galperin, B. and Orszag, S., eds., Cambridge University Press, pp. 287-314, 1993.
9. Menon, S. and Chakravarthy, V. K., Large-Eddy Simulations of Premixed Flames in Couette Flow, AIAA Paper No. 96-3077, 32nd AIAA/ASME/SAE/ASEE Joint Propulsion Conference, Lake Buena Vista, FL, July 1996.
10. Smith, T. and Menon, S., "Model Simulations of Freely Propagating Turbulent Premixed Flames", *Symposium (International) on Combustion*, 26, 1996 (to appear).
11. Menon, S and Calhoon, W., "Subgrid Mixing and Molecular Transport Modeling for Large-Eddy Simulations of Turbulent Reacting Flows", *Symposium (International) on Combustion*, 26, 1996 (to appear).
12. Calhoon, W. H. and Menon, S., "Linear Eddy Subgrid Modeling for Reacting Large-Eddy Simulations: Heat Release Effects," AIAA-97-0368, 35th Aerospace Sciences Meeting, Reno, NV, January 6-9, 1997.
13. Chakravarthy, K. and Menon, S., "On Large-Eddy Simulations of Non-Homogeneous Flows," AIAA 97-0652, 35th Aerospace Sciences Meeting Reno, NV, January 6-9, 1997.

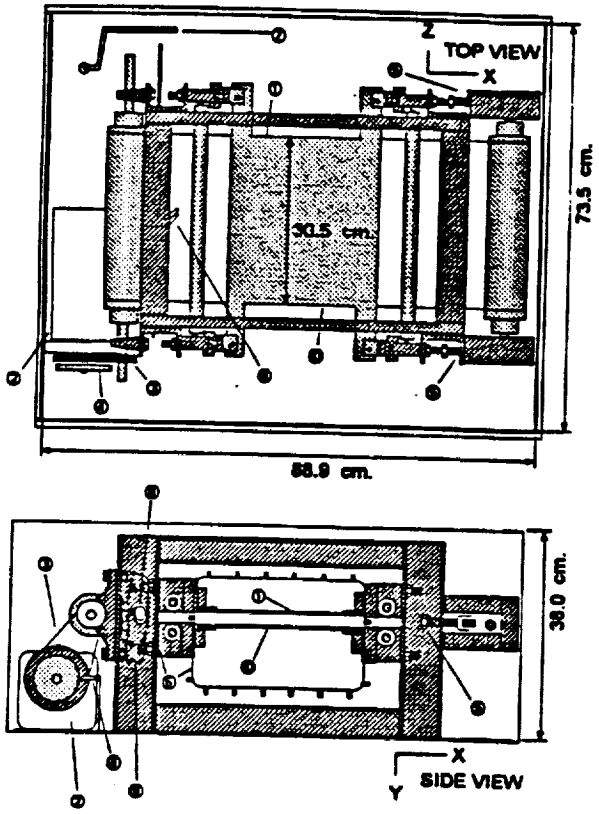

Figure 1. Setup of the experimental facility.

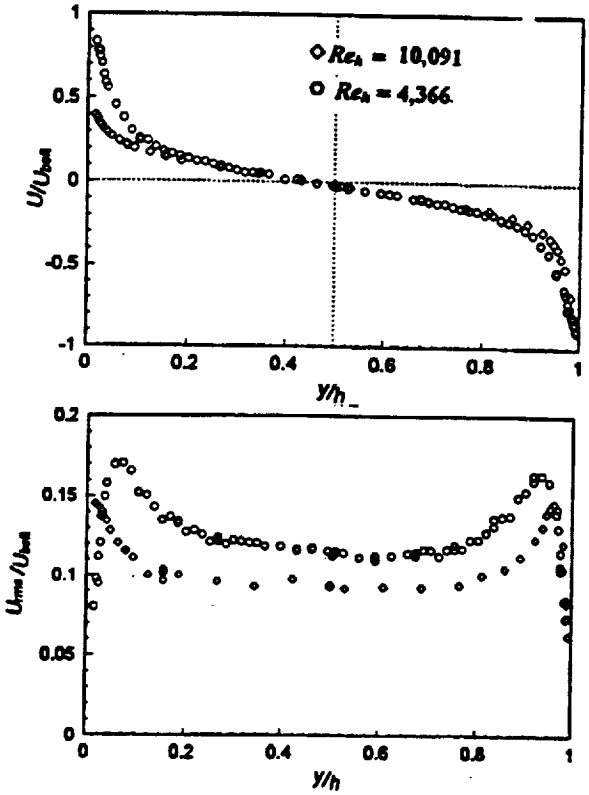

Figure 2. Mean (a) and rms (b) velocity fluctuations.

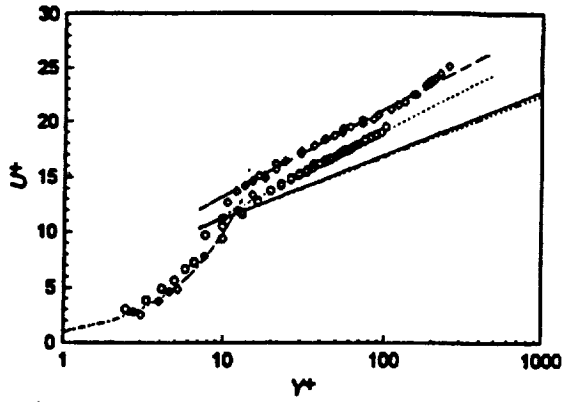

Figure 3. Non-dimensionalized near-wall velocity profile. Solid and dotted lines indicate curve fit to earlier data (refs. 3-7).

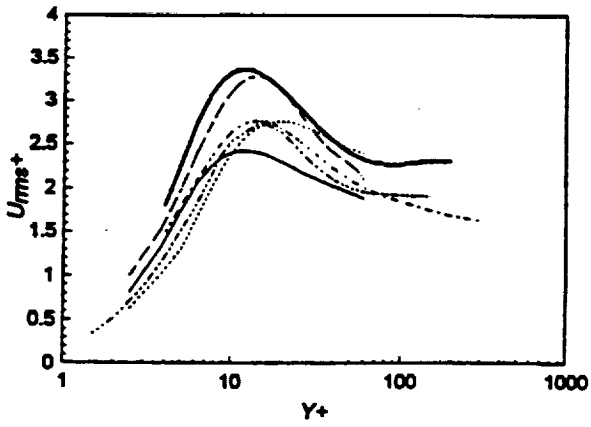

Figure 4. Comparison of present turbulence velocity fluctuation (shown as a bold line) with earlier experimental data (refs. 3-7).

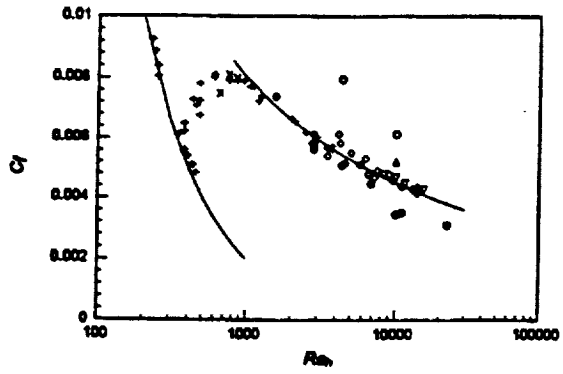

Figure 5. Skin friction coefficient comparison with earlier data. Solid circle: present study near wall; open circle: present study in the core. Other symbols correspond to data in refs. 3-7.

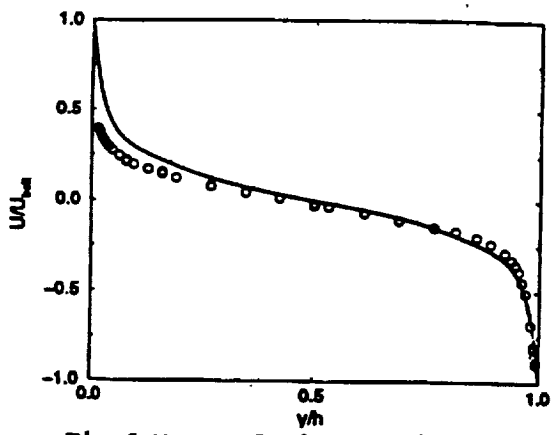

Fig.6:Mean velocity profiles
solidline:LES,symbols:expt.

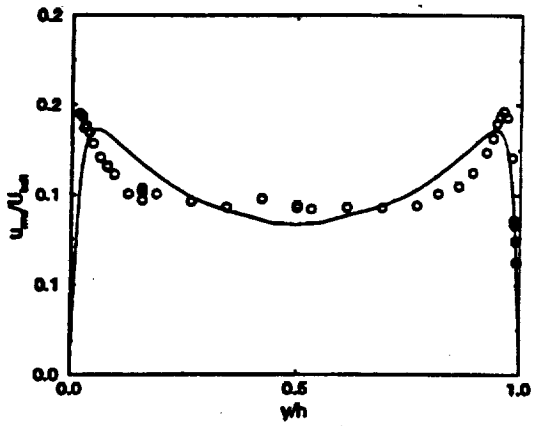

Fig.7:urms profiles
solidline:LES,symbols:expt.

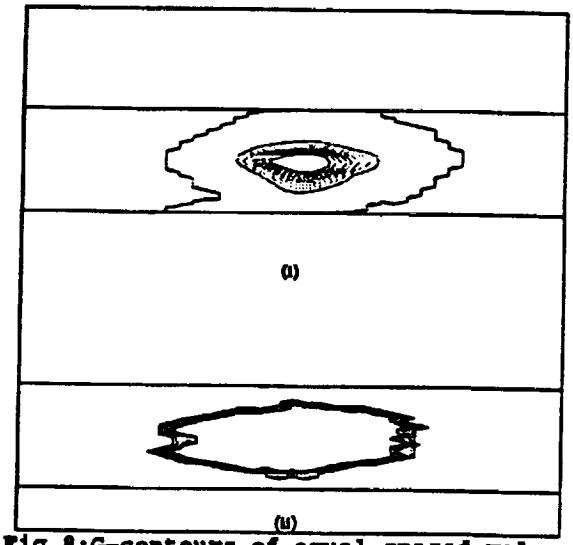

Fig.8:G-contours of equal spaced values
(i) Yakhot's model, (ii) LEM

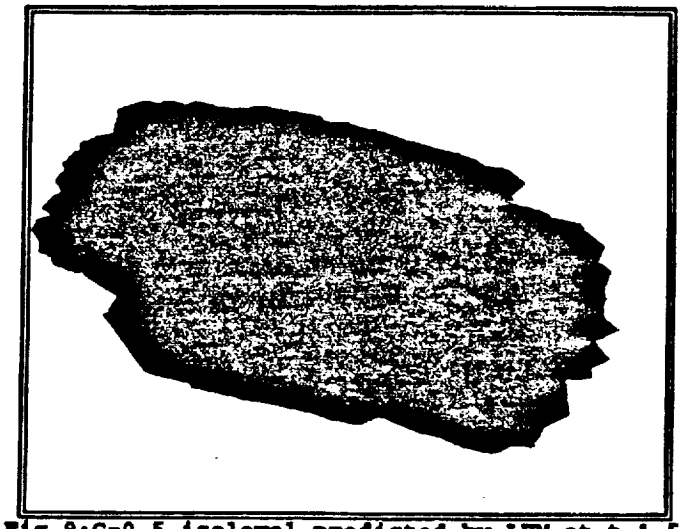

Fig.9:G=0.5 isolevel predicted by LEM at t=1.5
(t non-dimensionalized U_w and h)

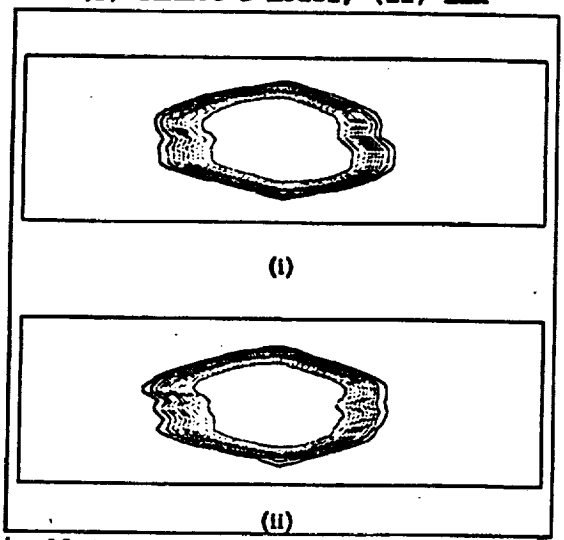

Fig.10:G-contours of equal spaced values
(i) zero gravity, (ii) gravity on earth

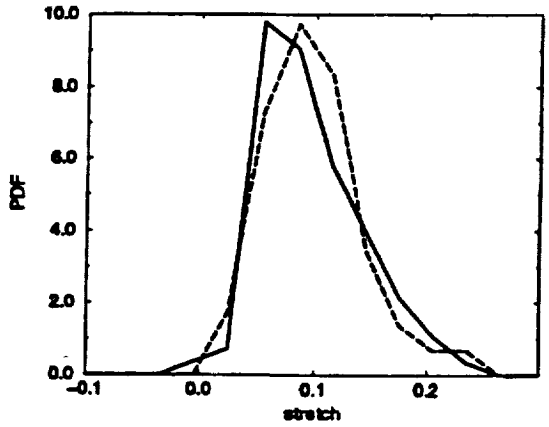

Fig.11:PDF of flame stretch
solid line: no gravity, dashed line:with gravity

AIAA 97-3331

Characteristics of a Subgrid Model for Turbulent Premixed Combustion

V.K. Chakravarthy and S. Menon
School of Aerospace Engineering
Georgia Institute of Technology
Atlanta, GA 30332-0150.

33rd AIAA/ASME/SAE/ASEEJoint Propulsion Conference & Exhibit
July 6 - 9, 1997 / Seattle, WA

Characteristics of a Subgrid Model for Turbulent Premixed Flames*

V. K. Chakravarthy ‡ & S. Menon†
School of Aerospace Engineering
Georgia Institute of Technology
Atlanta, GA 30332-0150

Abstract

A modified version of the linear eddy model (LEM) for subgrid combustion is developed and used for studying the properties of turbulent premixed flames in the core region of Couette flow. The handling of the burning (diffusion/reaction) and specie transport, in this new approach, is fully deterministic. The model is, therefore, found to predict the correct laminar flame speed in the limit of zero turbulence. The effect of three dimensional eddies on scalar fields at the subgrid scales is modeled using a stochastic Lagrangian rearrangement procedure. The derivation of this procedure from the inertial range scaling laws necessitates a calibration procedure since the numerical values of the constants in these laws are unknown. The present LEM approach relates the constant needed to the coefficient of eddy viscosity that is evaluated in a LES, under the assumption of constant turbulent Prandtl and Schmidt numbers. The new approach is found to predict the turbulent flame speed with fair amount of accuracy. The chemistry is modeled using a self propagating scalar field (G-equation) approach and within the limitations of this model, LEM is found to capture the right trends in evolution of flame structure, effects of heat release and turbulence. The encouraging results obtained here warrant further research into extending this subgrid model for cases of finite rate chemistry and inclusion of thermodiffusive mechanisms such as the Lewis number effects.

1 Introduction

The simulation of turbulent phenomena in engineering is, in the present day greatly limited by the available computational resources. This neccesitates the development of modeling tools that would enable us to simulate these phenomena within the realm of available resources. One such approach is Large Eddy Simulation (LES) in which the large scale structure of the flow is determined by solving the governing equations that are augmented with additional (approximate) model terms to account for the effect of small scales. Dissipation of kinetic energy is the only physical phenomenon of importance in non-reacting flows that occurs at small scales. Separating these small scales and the large scales (of the size of the characteristic geometric length in the flow) is the inertial range which acts purely as an energy cascade for supplying kinetic energy to the small scales from the large scales. The near universal behavior of the inertial range along with the assumption of local small scale isotropy has aided the modeling of turbulent flows using the eddy viscosity assumption.

However, there is no universally valid form of the scalar spectrum at small scales. There exist several forms of the of scalar spectrum depending on the local Schmidt number (for species) or Prandtl number (for temperature). Independent of these parameters, scalar mixing using an eddy diffusivity, nevertheless, is often used in the present day modeling studies. This approach is severely in error in cases where scalar counter gradient diffusion occurs. Further, if the fluid is reacting, the interaction between the molecular mixing and chemical reactions occuring at smallest of the scales (Kolmogorov and Batchelor scales) have significant effects on large scale fluid/flame structure. The additional non-linearity in the governing equations in case of reactive systems also needs to be handled perhaps with greater care for accurate modeling of reacting flows.

In many practical engineering systems, combustion takes place in a regime of parameter space called the corrugated flamelet zone. The flame thickness is very small as compared to any relevant fluid dynamic length scales

† Professor, Senior Member, AIAA.
‡ Graduate Research Assistant.

(Kolmogorov length scale). In this region of parameter space, the flame is wrinkled by turbulence but the local burning is laminar. The turbulent flame consists of an ensemble of locally laminar flames whose self propagation speed (laminar flame speed) is governed by the balance between temperature and specie diffusion. The probability density function (PDF) and moment closure approaches are, at the present day, inadequate in handling the diffusion processes and hence it is difficult to predict the correct reaction rate in the subgrid when these approaches are used.

When the reaction system is dominated by one physical phenomenon, there are several models that work well. Yakhot's model [1] and Fractal models [2](for thin premixed flames with low or no heat release) that concentrate on the kinematic structure of the flame and characterize the model in terms of incoming turbulence, Fureby and Moller model [3] which uses the turbulent reaction rate based on local turbulent and chemical time scales, are a few examples. Approaches such as these could be used to arrive (often empirically) at simple inexpensive models that, on calibration over certain regions of parameter space, could work for specific class of flows.

The Linear Eddy Mixing (LEM) model seeks to separate and model independently the effects of molecular mixing from the turbulent effects on the flame. The implementation is on a one-dimensional domain which considerably reduces the modeling cost. By carrying these one-dimensional domains in each of the LES cells to account for the effects of unresolved turbulence on scalar transport and production/destruction, this approach has been extended for use in LES [4]. The linear eddy model(LEM) is further capable of accounting for the thermodynamic effects such as volumetric dilatation, differential diffusion, viscosity variation with temperature etc. There is yet another important feature of this model that is very advantageous in modeling reacting flows once the advection (due to resolved scales) is modeled correctly. That is the adequate numerical resolution of the flame. Thin flames produce steep gradients in flow properties that could become very difficult to handle computationally if one uses finite volume or finite difference schemes. If not adequately resolved, most numerical schemes cause unphysical oscillations near the flame that threaten to destabilize the numerical solution. Generally used robust schemes usually are dissipative in nature and smear out the physical gradients, thus, artificially thickening the flame. The LEM approach handles the scalar transport in a Lagrangian manner circumventing this problem.

The Linear eddy model has been used in several numerical combustion studies. The kinematic structure of premixed flames was modeled earlier by Menon et al.[4] and this approach was extended for modeling the kinematics of a self propagating scalar interface in a wall bounded shear flow using LES with dynamic K-equation model [5]. This study utilized the G-equation [6] which models the motion of self propagating kinematic surface (model for cold flame). A subgrid kinetic energy equation model with dynamic evaluation of the model coefficients is used as the subgrid model for momentum transport. This study proves the feasibility of an online implementation of the LEM approach in a 3D LES but asks for further research into species advection modeling and inclusion of heat release effects. Some inadequacies in the advection algorithm were overcome by Calhoon and Menon [7] in their two dimensional simulation of reacting mixing layers including effects of heat release. However, as noted in [8], the inadequacies in this advection seem to cause significant errors in premixed flames as against non-premixed flames. A modified version of the advection algorithm is reported here.

The present research seeks to validate (independently) and combine the various different modeling procedures (for each of the underlying physical phenomena) to arrive at a comprehensive modeling approach for use in LES. Using this approach, the structure of premixed flames in turbulent Couette flow at Re (based on channel width and wall velocity difference) of 20000 is analysed. Experimental data from [9] is available at that Re for validation of cold flow LES. The Couette flow has a wide core region where the mean flow is small and the turbulent intensity is nearly constant. The turbulent intensity in this region can be used as a parameter against which the flame characteristics (like turbulent flame speed, flame stretch etc.) could be characterized. Also reported here are the effects of heat release on the flame structural properties.

The flame generated turbulence is found to be a significant factor in determining the flame speed. The precise nature of it's effects needs to be studied can be studied using a stationary flame problem. To this end, a premixed turbulent stagnation point flame is under study using LES. Some preliminary observations are reported here.

An eddy viscosity approach based on the model K-

equation (subgrid kinetic energy equation), discussed in section 2. is used to model momentum transport. A zero Mach number fractional step method is used to numerically integrate the LES equations on a non-staggered grid. The version of the LEM approach used here is outlined in section 3. The results are analysed in section 4 and directions for future research are discussed in section 5.

2 Governing equations for LES

The Navier Stokes equations on convolution with a spatial filter (after filtering), reduce to the following LES equations.

$$\frac{\mathrm{d}\rho}{\mathrm{d}t} + \rho\frac{\partial \overline{U}_i}{\partial x_i} = 0 \tag{1}$$

$$\frac{\mathrm{d}\rho\overline{U}_i}{\mathrm{d}t} = -\frac{\partial \overline{p}}{\partial x_i} + \frac{\partial \tau_{ij}}{\partial x_j} + \frac{\partial \tau_{ij}^{viscous}}{\partial x_j} \tag{2}$$

The volumetric dilatation $\partial\overline{U}_i/\partial x_i$ is obtained from the zero Mach number approximation of the energy equation arrived at by assuming a fast acoustic time scale approximation from the equations. The physical consequence of this is to remove any gradients in thermodynamic pressure (because of infinite propagation speed). The normal stress associated with the momentum gradients (as in incompressible flows) is however spatially dependent.

For a closed set of equations , one needs to approximate the subgrid stresses using a model. The velocity variations in the scales below the characteristic filter width Δ are unresolved in a LES. Due to the nonlinear nature of the Navier-Stokes equations, these small scale fluctuations effect the large scale motions. This effect comes from the subgrid stress, which in the present study is approximated as $\tau_{ij} = -\frac{2}{3}\rho K\delta_{ij} + 2\mu_t\overline{S_{ij}}$, where $\overline{S_{ij}} = \frac{1}{2}\left[\partial\overline{U}_i/\partial x_j + \partial\overline{U}_j/\partial x_i\right]$ is the resolved strain tensor, μ_t is subgrid eddy viscosity (to be defined later) and $K = -\frac{1}{2}(\overline{U_i\ U_i} - \overline{U_i}\overline{U_i})$ is the subgrid kinetic energy. Filtered variables are also called supergrid variables because they carry information about a variables at all length scales above the filter width (grid spacing).

A K-equation (for the subgrid kinetic energy) model [10] is used as the subgrid model. The advantage of this model is that it solves a single scalar equation for the subgrid kinetic energy which characterizes the velocity scale of subgrid turbulence. The subgrid kinetic energy has in it terms accounting for production, transport and dissipation. It is a representation of the temporal non-equilibrium of the subgrid scales because the production does not neccesarily equal the dissipation (even on an average).

A variable density version of the model (for use in zero Mach number equations) is used here. The eddy viscosity and subgrid dissipation are given as follows.

$$\mu_t = \rho C_\nu K^{\frac{1}{2}}\Delta, \tag{3}$$

$$\epsilon^{sgs} = C_\epsilon\frac{\rho K^{\frac{3}{2}}}{\Delta} \tag{4}$$

For the transport term, a gradient diffusion model based on eddy diffusivity model (with unit eddy Prandtl number) has been proposed and studied by Menon and Kim [11]. This approximation was found to adequately model the transport terms. Hence, this is used in a similar form in this study. The dynamic equation for K can now be written as:

$$\frac{\partial\rho K}{\partial t} + \frac{(\partial\rho K\overline{U_j})}{\partial x_j} = \tau_{ij}\frac{\partial\overline{U_i}}{\partial x_j} - \epsilon^{sgs} + \frac{\partial}{\partial x_j}\left[\mu_t\frac{\partial K}{\partial x_j}\right] \tag{5}$$

The turbulent dissipation due to compressibility and dilatational effects is assumed to be insignificant at the low Mach that are to be encountered. C_ν and C_ϵ are the model constants that need to be specified. These constants, however, are not universal and differ with flow fields in general. This suggests that these constants also depend on the local (supergrid) structure of the flow field. It is, then appropriate to refer to them as coefficients rather than constants. A dynamic approach is applied here to evaluate these coefficients, thus removing the arbitrariness in prescribing these coefficients. The approach is based on the concept of subgrid stress similarity supported by experiments in jets (Liu et al. [12]). In this approach, a test filter (similar to the LES filter) of characteristic width 2Δ is defined and the corresponding filtered velocity field is denoted by $\widetilde{U_i}$. This new velocity field is obtained by convolution of the LES filtered velocity with the test filter. The subgrid stress corresponding to the scales in between the grid filter width and the test filter width is termed the test filter stress. Assuming stress similarity between the test filter stress and the subgrid stress, along with equations similar to eq.(3) and eq.(4) the test filter variables, one can arrive

at equations for the model coefficients. These equations can be found in [13] and are omitted here for brevity.

The equations are discretized on a non-staggered grid (with spacing corresponding to the characteristic filter width Δ) and numerically integrated using a two step semi-implicit fractional step method. The Poisson equation in this method is solved numerically using an elliptic solver that uses a four-level multigrid scheme to converge the solution. The species transport between cells is handled in a Lagrangian manner and thus the species equation need no integration on the supergrid level.

3 Linear Eddy subgrid model

A subgrid modeling approach based on linear eddy mixing model (Kerstein, [14-17]) was proposed by Menon et al. ([18].[19],[20]). In this approach, the turbulent stirring of the scalar field and molecular diffusion (leading to laminar propagation) are accounted for distinctly. The effects of each of these phenomena on flame characteristics can hence be studied in isolation. The modeling procedure with appropriate justification is presented here in brief.

The subgrid modeling is conducted on a one-dimensional domain (in each of the LES cells) representing a ray of length Δ across the turbulent flame brush. This domain is divided into number (specification to be explained later) of cells each representing a finite volume with the total volume adding upto the volume of the LES cell.

A field equation for self propagating scalar interface called the G-equation [6] is used to model the laminar flame propagation in this study. This equation is designed to propagate a scalar interface at the laminar flame speed in stagnant flow and has the following form.

$$\frac{\partial G}{\partial t} = S_l|\nabla G| \qquad (6)$$

For the case of moving fluid, the interface also gets convected along with self propagation and a convection term needs to be added to the above equation.

The scalar G here, is a representation of the rate of advancement in a premixed reaction. It has a binary representation on the subgrid one-dimensional domain (later refered as the linear eddy domain). $G = 1$ represents an unburnt state and $G = 0$ represents a burnt state on each LEM cell. The interface between two dissimilar adjacent cells is considered to be an infinitely thin flame that propagates into the unburnt zone at a specified flame speed. The temperature rise due to the reaction is modeled by assuming the temperature to be a linear function of G. In this way, the G-equation replaces the reaction-diffusion equations for both species and temperature (that, in conjunction make the premixed flame self propagating). In the burnt state, the temperature rises to the prescribed value of the product temperature. Since the thermodynamic pressure is assumed to be constant (which is the case across premixed flames governed by second order chemical kinetics), the density varies inversely with temperature. Since the transport and diffusive properties of G and temperature would be closely correlated in this approach, it is to be assumed that these simulations correspond to a case of constant Le (Lewis number), specifically 1.0.

As can be seen in the above equation, the G-equation does not include any convective term. The effect of subgrid velocity (turbulence) is modeled separately using a stochastic process. A Lagrangian rearrangement is used to model the effect of fluid dynamic eddies on the scalar field. The length scale of the eddy (segment size on which this rearrangement process is to be conducted) and the frequency of stirring at that length scale are determined using isotropic inertial range (assumed to exist in the subgrid scales of the LES) scaling laws. There is no universality of the rearrangement scheme. It can be arbitrary but it should mimic the effect of hydrodynamic eddies on the scalar field and be conservative (retain the lowest scalar moments invariant).

A triplet map [17] is chosen for the present study. In this mapping, the chosen segment is divided into three equal parts. All spatial gradients are increased by a factor of 3 in the portions at the ends, and a factor of -3 in the middle portion. The scalar field in the three segments is pieced together to give a continuous scalar field with scalar values at the end points of the segment remaining the same as before and the scalar gradients increased by 3 times in magnitude (as illustrated in [5]). These increased gradients cause increased scalar diffusion in accordance with what has been observed as the effect of turbulence on scalar transport and dispersion. The number of finite volume cells in each subgrid domain is so chosen that a stirring event at the smallest relevant (energetic possessing) scale could be implemented. This is assumed to be the Kolmogorov length scale η. A line segment needs to have atleast 6 cells to implement a triplet map, so the cell size should be no less than $\eta/6$.

So the total number of cells is $6\Delta/\eta$.

The triplet map causes particle dispersion with mean square displacement of $4l^2/27$, where l is the length of the segment. The diffusivity associated with such a process would be $2\lambda l^3/27$, where λ is the frequency per unit length. The diffusivity due to turbulence for all length scales below l can be determined from the inertial range scaling laws (relevant dimensional analysis) in terms of the η, l and ν. It can be shown that it has the same form as eddy viscosity at that length scale, only difference being the constant of proportionality is now C_ν/Pr_t instead of C_ν. C_ν is determined as explained in the earlier section and it is assumed that Pr_t is 1.0. Thus the constant of proportionality is arrived at from analytical reasoning rather than a calibrating procedure undertaken in [7]. Equating the value of diffusivity to the corresponding integrated effect of triplet mappings at various length scales, one can arrive at the PDF for length scale l and the stirring frequency (using the procedure adopted in [5]). The stirring procedure in conjunction with the molecular diffusion has been shown to effectively model the effect of three dimensional inertial range turbulence on the scalar fields [21].

Advection due to the supergrid velocity brings about transport of chemical species from one LES cell into it's neighbouring cells. This is modeled using a procedure termed as "splicing"[17]. The scalar flux across each LES cell face is computed using the filtered velocity on the cell face. The number of subgrid cells corresponding to the scalar flux are transfered from one cell to it's neighbour across the cell face in accordance with the direction of the scalar flux.

Instead of picking these cells from a random location on the donor subgrid domain like in the earlier research [5], cells are tranfered from one end of the subgrid domain. The cells that are spliced in are put at the opposite end of the domain. In time, the linear eddy cells to be spliced in first get spliced out first. In the laminar limit (acheived by removing stirring), the flame travels from one end to another end of the cell at the rate of S_l, the laminar flame speed. When a LES cell is fully burnt the flame crosses over to the next LES cell and this process is found to predict the right laminar flame speed on the supergrid (on an average). The earlier splicing algoritm with randomly chosen locations for transfer of subgrid segments does not ensure this. Further, the introduction of cells spliced into the receiver subgrid domain can cause extra flames at the interface (between the cells put in and the existing cells). The splicing algorithm models advection and is not supposed to create any scalar gradients (flames in the present case) on the linear eddy domain. So, in the event of an artificial flame being created at the interface, the spliced in cells are rearranged to remove this extra flame. The only exception to this procedure is the case of burning initiation in a fully unburnt cell in which case one flame caused at the interface is retained. This procedure prevents the existence of more than one flame in laminar flows (there is no flame brush in laminar flames). This approach was found necessary to obtain the correct laminar propagation on the supergrid especially in case of curved flames (cylindrical and spherical). In the turbulent case, the stirring could cause multiple flames to exist on the same subgrid domain and this could be interpreted as a stochastic representation of flame brush in each cell.

Finally the average density along the subgrid domain is used as the filtered density on the supergrid and is used to compute the volumetric dilatation on the supergrid.

4 Results and Discussions.

The LES numerical code is validated against the experimental results obtained from turbulent Couette flow experiments[9]. Shown in fig. 1 and fig. 2, respectively, are the profiles of mean velocity and *rms* of axial velocity for Couette flow at Re of 20000. A 49x49x33 is utilized for this simulation. Hyperbolic tangent stretching is used for the grid spacing along the wall normal direction. As can be seen, the mean velocity profile is anti-symmetric about the centre-line where as the experimental prediction is not. It was argued that this does not cause any bias in the u' profile which is in fact found to be symmetric. The peak in u' profile is much closer to the walls in experimental data than in the LES. The cause of this discrepancy is unknown. It is likely that the wall layer needs more resolution or the experimental results may be in error due to moving wall (belt) vibrations which make the flow noisy. This LES approach has earlier been validated by simulating turbulent Couette flow at Re of 5200 by comparing with experiments in [5].

In order to ease the implementation of LEM on LES grid, the mid 78 percent of the grid is made uniform. The simulations are stopped once the flame reaches the boundaries of this uniform region. The capability of linear eddy subgrid model in capturing thin flames is illustrated in fig. 3. For comparison, starting with the

same initial conditions, LES is conducted using a finite difference implementation of G-equation with turbulent flame speed obtained using the Yakhot's model [1]. Nine contours corresponding to nine equally spaced values of G are shown in fig. 3. The finite difference implementation of chemistry is seen to thicken the flame front, thus, reducing the gradients. This in turn causes a reduction in flame speed. As was sought from the conclusions of earlier LEM research [5], the linear eddy model (with the new advection modeling approach) now propagates the laminar flame on the supergrid at the correct flame speed for both planar and spherical flames. This removes the arbitrariness in advection algorithm [5] and the calibration procedure for diffusion/burning [7]. The turbulent stirring becomes the only stochastic part of the approach and the only arbitrariness is in prescribing Pr_t.

The premixed flame propagation is simulated for values of u'/S_l : 1.0, 4.0 and 8.0. For all these cases, simulations are conducted for three different values of product temperatures (T_p). T_p/T_f of 1.0, 4.0 and 7.0 are used. So there are nine cases in the parameter space. Since the flames are not stationary, one needs several realizations of the flow at the same time after ignition for statistical analysis. For each of the above cases, several LES realizations (starting from different realizations of non-reacting flow LES as initial conditions before igniting the flame) of the flow are simulated till the statistics converge.

The temporal evolution of the flame structure is discussed first, followed by analysis of effects of increasing relative (to S_l) turbulent intensity. Since the cold flames have been studied earlier, this analysis is done for flames in the presence of heat release. The effects of increasing heat release are discussed later.

The local structure of the flame can be characterized using the principle radii of curvature. These are computed from the eigen values of the curvature tensor [22]. The ratio of smaller radius to the higher, is refered to as the shape factor. It lies between -1 (corresponding to a saddle point) and 1 (spherical shape). The value of 0 corresponds to a cylindrical shape. The hydrodynamic effects on the flame are mainly characterized by two quantities, the tangential strain rate in the plane of the flame and the flame stretch which is defined as the rate of change of a Lagrangian flame surface at a given location. Mathematical means of computing these quantities can be found in [22]. The strain rate gives an estimate of the hydrodynamic force acting in the plane of the flame. The flame stretch determines the rate at which the flame is deforming with the effects of self propagation included. Positive stretch indicates a tendency of the flame to replanarize thus reducing the curvature and hence also the turbulent flame speed. In the limit of a material surface ($S_l = 0$), the tangential strain rate and the flame stretch are highly correlated. Probability density functions (PDFs) of each of these local flame properties are constructed in order to characterize the gross nature of the flame. The strain rate and flame stretch are non-dimensionalized using the Kolmogorov time scale and the curvature is non-dimensionalized using the integral length scale (prescribed).

In fig. 4, the transition from a spherical to (locally) cylindrical nature of the flame is shown for the case of u'/S_l of 8.0 and T_p/T_f of 7.0. When the fuel is ignited at a point source, the initial growth is (globally) spherical. With increasing time the effect of turbulence is realized in terms of wrinkles that are characterized by increase in shape factor PDF near cylindrical zone. Eventually the effect of mean velocity comes in and elongates the flame and the turbulence wrinkles the flame front. This is illustrated graphically to a certian extent in fig. 5. Then the flame becomes mostly cylindrical and finally, towards the end of the simulation, some saddle nature is noticed. This trend of PDF shifting towards the saddle zone from mostly cylindrical nature (once the effect of turbulence is fully realized) is also noticed as the shear layer evolves spatially in [22]. In fig. 6 is shown the evolution of flame stretch PDF with time. The time here is non-dimensionalized by the total time of the simulation (just before the flame leaves the domain where LEM is implemented). For an outward burning hot flame, the curvature and volumetric dilatation (expansion) are always positive leading to positive flame stretch. As the flame expands, the curvature effect reduces and turbulence effect is felt more. In isotropic turbulence, the stretch is nearly symmetric except that the self propagation contribution skews the PDF slightly towards the positive side. This skewness reduces with increasing u'/S_l and PDF is very nearly symmetric for material surfaces [23]. The flame is indeed found to transition towards this nature gradually from it's initial state of fully positive stretch.

The simulations with T_p/T_f of 7.0 are analyzed to study the effects of reducing S_l with same u' (increasing u'/S_l). The tangential strain rate PDFs for three cases of u'/S_l are shown in fig. 7. Increasing the flame speed causes the negative curvature to decrease and positive

curvature (concave to the fuel side) to increase. Due to positive volumetric dilatation on the burnt side, regions of positive curvature experience high strain rates on the surface. So the PDF is more skewed to the right for the case of higher S_l. Alternately, as turbulence intensity increases relative to S_l, the nature of the flame tends more towards that of a material surface thus reducing the skewness. As noticed in earlier studies [22] involving spatial mixing layers, the mean curvature PDF (fig. 8) is slightly shifted to the right (because of finite S_l) and is found to be independent of u'/S_l. The flame stretch (fig. 9) is found to behave in much the same fashion as the tangential strain rate because the curvature remains unchanged. Because of slight positive skewness in curvature PDF, it is easy to see from the expression for flame stretch, that the flame stretch skewness is slightly reduced as compared to flame strain rate.

The relative alignment of the flame normal with the direction of most compressive strain rate (eigen vector corresponding to the lowest eigen value of the strain tensor) is computed and plotted in fig. 10. Contrary to the previous reports [24] of the PDF peak at an alignment angle of 30° in shear driven flows, the peak is closer to 0° indicating a tendency of the flame normal to align with the compressive strain rate direction. This was observed in isotropic turbulence simulations earlier [24]. Two reasons could perhaps be attributed for this behavior. First, the mean shear is very small in the core region and hence the turbulence may be close to being locally isotropic. Second, in the presence of heat release, the mean shear effect may be insignificant because the flow is modified drastically due to density changes. The volumetric dilatation tries to accelarate the flame propagation thus trying to compress the flame brush. In such cases, the higher two eigenvalues are both most likely positive thus making the tangential strain rate highly positive for high heat release cases as noticed in fig. 7.

The effects of increasing heat release on the flame structure are analyzed using cases with u'/S_l of 4.0. The tangential strain rate is plotted, for the three values of heat release under consideration, in fig. 11. As seen earlier, the most compressive principle strain rate aligns closely with the flame normal at most of the points. The sum of the three principle strains is positive and increases with increasing heat release. Since the strain rate normal to the flame is negative, it is very likely that the two higher values of the principle strain rates are positive leading to an overall positive strain rate in the plane of the flame. Mean curvature (shown in fig. 12) is slightly biased towards the positive side. The likelihood of regions on the flame with higher mean curvature is found to increase with heat release. The heat release causes faster flame growth due to dilatation but this acceleration could dewrinkle the flame, thereby reducing the local radii of curvature (increasing curvature). The flame stretch is plotted in fig. 13 and is found to correlate well with the behavior of the tangential strain rate since the curvature is nearly symmetric.

The turbulent propagation rate of the premixed flames, while they are in the core region, is characterized against the turbulent intensity of the cold flow into which the flame is propagating. The turbulent flame speed predictions (experimental and theoretical) exhibit a large amount of scatter. The key reason for this being the fact that there may be parameters that are different in various studies and, hence, comparing the results from these to arrive at some definite conclusions cannot be rationalized. Bradley et al. [25] in their survey of available of experimental results for characterizing turbulent flame speed against inflow turbulence, found it necessary to consider the dimensionless Karlovitz stretch factor as a relevant parameter. It is a measure of chemical time against the eddy time and is given as [26]:

$$K = 0.157\left(\frac{u'}{S_l}\right)^2 R_l^{-0.5} \qquad (7)$$

where R_l is the turbulent Reynolds number based on the integral length scale.

The results reported were therefore separated into different zones depending on the value of this parameter times the Lewis number. They report results that fall into two zones corresponding to mean values of $K.Le$ values of 0.1 and 1.0 with a scatter of about 25 precent. Some of these experimental results are plotted along with the predictions from the current study in fig. 14. The values of the above mentioned parameter are 0.01, 0.15 and 0.46 respectively for u'/S_l values of 1.0, 4.0 and 7.0. Also included are the best fit lines to experimental predictions at $K.Le$ of 0.1 and 1.0. It is found that the cold flame front propagation matches the experimental data rather well. However, the turbulent flame propagation is much faster in cases with heat release. The compounded effect of two factors could be the reason for the observed increase with heat release. Flames that are primarily convex (burning outwards from burnt side) experience some amount of outward accelaration. The

countering effect would be that this increases the flame stretch thus reducing the flame speed. Also, a wrinkled exothermic propagating front generates some fluid dynamic diturbances which in turn change the flame propagation speed. These disturbances (termed flame generated turbulence) add onto the incoming turbulence and one can define an "effective turbulence intensity" [26] that determines the flame structure. Leisenheimer and Leuckel [27] were able to measure this effective intensity in a premixed flame propagating radially. Radial symmetry (in their study) on an average allowed for decomposition of the flow into an average field and turbulence. There is no way of studying this phenomenon using an arbitrary non-stationary flames and is left as an objective for future research.

The LEM approaches is being currently used to simulate turbulent premixed stagnation point flows. This flame is stationary and also is two-dimensional on an average. This presents one with opportunity to study, statistically, several phenomena in turbulent combustion at a lowered compututional expense. A 65x49x33 grid is being used to simulate this flow on a domain that is 70mm x 200mm in wall normal and lateral directions. The width in the third direction is set at 70mm. The inflow velocity is 5.0m/s with 10.0 percent turbulence. These parameters are being used with an aim of simulating the flames studied in [27].

With the conditions being used, the turbulent flame speed turns out to be about 4 times the laminar flame speed (for $S_l = u'$) which is unusually high. It is found that this could be reduced by decreasing the frequency of stirring (when put to zero, the LEM predicts the laminar flame speed). The reason for stirring being higher than required is that the subgrid kinetic energy that determines the frequency, is probably not being predicted correctly. The inflow subgrid is set at 0.1 times the turbulence level rather arbitrarily and this may be in error.

The increased stirring rate in LES of stagnation point flame is found to reduce the wrinkling of the flame on the supergrid. Some 3-dimensional wrinkling is nevertheless seen in fig. 15. Contours corresponding to G level of 0.5 are plotted for several locations along the homogeneous direction, in fig. 16. Instantaneous burning is found to occur in supergrid cells that are within two grid points distance from the mean position of the flame. This indicates that the LEM approach is able to capture the flame brush in just a few grid prints.

5 Conclusions

In summary, it can be concluded that the modified advection algorithm overcomes the inadequacies noted in earlier research. The linear eddy subgrid approach, in the absence of turbulent stirring, is found to model laminar flame propagation correctly. In the presence of stirring (the only non-deterministic part of the approach), it is found to also predict the turbulent flame speed with fair amount of accuracy. The trends in evolution of the spatial structure of the premixed flames are also in agreement with experimental and DNS predictions. The present approach is however limited by the G equation and the corresponding state equation for temperature. The LEM needs to be extended to flames involving real chemical kinetics in order to account for effects of thermodiffusive mechanisms. Also intended for future research is the subject of flame generated turbulence. The preliminary results from LES of premixed flames in stagnation point flames are found to be quite encouraging. In fact, this problem could provide the platform necessary for studying flame generated turbulence.

Acknowledgements

This research was supported by the NASA Lewis Research Center under Grant no. NAG3-1610.

References

1. Yakhot, V. (1988) "Propagation velocity of premixed turbulent flames", *Combust Sci. Tech.*, 60, 443-450.

2. Menon, S. and Kerstein, A. R. (1992) "Stochastic simulation of the structure and propagation rate of turbulent premixed flames", *Twenty fourth symposium (Int.) on combustion*, The Combustion Institute, 443-450.

3. Fureby, C. and Moller, S.-I. (1995) "Large eddy simulation of reacting flows applied to bluff body stabilized flames", *AIAA J.*, **12**, 2339-2347.

4. Menon, S., McMurtry, P. A., and Kerstein, A. R. (1993) "A linear eddy subgrid model for turbulent combustion: Application to premixed combustion", *AIAA paper 93-0107, AIAA 31st Aerospace Sciences Meeting.*

5. Menon, S. and Chakravarthy V. K. (1996) "Large eddy simulation of premixed flames in Couette flow",

AIAA paper 96-3077, 32nd AIAA/ASME/SAE/ASEE Joint Propulsion Conference.

6. Kerstein, A. R., Ashurst, W. and Williams, F. A. (1988) "Field equation for interface propagation in an unsteady homogeneous flow field", *Physical Review*, **A37**, 2728-2731.

7. Calhoon, W. H. and Menon, S. (1997) "Linear-eddy subgrid model for reacting large eddy simulations: heat release effects", *AIAA paper 97-0368, AIAA* 35^{th} *Aerospace Sciences Meeting*, Reno.

8. Smith, T. M. and Menon, S. (1997) "Large-eddy simulation of turbulent reacting stagnation point flows", *AIAA paper 97-0872, AIAA* 35^{th} *Aerospace Sciences Meeting.*

9. Menon, S., Disseau, M., Chakravarthy, V. K. and Jagoda, J. (1997) "Turbulent premixed flame propagation in microgravity", Proceedings of the *Fourth International Microgravity Combustion Workshop*, 155-160.

10. U. Schumann. (1975) "Subgrid scale model for finite difference simulations of turbulent flows in plane channels and annuli", J. Comp. Phys. 18, 376-404.

11. Menon, S., and W.-W. Kim. (1996) "High Reynolds number flow simulations using the localized dynamic subgrid scale model", *AIAA Paper 96-0425,* 34^{th} *Aerospace Sciences Meeting and Exhibit.*

12. Liu, S., Meneveau, S. and J. Katz (1994) "On the properties of similarity subgrid scale models as deduced from measurements in a turbulent jet", 1994, *J. Fluid Mech.*, **275**, 83.

13. Nelson, C. C. (1997) "Simulation of spatially evolving compressible turbulence using a local dynamic subgrid model", Ph.D thesis (in preparation).

14. Kerstein, A. R. (1988) "Linear eddy model of turbulent scalar transport and mixing", *Combust. Sci. Tech.*, **60**, 391-421.

15. Kerstein, A. R. (1989) "Linear eddy model of turbulent transport II. Application to shear layer mixing", *Comb. Flame*, **75**, 397-413.

16. Kerstein, A. R. (1990) "Linear eddy model of turbulent transport III. Mixing and differential molecular diffusion in round jets", *J.Fluid.Mech.*, **216**, 411-435.

17. Kerstein, A. R. (1991) "Linear eddy model of turbulent transport. Part 6:i Microstructure of diffusive scalar fields", *J.Fluid.Mech.*, **231**, 361-394.

18. Menon, S. (1991) "A new subgrid model for large eddy simulations of turbulent reacting flows",*QUEST Technical Report No. 535*, NASA Contract No. NAS2-13354.

19. Menon, S., McMurtry, P. A. and Kerstein, A. R. (1994) "A linear eddy mixing model for LES of turbulent combustion", in *LES of Complex Engineering and Geophysical flows* (Galerpin, B. and Orszag, S. ed.). Cambridge Univ. Press.

20. McMurtry, P. A., Menon, S., and Kerstein, A. R. (1992) "A subgrid mixing model for LES of non-premixed turbulent combustion", *AIAA paper 92-0234. AIAA* 30^{th} *Aerospace Sciences Meeting.*

21. Smith, T. M. and Menon, S. (1997) "One-dimensional simulations of freely propagating turbulent premixed flames", accepted for publication in *Combust. Sci. and Tech.*.

22. Smith, T. M. and Menon, S. (1996) "The structure of premixed flames in a spatally evolving turbulent flow", *Combust. Sci. and Tech.*, **119**, 77-106.

23. Yeung, P. K., Girimaji, S. S. and Pope, S. (1990) "Straining and scalar dissipation on material surfaces in turbulence: Implications for flamelets", *Combustion and flame*, **79**, 340-365.

24. Ashurst, Wm. T., Kerstein, A., Kerr, R. M. and Gibson, C. H. (1987) "Alignment of vorticity and scalar gradient with the strain rate in simulated Navier-Stokes turulence", *Phys. Fluids A*, **30**, 77-106.

25. Bradley, D., Lau, A. K. C. and Lawes, M. (1992) "Flame stretch rate as a determinant of turbulent burning velocity", *Phil. Trans. R. Soc. London. A.* **338**, 359-387.

26. Leisenheimer, B. and Leuckel, W. (1996) "Self-Generated Acceleration of confined deflagrative flame fronts", *Combust. Sci. and Tech.*, **118**, 147-164.

27. Cho, P., Law, C. K., Cheng, R. K. and Shepherd, I. G. (1988) "Velocity and scalar fields of turbulent premixed flames in stagnation flow", *Twenty second symposium (Int.) on combustion*, The Combustion Institute, 739-745.

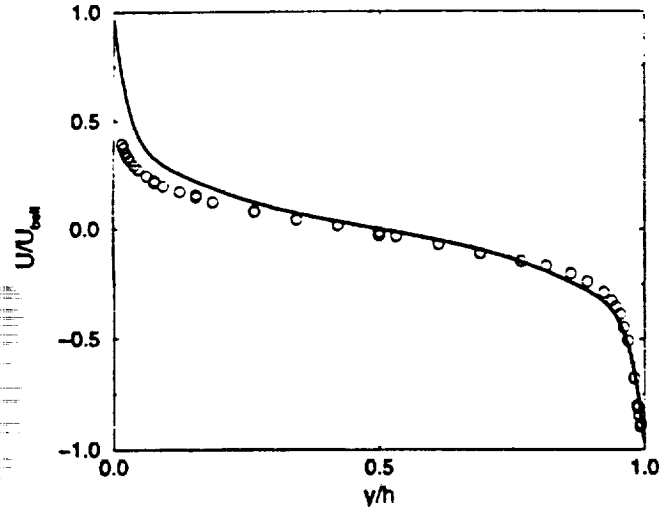

Figure.1 : Mean velocity profile in turbulent Couette flow.
Solid line : LES, symbols : experiments [9]

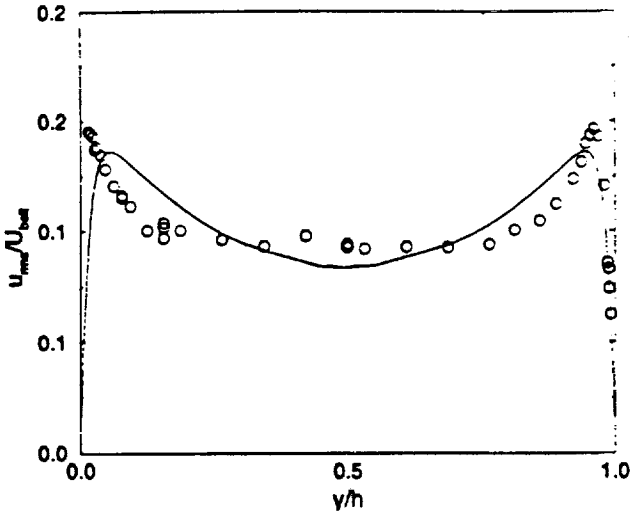

Figure.2 : Axial *rms* velocity profile in turbulent Couette flow.
Solid line : LES, symbols : experiments [9]

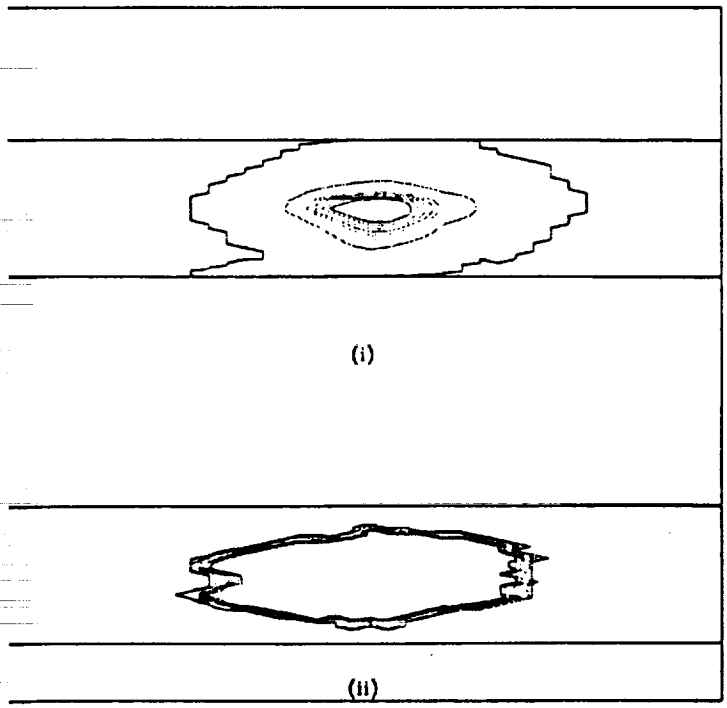

Figure.3 : G-level surface contours.
(I) Finite difference method, (ii) LEM

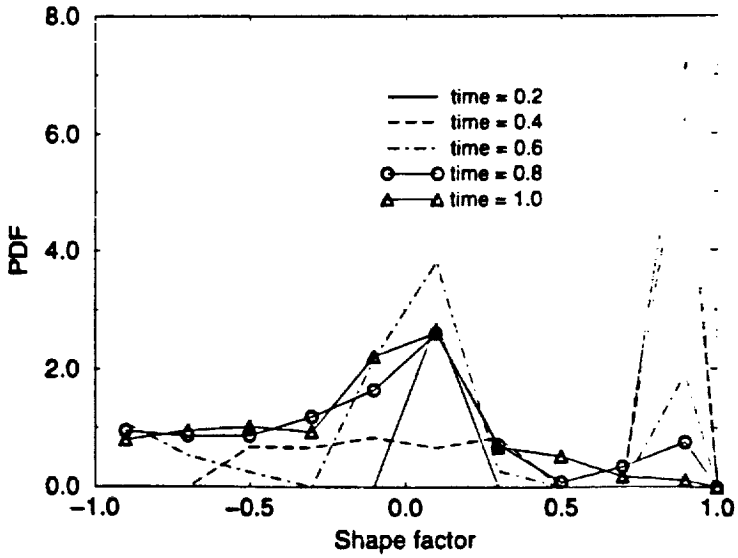

Figure.4 : LEM predicted temporal evolution of flame structure.

(i) (ii)

Figure.5 : Geometry of the flame surface.
(i) t = 0.6, (ii) t = 1.0

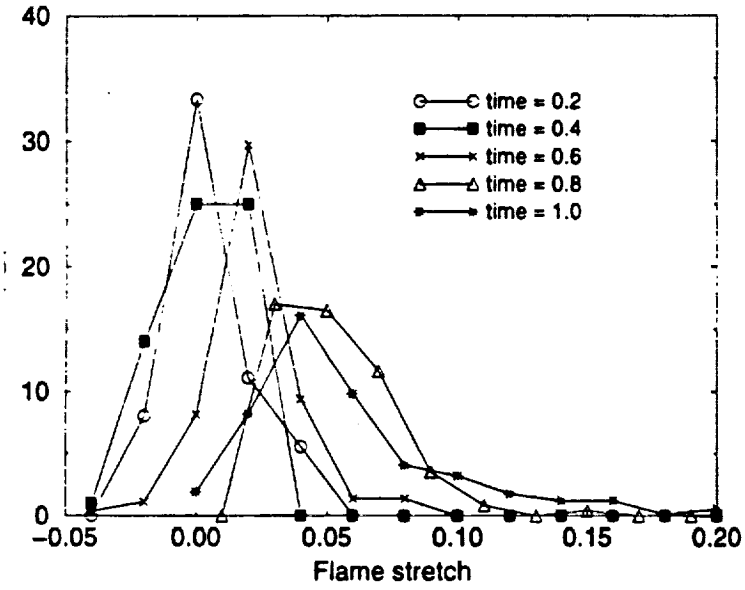

Figure.6 : Evolution of flame stretch in time.

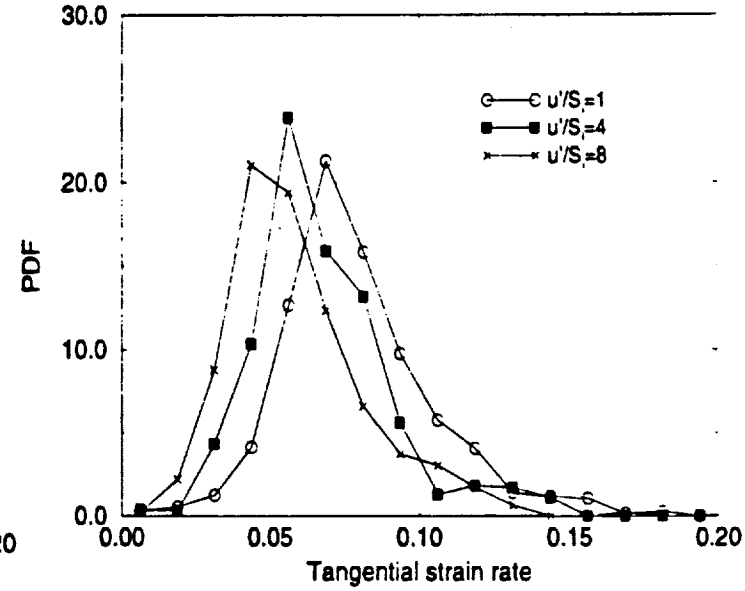

Figure.7 : Effect of laminar flame speed (relative to a constant turbulence level) on the tangential strain rate.

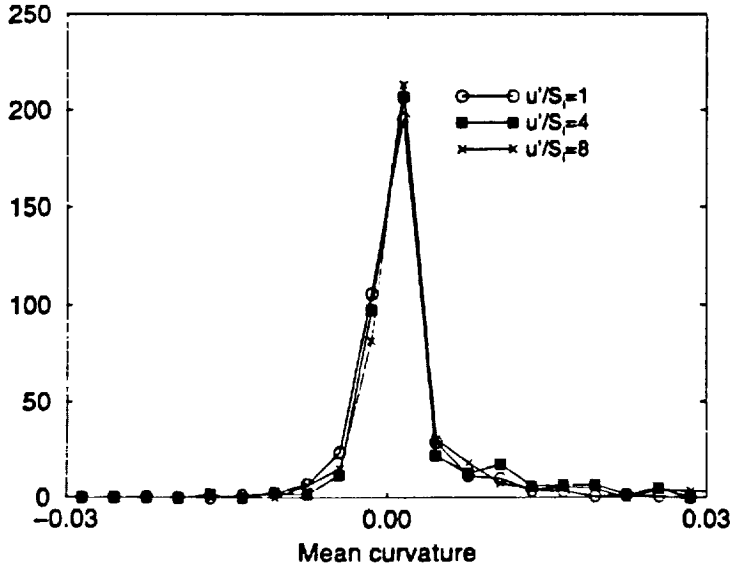

Figure.8 : Effect of laminar flame speed (relative to a constant turbulence level) on the mean curvature.

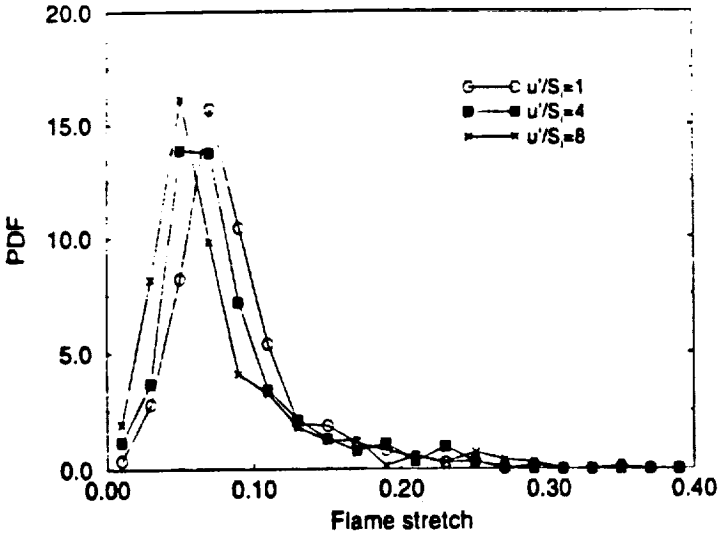

Figure.9 : Effect of laminar flame speed (relative to a constant turbulence level) on the flame stretch.

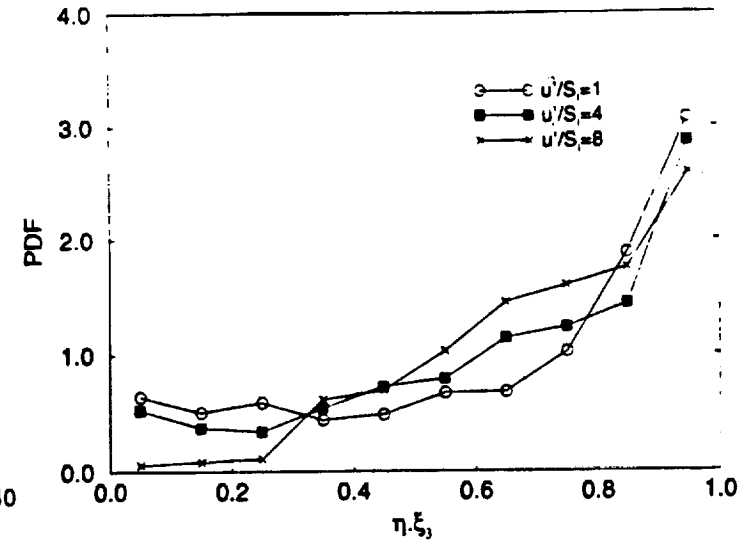

Figure.10 : Effect of laminar flame speed (relative to a constant turbulence level) on the flame normal alignment relative to the most compressive strain direction.

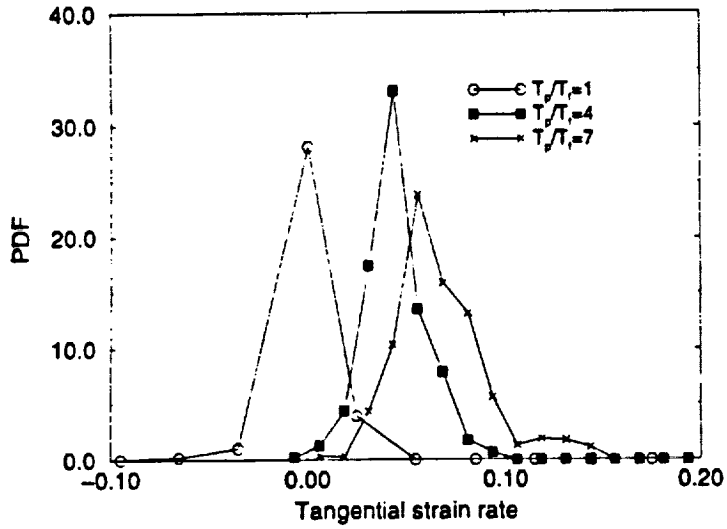

Figure.11 : Effect of heat release on the tangential strain on the flame surface.

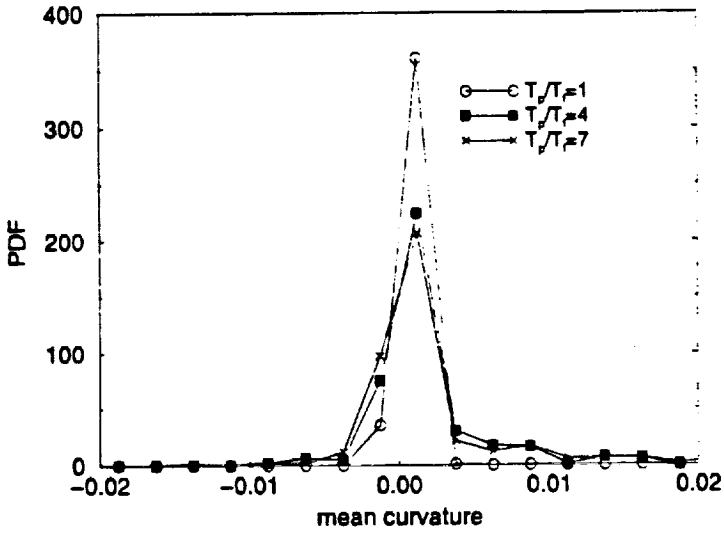

Figure.12 : Effect of heat release on mean curvature of theflame surface.

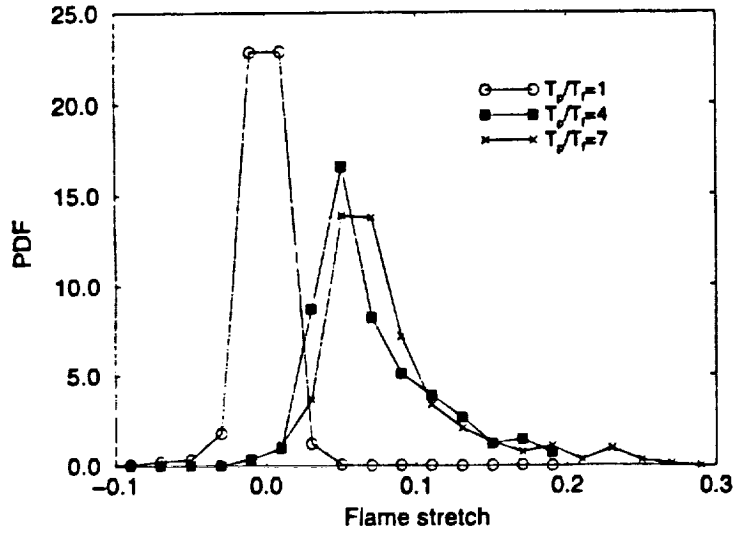

Figure.13 : Effect of heat release on flame stretch.

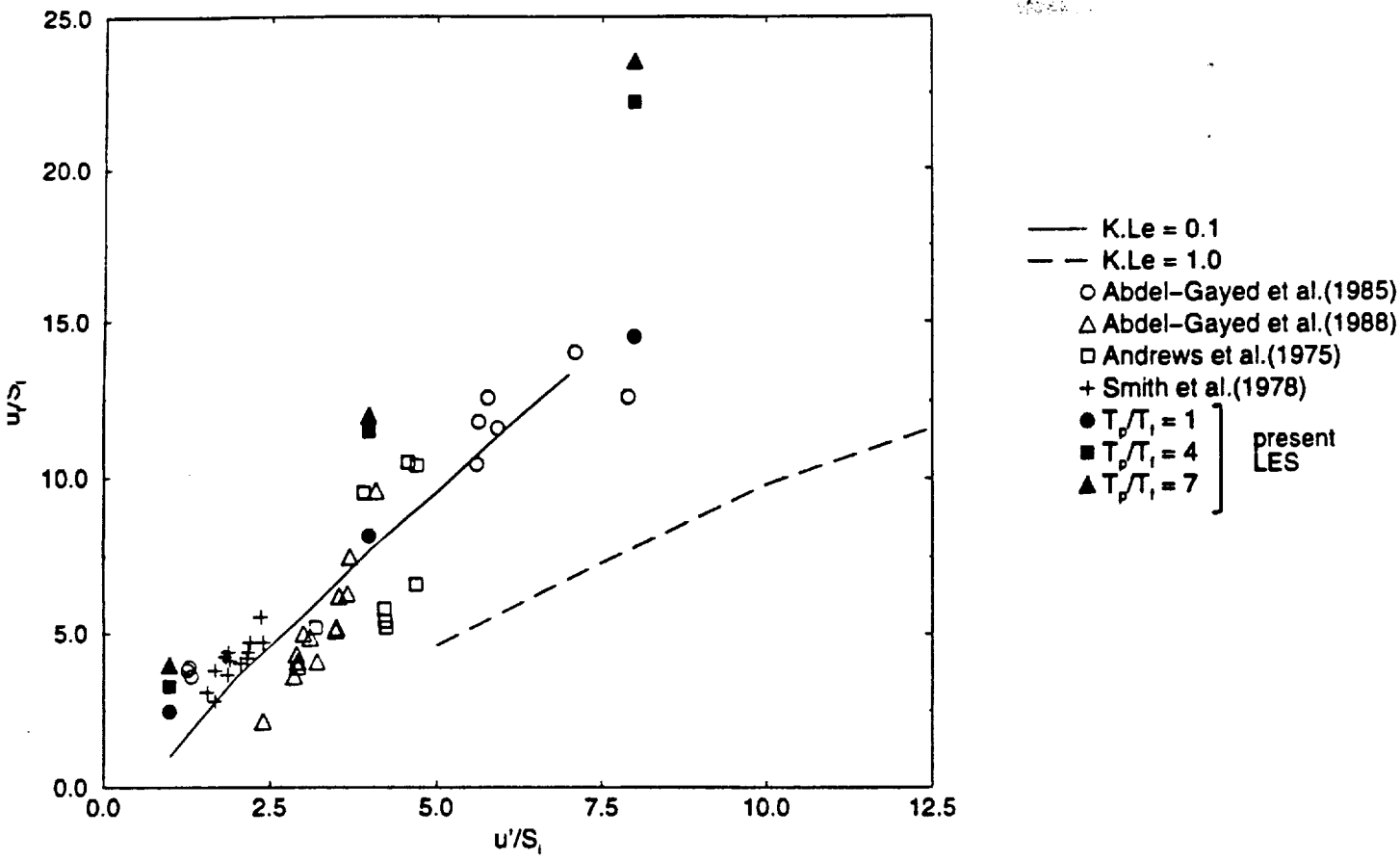

Figure.14 : Comparison of turbulent flame speed predictions with experimental data. (K = Karlovitz stretch factor [26], Le = Lewis number)

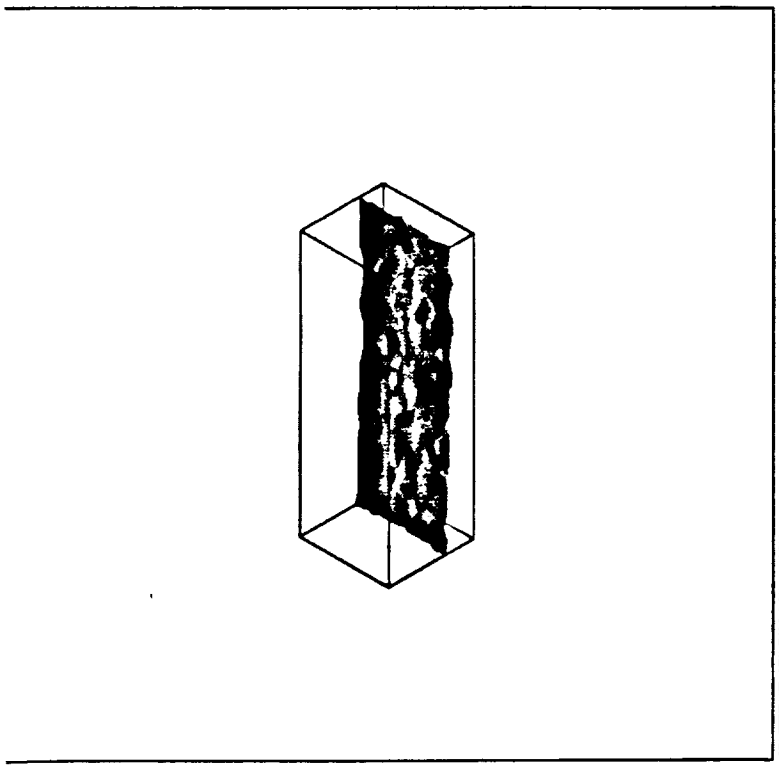

Figure.15 : 3-dimensional structure of the flame in stagnation point flow.

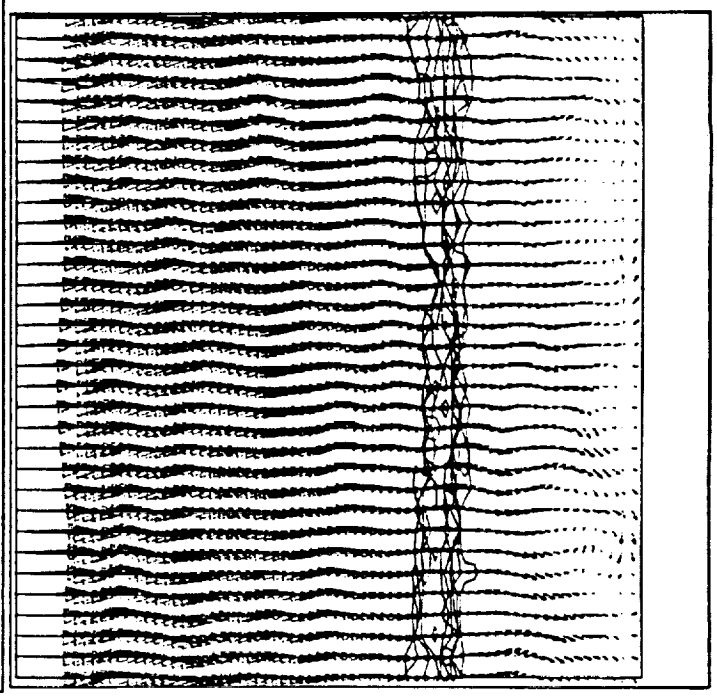

Figure.16 : Superposition of G=0.5 (flame) contours along the homogeneous direction and the instantaneous streak lines.

AIAA 97-0672

The Effect of Gravity on Turbulent Premixed Flame Propagation - a Preliminary Cold Flow Study

M. Disseau, S. Menon, J. Jagoda and R. Sujith
Georgia Institute of Technology
School of Aerospace Engineering
Atlanta, GA

35th Aerospace Sciences Meeting & Exhibit
January 6-10, 1997 / Reno, NV

THE EFFECT OF GRAVITY ON TURBULENT, PREMIXED FLAME PROPAGATION - A PRELIMINARY COLD FLOW STUDY

M. Disseau*, S. Menon†, J. Jagoda‡, and R. Sujith§
Georgia Institute of Technology
School of Aerospace Engineering
Atlanta, Georgia

Nomenclature

x, y, z = axis system (see Fig. 1)
h = height of channel
w = width of channel
L = integral scale
η = Kolmogorov scale
u' = magnitude of large scale turbulent velocity
υ = magnitude of small scale turbulent velocity
U = x component of mean velocity
V = y component of mean velocity
U_i = i^{th} component of mean velocity
$U_{wall} = U_{belt}$ = belt velocity
U_{rms} = x component of root mean square velocity
V_{rms} = y component of root mean square velocity
u_i = i^{th} component of velocity fluctuation
U^* = shear or friction velocity
C_f = coefficient of friction
$Re_h = U_{belt} h / \nu$
$Re_L = u' L / \nu$
τ_y = shear stress
τ_{wall} = wall shear stress
μ = viscosity
ν = kinematic viscosity
ρ = density
k = wave number of spectra
f = frequency of spectra
$\overline{u_i^2}(f)$ = power in frequency space, for the i^{th} velocity component
ϕ_{u_i} = spectral density

* Graduate Research Assistant - AIAA Student Member
† Associate Professor - AIAA Member
‡ Professor and Associate Chair for Research and Graduate Studies - AIAA Member
§ Now Lecturer - School of Aerospace Engineering, IIT Madras

Abstract

Turbulent premixed combustion, while of increased practical importance, is still not fully understood. A serious barrier to further progress in this area lies in the fact that at the high Reynolds numbers encountered in most turbulent reacting flows the Kolmogorov scale is too small to resolve experimentally. When tests at lower Reynolds number are run, the effects of buoyancy become important. In the present study the effect of buoyancy is removed from a turbulent Couette flow by testing it under conditions of microgravity. In the work reported here the velocity field of the cold flow under normal gravity forces was fully characterized. The feasibility of using acetone planar laser induced fluorescence to measure turbulent passive scalar diffusion was confirmed. It was determined that the full range of turbulence scales could be observed experimentally for Reynolds numbers of interest in subsequent combustion studies.

Introduction

Recently there has been a rising interest in premixed combustion because of the ability to control local temperatures, which leads to reductions in NO_x emissions. Practical premixed combustors are turbulent, however, and there are still a number of unresolved issues related to turbulent premixed combustion. This means that these types of reacting flows are not accurately predictable[1]. The overall objective of this study is to increase our understanding of turbulent premixed flames by characterizing their behavior. Particular attention will be paid to flame speeds, flame wrinkles, and flame thickness. This experimental study is being carried out in parallel with a computational study by Menon and Chakravarthy[2].

A number of important factors have to be considered when studying turbulent reacting flows. First of all it is important to have access to all the scales involved from L, the integral length scale, to η, the Kolmogorov

scale. Their magnitutes change, relative to each other, with Re_L by the relation

$$L / \eta = (Re_L)^{3/4} \quad (1)$$

This implies that for a given L, which is the case in most experimental flow fields, low Reynolds numbers ensure relatively large Kolmogorov scales, making them easier to measure. However, turbulence in practical devices is usually associated with high Reynolds numbers. An additional problem is encountered when trying to simulate a high Reynolds number reacting flow by a flow with low Reynolds number. At high Reynolds numbers large scale turbulent stresses are responsible for momentum transport. These stresses, however, can be overwhelmed by buoyancy forces in lower Reynolds number flows.

To remove the effect of buoyancy in a low Reynolds number turbulent reacting flow field a microgravity environment is required. As stated by King[3] microgravity has numerous benefits in combustion science including, but not limited to: increased scalar resolution by allowing the use of larger scales, truly one dimensional geometries, or at least geometries not deformed by buoyancy, and more uniform flames, since buoyancy is temperature dependent, and thus affects different areas of the flame differently. This enables a more accurate study of the combustion processes, which leads to an increased understanding of turbulent combustion.

A Couette flow configuration was selected to generate a turbulent flow at relatively low Reynolds numbers for this study. A Couette flow is a classical shear layer flow produced between two parallel plates moving in opposite directions each at a fixed velocity U_{wall}. This flow has the benefit that the shear stress is constant though-out the cross-section, and that the intensity of turbulent fluctuation is constant for most of the cross-section. Due to these and other characteristics, Couette flow has been widely studied over the years[4,5,6,7]. In addition, such a flow can be generated in the confined space available in the drop tower facility described below.

The NASA Lewis 2.2 Second Drop tower was chosen as the site of the microgravity experiments. This facility allows a 40.64cm by 96.52cm by 83.82cm experimental rig to experience 2.2 seconds of ~ 10^{-4}g followed by 0.2 sec deceleration (at 15 to 30 g). Due to the spatial and temporal restriction imposed by this experimental facility[8] the diagnostic techniques of choice, like laser Doppler velocimetry (LDV), cannot be used to study the flow field. To interpret the results from more basic diagnostic techniques, like OH fluorescence and Schlieren imaging, it is essential to fully understand the non-reacting flow field. Two techniques were used to date to characterize the non-reacting flow field. The velocity and shear flow field was mapped for different flow conditions using LDV. In addition turbulent diffusion of passive species are being visualized using acetone planar laser induced fluorescence (PLIF). This technique is used to measure the scales of the flow so as to determine the required resolution for future combustion visualization techniques. This paper will report the results of the cold flow study, and discuss the resulting requirements for the combustion experiments.

Experimental Facility

The experimental device used in this study is shown in Fig. 1. The device consists of a continuos Mylar belt ① which provides the "two parallel plates" moving in opposite directions. The belt runs over a series of rollers, two of which drive the belt while four are used

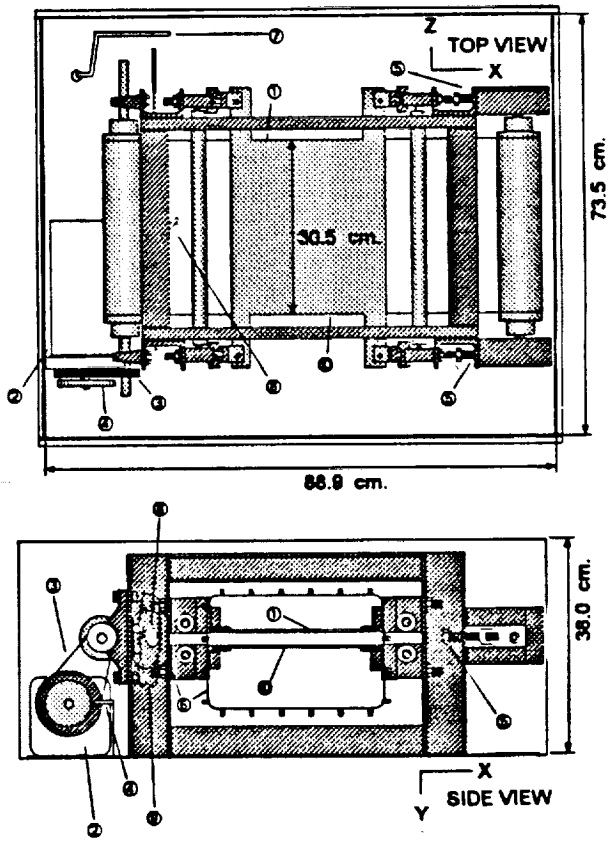

Figure 1- Current setup of the experimental device. Call-outs described in the text.

to adjust the spacing in the test section. It is driven by an adjustable DC motor ② connected to the drive roller by a set of pulleys and a v-belt ③. The rotational speed of the motor is sensed by a magnetic proximity sensor ④. Knowing the pulley ratio and the roller diameter, the speed of the belt can easily be determined. To prevent belt walking and to ease the insertion of a new belt, a set of tensioning screws ⑤ help position the far roller. The Reynolds number for the device, Re_h, can be changed by either changing the speed of the belt, U_{belt}, or by changing the belt spacing, h. The device is surrounded by a Plexiglas box to prevent any external influence on the flow without disturbing optical access to the experiment.

Because of the restrictions of the drop tower the device used in this study had to be more compact than those used in other Couette flow studies. A survey by Aydin *et al.*[4] shows that the current device has the smallest gap spacing, 2.54cm versus 3 to 12cm, the smallest length to gap ratio, 14 versus 30 to 158, and one of the smallest width to gap ratio, 12 versus 7 to 28, of air Couette devices. In addition, the current device operates in a closed loop, i.e. turbulent flow is forced to reenter the test section. Most other studies were carried in devices which, in essence, transition the flow from laminar to turbulent. As a result the flow field generated by the device developed for this study had to be extensively studied and the extent to which it deviates from an ideal Couette flow had to be documented.

The velocity flow field was mapped with a TSI 9100-7 two component laser Doppler velocimeter, which uses the 514.5nm and 488nm wavelengths of an 5 watt Ar^+ laser. After going through an expander and focusing using a 14mm aperture lens, with a 750mm focus, the probe volume was 0.13mm in diameter and 1.3mm long. The system was used in back scatter mode. The output signals were analyzed by a TSI IFA656 digital burst correlator, which can cope with lower signal to noise ratios than a traditional counter. One beam of each pair was frequency shifted by a Bragg cell to allow for measurement of negative velocities. Big central glass windows ⑥ were installed in the enclosure because it was soon discovered that the Plexiglas box absorbs too much light, and thus renders the scattered signal too faint. In order to avoid cutting off one of the two beams used to measure the velocity component normal to the belt the device was slightly tilted. The tilt angle was measured by plain geometry, using a HeNe laser as a pointer. Sub-micron TiO_2 particles were used to seed the flow. After passing though a fluidized bed, TiO_2 laden air is inserted into the device through a tube ⑦, which produces a cloud of seed around the moving belts that is then entrained into the Couette flow. This eliminates the possibility of biasing the data with artificial seeding velocities. FIND software, from TSI, was then used to statistically process the 50,000 samples obtained at each location. Data was velocity bias corrected according to the algorithm provided in FIND.

As discussed below early velocity data showed that the flow field between the belt is two dimensional. However a spectral analysis of the velocity data showed that the belt was vibrating. The vibrations were minimized by adding plates ⑩ on the outside of the belt.

Acetone PLIF is performed using a tunable Lambda Physik excimer laser running with KrF, to produce a laser pulse at a wavelength of 248nm. The beam is used to create a sheet which enteres through the quartz window ⑥. It penetrates in-between the Mylar sheets through a cut in the frame ⑨, and is turned by a mirror ⑧, to run along the mean flow direction. A micro-tube 0.254mm in diameter and with a hole cut in its side, is positioned perpendicular to the flow. Liquid acetone is introduced through the tube into the center of the flow. Here a droplet of acetone stays suspended in the flow while it vaporizes. When the excimer beam encounters the acetone vapor the latter fluoresces broadband in the blue (350-550nm), with peaks at 445nm and 480nm. The fluorescence is tracked with a Princeton Instruments Inc. intensified camera with a resolution of 384x576 pixels. At this resolution the camera can operate at a rate of two frames per second. The rate can be increased by decreasing the resolution, yielding 10 frames per seconds with a resolution of 192x288 pixels, and 20 frames per second with a resolution of 96x144 pixels.

A 55mm macro glass lens is used on the camera in order to absorb any scattered UV light from the beam. Images are background corrected to remove noise created by fluorescence due to UV scattering off parts of the device. This fluorescence is very prominent close to the belt and close to the needle. Therefore, these regions are not imaged.

Results

Velocity Field Mapping

Figure 2 shows the velocity distribution and, therefore the two dimentionality of the flow. The z/w = 0

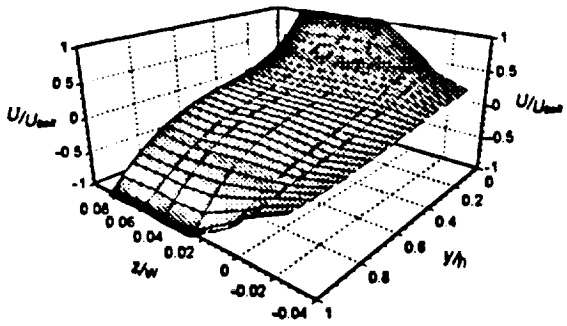

Figure 2 - Velocity distribution showing two dimesionality of the flow. This test was performed at the beginning of the project at a $Re_h = 2100$.

location corresponds to the edge of the belt. It can be seen that the velocity profile is constant for z/w up to 0.04, which corresponds to 1.2cm, from this edge. This yields a usable, two-dimensional test area that is 28.0cm wide. As a result most velocity data were obtained 2cm off-center, which gave better optical access.

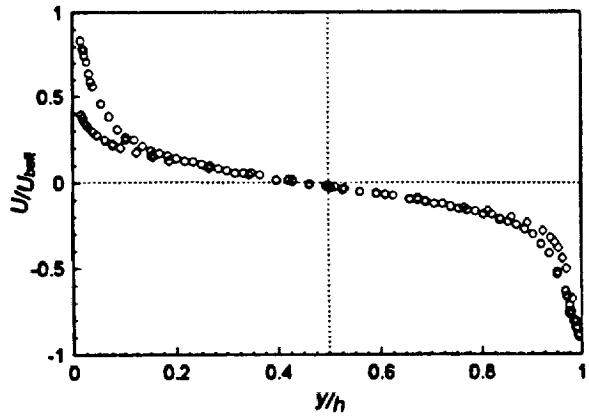

Figure 3 - Velocity distribution across the flow ◇ Re_h = 10,091, ○ Re_h = 4,366.

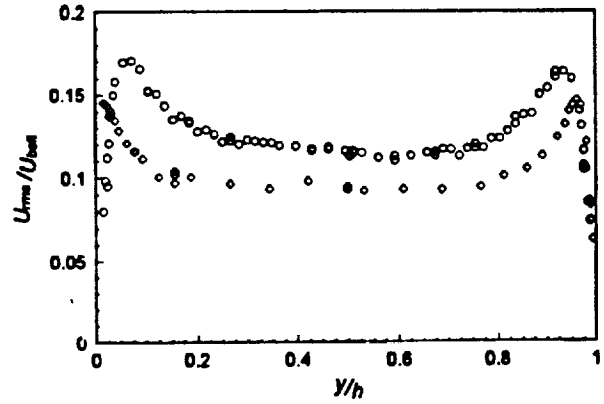

Figure 4 - Turbulent velocity fluctuation distribution across the flow: ◇ Re_h = 10,091, ○ Re_h = 4,366.

Figure 3 shows the velocity distribution across the flow field. Careful inspection of this plot shows that the velocity profile is not totally symmetric. The U component of velocity should go through zero at y/h = 0.5, but in reality it does so at y/h = 0.45. It was hypothesized that this was due to an asymmetry in the end regions where the driving rollers are located. To prove this the motor was set in reverse and, as expected, the crossing moved to y/h = 0.55. This feature does not seem to have any affect on the rms velocity as seen in Fig. 4, and as long as it is kept in mind while analyzing the combustion data, it is not deemed to be a problem.

As mentioned in the experimental section, there was a slight fluttering of the belt during early testing. This flutter was not visible to the naked eye, but was detected by frequency analysis of the velocity spectrum. A non-excited frequency spectrum should decay smoothly. The excited frequency spectrum that was encountered had peaks in the 100 Hz region, as shown in Fig. 5. A microphone was placed in the flow to check whether corresponding pressure oscillations

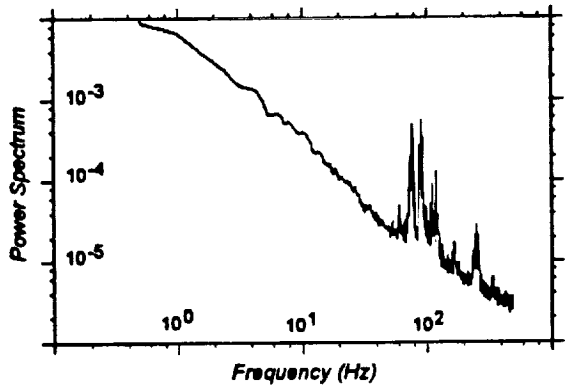

Figure 5 - Frequency spectrum for the case without plates.

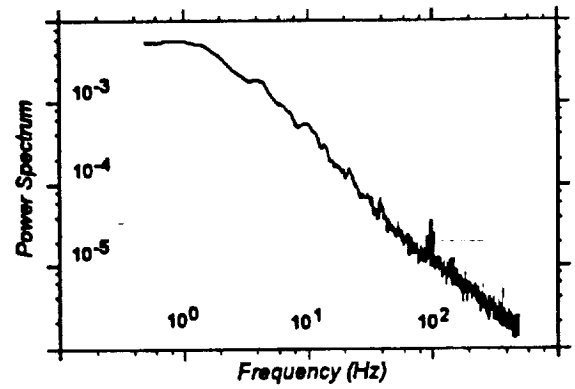

Figure 6 - Frequency spectrum for worst case with plates.

were encountered at that frequency, and they were. These oscillation were increasing the turbulence intensity, but their frequency was dependent on the belt tension, which could not be accurately measured or reproduced. Thus this situation was deemed unacceptable. With the plates in position the fluctuation were almost stopped completely. Figure 6 shows the worst case encountered where the oscillations were not fully damped.

To discuss the results further the following quantities have to be introduced. The shear stress τ_{ij} is given by

$$\tau_{ij} = \mu\left(\frac{\partial U_i}{\partial x_j} + \frac{\partial U_j}{\partial x_i}\right) - \rho\left(\overline{u_i u_j}\right) \qquad (2)$$

The first term represents the viscous stresses and the second represents the Reynolds stresses. In a pure Couette flow the shear stress is constant; though the Reynolds stresses are mainly concentrated in the center of the flow, and the viscous stresses are mainly present near the wall. Another useful quantity is the shear velocity U^*

$$U^* = \left(\frac{\tau_{wall}}{\rho}\right)^{1/2} \qquad (3)$$

The velocity and positions in the flow field are commonly non-dimesionalized as follows:

$$U^+ = \frac{U}{U^*} \quad V^+ = \frac{V}{U^*} \qquad (4)$$

$$U^+_{rms} = \frac{U_{rms}}{U^*} \quad V^+_{rms} = \frac{V_{rms}}{U^*} \qquad (5)$$

$$y^+ = \frac{yU^*}{\nu} \qquad (6)$$

Figure 7 shows U^+ as a function of y^+. The data clearly show the expected behavior for a wall bounded shear flow. The flow can be divided into two regions[10], the viscous sublayer ($y^+<5$), and the inertial sublayer ($30<y^+<1000$). The flow correlates well with the linear behavior at the wall in the viscous sublayer. The logarithmic behavior in the inertial sublayer is also clearly present. However the data at different Reynolds numbers do not exactly collapse into one single line when non dimesionalized, as predicted by theory and seen by others. This is probably due to the smaller dimensions and re-circulating nature of the present device.

Figure 8 shows U_{rms}^+ and V_{rms}^+ as functions of non-dimensional distance from the belt. As expected, U_{rms}^+ has a turbulence peak close to the wall before it reaches a uniform distribution in the core, and V_{rms}^+ gradually increases to a uniform distribution in the core. Figure 9 shows how velocity fluctuations vary

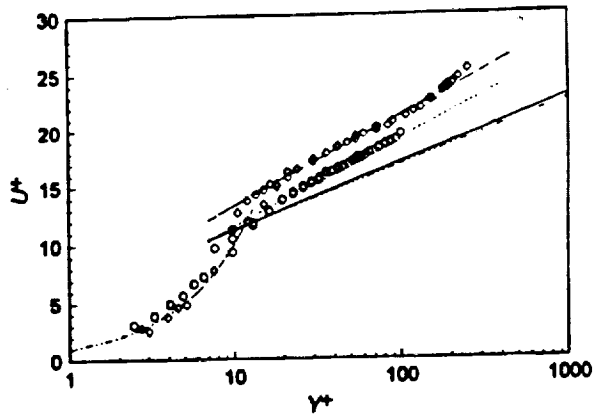

Figure 7 - Non-dimensionalized mean flow velocities and their curve fits: ◇ Re_h = 10,091, ○ Re_h = 4,366, -·- $Y^+ = U^+$, — $U^+ = 5.4 + 3.4\ln Y^+$ and ·· $U^+ = 3.9 + 3.3\ln Y^+$ for present study; -- $U^+ = 5.2 + 2.55\ln Y^+$ for El Telbany *et al.*[6]; -·- $U^+ = 5.6 + 2.43\ln Y^+$ for Robertson *et al.*[7]; and — $U^+ = 5.5 + 2.5\ln Y^+$ for Aydin *et al.*[4].

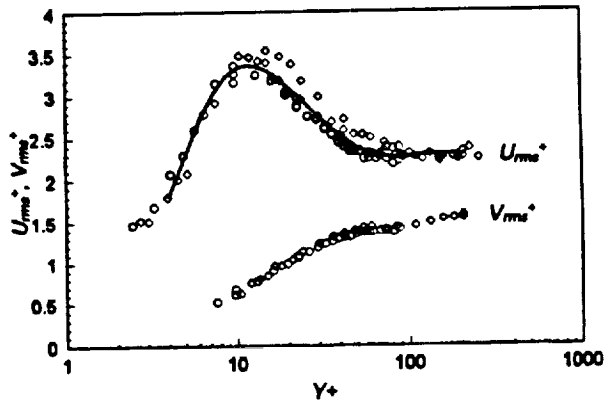

Figure 8 - Non- dimensionalized turbulent velocity fluctuation for present study: ◇ Re_h = 10,091, ○ Re_h = 4,366.

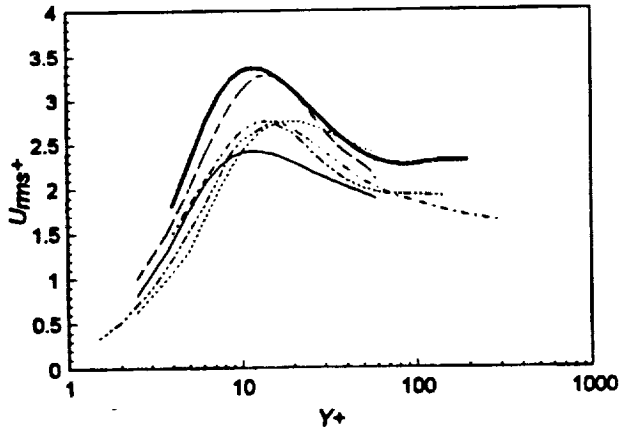

Figure 9 - Non-dimensionalized turbulent velocity fluoctuation: -·- Aydin *et al.*[4], — Clark[9], ·· El Telbany *et al.*[6] — Hussain *et al.*[6], -- Robertson *et al.*[4], — present study.

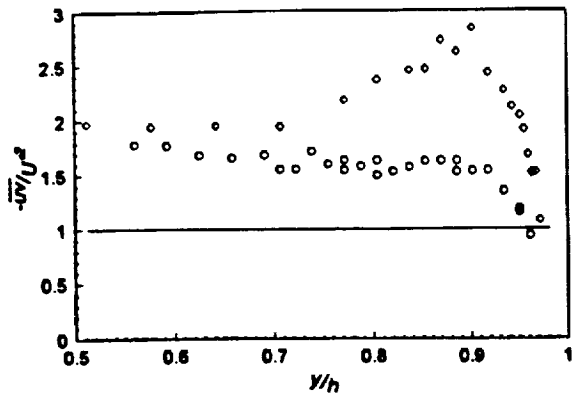

Figure 10 - Non-dimensionalized Reynolds stresses for present study: : ◇ Re_h = 10,091,and ○ Re_h = 4,366.

for different devices. Except for Clark's device, which was actually not a Couette, but a channel flow, it would seem that the flow in this device is more turbulent than those in other devices. This feature is also seen by looking at the Reynolds stresses.

It is convention to non-dimensionalize Reynolds stresses by U^{*2}. Inspection of Equations (2) and (3), and the velocity profile, shows that in theory the non-dimensional Reynolds stress should level out at a value of 1. Figure 10 shows that in this flow the turbulent stresses are higher then expected in a pure Couette flow. This is an advantage in this case since higher turbulence is produced at lower Reynolds numbers. In addition, a peak in Reynolds stress near the wall is seen at the higher Reynolds number. Such a peak has not been reported anywhere in the literature.

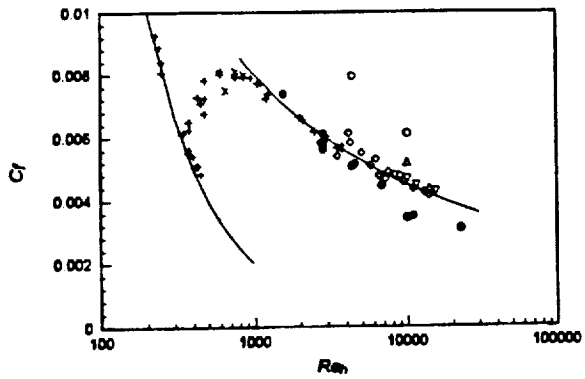

Figure 11 - Coefficient of Friction: + Couette in water[7], × Couette in air[7], △ Robertson in air (center)[7], ▽ Robertson in air (wall)[7], ◇ Robertson and Johnson in air[7], ● present study in air (wall), and ○ present study in air (center).

A way of quantifying the shear stresses is by measuring the coefficient of friction.

$$C_f = \frac{\tau_{ij}}{\frac{1}{2}\rho\, U_{wall}^2} \tag{7}$$

In general the coefficient of friction is more meaningful at the wall, and thus usually represents the viscous stresses. Since in pure Couette flow there is a uniform shear, the coefficient of friction measured at the center is supposed to yield the same approximate answer as the coefficient of friction measured at the wall. Figure 11 shows the coefficient of friction measured in this device compared to those in previous investigated Couette flows. C_f calculated from the center measurements of shear stress for this flow field are higher than the ones calculated at the wall. This is due to the higher than expected Reynolds stresses. Deviations from more ideal Couette flow are, once again, probably due to the recirculating nature of the flow in this compact device.

A parallel computational study of this flow assumes the existence of an inertial range in which the flow follow the $k^{-5/3}$ law. The experimental validation of this assumption requires the determination of a wave number spectra for this flow. Since LDV measurements are single point, wave number spectra can only be obtained from frequency spectra using Taylor's hypothesis[11]. One of the criteria for Taylor's hypothesis to hold is that $U/U_{rms}>>1$. This is clearly not the case, in what can be considered the inertial range of this device. However, it might still be interesting to examine the wavelength spectra to obtain some qualitative information, while keeping in mind the assumptions made in calculating the spectra.

Following Taylor's hypothesis a wave number can be defined as follows[9]:

$$k_1 = \frac{2\pi f}{U} \tag{8}$$

The absolute value of spectral density in wave number space is given as:

$$\phi_{u_u} = \frac{f}{k_1 y}\frac{\overline{u_1^2(f)}}{U^*} \tag{9}$$

If one now plots ϕ_{u_u} versus $k_1 y$, where y is the position from the wall, one can look at spectra for different regions in the flow and note which ones follow the $k^{-5/3}$ law.

Figure 12 shows $\phi_{u_{11}}(k_1)$ and $\phi_{u_{22}}(k_1)$ versus ky for different regions in the flow. These velocity spectra are for the case of Re_h=10,091. The U, and V spectra for

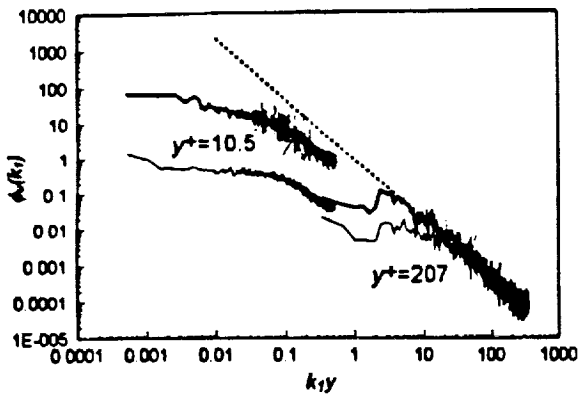

Figure 13 - Wave number spectral analysis: $\phi_{u_{11}}(k_1)$ $\phi_{u_{22}}(k_1)$, $k^{-5/3}$.

the y^+= 207 location follow the inertial layer law, but those for the y^+ = 10.5 location do not. As a matter of fact the inertial behavior can only be seen in spectra for the $y^+ > 60$ locations, which correspond to the region of constant U_{rms}. Thus the assumption of the existence of an inertial layer necessary for the parallel computational study is valid in the region of interest.

Visualization of Turbulent Diffusion

The hypodermic needle carrying the acetone drop was placed below the centerline where the flow runs from right to left. The fluorescence of the acetone in the region to the left of the needle was recorded. Flow in the lower half of the picture is expected to be acetone laden, while flow in the upper half of the picture is expected to be free of acetone. Figure 13 shows a snapshot of the resulting turbulent diffusion process. The light marking correspond to the presence of acetone. As expected high concentration of acetone is seen in the lower half of the image. Some large scales structures can be seen in this picture. It is not certain whether these are Couette flow structures or whether vortices are shed off the acetone supply line. The Reynolds number based on the diameter of the needle is of the order of 10, thus it is safe to assume that the needle does not produce structures. However the Reynolds number associated with the droplet is of the order of 150, thus making it very possible for it to shed vortices.

For the feasibility study reported here, the fluorescence measurements of acetone were carried out under steady conditions. In order to better determine the influence of turbulent passive scalar diffusion processes, it will be necessary to observe the leading edge of the acetone as it begins to diffuse into the flow. This will require a higher framing rate and a more sophisticated timing of the injector and camera, which are under preparation. However, the test reported here did show that it is possible to visualize diffusion in this flow using acetone PLIF.

Considerations on the Resolution of Scales

One of the premises of this study was the need to have access to a wide range of scales, to allow a better understanding of the turbulent combustion process. It is, therefore, important to consider the ability of the cold flow study to resolve these scales. As mentioned in the introduction L, the integral length scale, can be approximated as the significant length scale in the flow, which in this case is the belt spacing, h, and equals 25.4mm. The Kolmogorov scale, η, can be calculated from Equation (1) where the Reynolds number is determined from the turbulent velocities measured in the core of the flow. They were found to be 0.23mm for the Re_h = 4,366 case and 0.13mm for the Re_h = 10,091 case.

Considerations for LDV: The integral length scale can definitively be resolved by measuring full traverses with the LDV. The Kolmogorov scale, on the other hand needs to be more carefully considered. The seed particle size is sub-micron, much smaller than η, while the LDV probe volume is of the order of the η. This implies that the scale can just be spacially resolved during two point correlation measurements. However smaller scales may be temporally resolved. Since the scales are moving, residence time inside the probe volume is a more accurate measurement of scale resolution. The velocity of the scale can be estimated by using the relation between Kolmogorov velocity scale and the magnitude of turbulent velocity:

$$u'/v = (Re_L)^{1/4} \qquad (10)$$

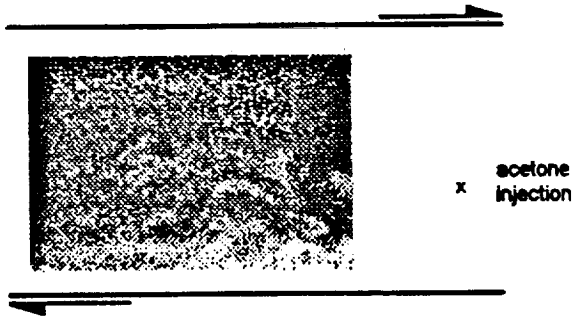

Figure 12 - Picture of acetone PLIF signal. The light regions correspond to the presence of acetone in the flow. To the right of the picture is acetone injection system The arrows correspond to direction the belt is moving in.

Based on the probe volume dimensions and Equation (10) a residence time and, therefore, a frequency can be calculated to be 590Hz for the Re_λ = 4,366 case and 1,030Hz for the Re_λ = 10,091 case. This means that the data rate for the LDV should be grater than 2,060Hz to resolve Kolmogorov scales temporally. Because of the high noise levels in the system, this is difficult to achieve. It thus requires considerable attention to alignment and seeding to obtain information on the smallest scales in the flow.

Consideration for PLIF: Again the integral length scale can be resolved without a problem. On the other hand, the full resolution of the camera combined with the macro lens used yields a pixel dimension of 0.05 mm squared. This results in approximately 3 x 3 pixels per Kolmogorov scale, for Re_λ= 10,091, and 5 x 5 pixels per Kolmogorov scale for Re_λ = 4,366. Decreased resolution to achieve higher frame rates would of course decrease these estimates. However, reduced areas of interest can be viewed with higher magnification lenses, which would increase the resolution significantly.

Combustion Considerations

The wrinkledness of a turbulent premixed flame depends upon the ratio between the turbulent velocity fluctuation and the laminar flame speed. In the Re_λ = 10,091 flow the core has a U_{rms} of 0.75 m/sec, which is 4 times bigger than the laminar flame speed for lean limit methane air combustion. Since this Reynolds number also lies at the limit of the Kolmogorov scale resolution, most test will be carried out under this flow regime.

Conclusions

A facility in which Couette like, non-reacting and reacting flows could be generated in a microgravity environment was designed and built. To fit into the NASA Lewis drop tower the device has to be very compact. This means that edge effects and flow re-circulation were expected to affect the flow.

The flow field was thoroughly investigated using laser Doppler velocimetry. The flow was found to be largely two dimensional with constant turbulence intensities near the core. Slight flow asymmetries are introduced by the non symmetric re-circulation of the fluid outside the test region. Belt flutter problems were remedied by adding a pair of guide plates to the belt. In general the flow field was found to be quite similar to previously investigated Couette flows. However, turbulence levels and associated shear stresses were higher. This is probably due to the confined re-circulation zone reintroducing turbulence into the test section.

The feasibility of measuring turbulent scalar diffusion in the Couette flow was confirmed by suspending droplets of acetone and visualizing their acetone vapor as it diffuses in the flow by planar laser induced fluorescence. Turbulence scales were compared with the spatial and temporal resolution of the experimental techniques and it was determined that for Reynolds numbers of about 10,000 structures down to the Kolmogorov scale could be resolved.

Acknowledgments

This Research was sponsored by a grant (No. NAG 3-1610) from the NASA Lewis Research Center,. The authors wish to recognize the support provided by the staff of the Aerospace Combustion Laboratory at Georgia Tech, by Dr. J. Seitzman, and by Dr. P.K. Yeung.

References

1. Williams, F.A., *Combustion Theory*, 2nd Ed., Addison-Wesley, New York, 1985, pp. 411-437.

2. Menon, S., and Chakravarthy, V. K., *Large-Eddy Simulations of Premixed Flames in Couette Flow*, 32nd AIAA/ASME/SAE/ASEE Joint Propulsion Conference, Lake Buena Vista, FL, July 1996.

3. King, M.K., "Overview: NASA Microgravity Combustion Science Program," *Proceedings of the Third international Microgravity Combustion Workshop*, 1995, pp. 3-8.

4. Aydin, E. M., and Leutheusser, H. J., "Plane-Couette flow between smooth and rough walls," *Experiments in Fluids*, Vol. 11, 1991, pp. 302-312

5. Bech, K.H., Tillmark, N., Alfredsson, P.H., Andersson, H.I., " An Investigation of Turbulent Plane Couette Flow at low Reynolds Numbers," *Journal of Fluid Mechanics*, Vol. 285, 1995, pp. 291-325.

6. El Telbany, M.M.M., Reynolds, A.J., "The Structure of Turbulent Plane Couette Flow," *Journal of Fluids Engineering*, Vol. 104, 1982, pp. 367-372.

7. Robertson, J. M., and Johnson, H. F. (1970), "Turbulence Structure in Plane Couette Flow," *J. Eng. Mech.*, Proc. of Am. Soc. of Civil Engg., Vol. 6, pp. 1171-1182.

8. Lekan, J., Gotti, D.J., Jenkins, A.J., Owens, J.C., Johnston, M.R., "User Guide for the 2.2 Second Drop Tower of the NASA Lewis Research Center," *NASA Technical Memorandum 107090*, 1996.

9. Clark, J.A., "A Study of Incompressible Turbulent Boundary Layers in Channel Flow," ASME *Journal of Basic Engineering*, Vol. 90, 1968, pp.455-468.

10. Pope, S.B., *Turbulent Flows (Draft of Chapter 1-7)*, to be published, pp. 249-274.

11. Hinze, J.O., *Turbulence*, 2nd edition, McGraw-Hill, New York, 1987, pp.44-48.

AIAA 96-3077
Large-Eddy Simulations of Premixed Flames in Couette Flow

S. Menon and V. K. Chakravarthy
School of Aerospace Engineering
Georgia Institute of Technology
Atlanta, Georgia

32nd AIAA/ASME/SAE/ASEE
Joint Propulsion Conference
July 1-3, 1996 / Lake Buena Vista, FL

Large eddy simulation of premixed flames in Couette flow*

S. Menon† & V. K. Chakravarthy ‡
School of Aerospace Engineering
Georgia Institute of Technology
Atlanta, GA 30332-0150

Abstract

Large eddy simulations in a wall bounded domain are conducted in order to study the kinematic structure of premixed turbulent flame. The linear eddy model presents a prospect of isolating the effects of each of the physical mechanisms that underly turbulent combustion. In the present study, we investigate the flame structure in the absence of thermodyamic effects such as heat release using this model and compare the results to predictions arrived at using Yakhot's model. The momentum transport is modeled using an eddy viscosity approach based on the dynamic subgrid kinetic energy equation. The LEM approach is found to be fairly accurate in non-homogeneous shear flows such as the Couette flow. It is found that the effects of turbulence on the flame geometry are modeled well using this approach. The model however, needs to modified for the limiting case of near laminar propagation in regions of space with little or no turbulence.

1 Introduction

The main goal of large eddy simulation (LES) is to simulate the large scale structure of the flow by accounting for the small scale effects using a model. Dissipation of kinetic energy is the only physical phenomenon of importance in non-reacting flows that occurs at small scales. Separating these small scales and the large scales (of the size of the characteristic geometric length in the flow) is the inertial range which acts purely as an energy cascade for supplying kinetic energy to the small scales from the large scales. The near universal behavior of the inertial range along with the assumption of local isotropy in this range have been used to model turbulent flows using the eddy viscosity assumption. However, modeling of these small scale effects in scalar mixing/reactions is more complicated than in momentum transport, posing a bigger challenge in the field of continuum studies. There are various forms of scalar spectrum in the inertial and dissipative ranges depending on the local Schmidt number (or Prandtl number). Similar parameterization of scalar mixing using an eddy diffusivity, however, often seems to fail especially if the scalar is not passive. If the fluid is reacting, there are phenomena like the molecular mixing and chemical reactions occuring at smallest of the scales (Kolmogorov and Batchelor scales). These need to be adequately modeled within the constraints of available computational resources.

Computational approaches in mixing studies, in most cases, can be classified into two groups: moment methods and the probability density function(PDF) methods. In moment methods, the flow variables are decomposed into mean and fluctuating components. The numerical procedure involves solving for the mean values and a few lower moments (correlations) of chemical and fluid dynamic quantities. A comprehensive account on this method can be found in Ref[1] (Patterson, 1981). In the PDF approach, the objective is to arrive at the PDF of the chemical quantities. This approach is outlined in Ref[2](Pope, 1985).

In moment methods, the reaction rate terms and the turbulent stirring term need to be modeled. Because of the nonlinearity of the reaction rate term, one needs a good global mechanism to cut down on the cost. Fast kinetics (infinite rate) further allow for reasonable approximations which seem to be valid for some hydrocarbon reactions. The turbulent fluxes are modeled using a gradient diffusion assumption. The turbulent diffusivity is obtained using passive scalar transport theories, which do not account for thermodynamic effects like heat release. Hence, the gradient diffusion assumption, while adequate for passive scalar transport, fails in case of reacting flows. Furthermore, in many practical engineering systems, combustion takes place in a regime of parameter space called the

† Associate Professor, Senior Member, AIAA.
‡ Graduate Research Assistant.

corrugated flamelet zone. In this region of parameter space, the flame is wrinkled by turbulence but the local burning is laminar. The turbulent flame is an ensemble of local laminar flamelets whose size spans over several decades of length scales. Hence, there are reaction zones that occur with characteristic length scales extending to such small values that molecular diffusion becomes very significant. The molecular diffusion is what causes the local laminar propagation. However, in the moment methods, the effects of molecular diffusion cannot be captured adequately. Further, the moments chosen that are used to characterize the chemistry in a flow field are arbitrary. It cannot be based on numerical values of these moments because some moments, while insignificant in terms of quantities, need to be predicted accurately (eg. NO_x emissions).

In PDF methods, the solution is arrived at, in either of the two ways: evolve a PDF in time using a dynamic equation or assume a specific form for the PDF in terms of a few parameters and predict their values by modeling. The assumed PDF method was extended for LES by Frankel et al. (1993). Gao and O'Brien (1993) suggest solving the PDF evolution equation (Pope 1990) for LES. Their work is far from complete and needs further development. The PDF methods have one main advantage that the chemical reaction term is closed. Molecular diffusion needs to be modeled and is usually done using variants of the coalescence-dispersion models. This aspect is the subject of ongoing research and at the present day greatly limits the capability of the PDF models.

When the reaction system is dominated by one physical phenomenon, there are several models that work well. Yakhot's model[6], Fractal models[7](for premixed combustion with low or no heat release) that concentrate on the kinematic structure of the flame and characterize the model in terms of incoming turbulence, Fureby and Moller model[8] which uses the turbulent reaction rate based on local turbulent and chemical time scales, are a few examples. Such models are far from representing the correct physics in many cases and are approaches suitable for case based model development studies.

A field equation for interface propagation [9] called the G-equation is used in this scalar transport study. This model was used earlier by several researchers to study the structure of a self propagating front in unsteady flow fields [9]. When the self-propagation speed is set equal to the laminar flame speed, any level surface of this scalar in space could be considered a cold flame. The primary advantage of the G-equation approach is the explicit inclusion of the flame speed in the equation, thereby avoiding the need for solving the finite rate kinetics in multiple scalar equation.

Using the G-equation as representative of all the chemistry, the kinematic structure of premixed flames in a wall bounded shear flow is investigated. A linear eddy model [18] is used to model the subgrid combustion related processes and a subgrid kinetic energy equation model with dynamic evaluation of the model coefficients is used as the subgrid model for momentum transport. A turbulent Couette flow is chosen for the present study, because it has a wide core region with near constant values of *rms* velocity fluctuations. The turbulent intensity is then nearly constant in this region and when the flames are contained in here, the near constant value of the turbulence intensity can be used as a reference value for characterization of the results. All level G-surfaces enclosed fully in this region are considered to be flames and this gives several realizations of the flame to collect statistics over. The linear eddy model(LEM) is capable of accounting for the thermodynamic effects such as volumetric dilatation, viscosity variation with temperature etc. Heat release and finite rate chemical kinetics can be accounted for in this subgrid model in a deterministic way which makes stochastic part of the algorithm more crucial. So, we choose to investigate the LEM predictions of the kinematic structure of the flame using cold chemisty model. The results are compared to predictions from conventional LES using the Yakhot's model (which is known to predict reasonably correct values of the turbulent flame speed for $\frac{u'}{S_l}$ between 1 and 10). Here, u' is the turbulent intensity and S_l is the laminar flame speed.

An outline of the numerical and the LES model method are provided in section 2 and section 3 respectively. The linear eddy model is formulated in section 4. In section 5 are discussed the results from this study and the possible directions for future research are proposed.

2 Numerical method

The Navier-Stokes equations, on convolution with a spatial filter, reduce to the following set of LES equations.

$$\frac{\partial \overline{U}_i}{\partial x_i} = 0 \tag{1}$$

$$\frac{\mathrm{d}\overline{U}_i}{\mathrm{d}t} = -\frac{\partial \overline{p}}{\partial x_i} + \nu \frac{\partial^2 \overline{U}_i}{\partial x_k \partial x_k} + \frac{\partial \tau_{ij}}{\partial x_j} \tag{2}$$

where the overbar indicates a filtered variable, $\tau_{ij} = (\overline{U_i\ U_j} - \overline{U_i U_j})$ is the subgrid stress. For a closed set of

quations , one needs to approximate the subgrid stresses ısing a model. The velocity variations in the scales below he characteristic filter width Δ are unresolved in a LES. Due to the nonlinear nature of the Navier-Stokes equations, hese small scale fluctuations effect the large scale motions. This effect comes from the subgrid stress, which in the resent study is approximated as $\tau_{ij} = -\frac{2}{3}K\delta_{ij} + 2\nu_t\overline{S_{ij}}$, here $\overline{S_{ij}} = \frac{1}{2}\left[\frac{\partial\overline{U_i}}{\partial x_j} + \frac{\partial\overline{U_j}}{\partial x_i}\right]$ is the resolved strain tenor, ν_t is subgrid eddy viscosity (to be defined later) and $K = -\frac{1}{2}(\overline{U_i}\ \overline{U_i} - \overline{U_iU_i})$ is the subgrid kinetic energy. Filered variables are also called supergrid variables because hey carry information about a variables at all length scales bove the filter width (grid spacing). The model equations or the subgrid kinetic energy and the eddy viscosity are resented in the next section. The equations are discretized n a non-staggered grid (with spacing corresponding to the haracteristic filter width Δ) and numerically integrated usng a two step semi-implicit fractional step method. In this nethod, all of the primitive variables are defined at the grid oints. The well known checker board type oscillations ocur in velocity field due velocity-pressure decoupling when ne uses central finite difference schemes for approximating he spatial derivatives. Use of QUICK scheme for calcuation of velocity gradients that arise in the source term f the elliptic equation for pressure is found to effectively ouple the velocity and pressure fields thus removing these scillations [10]. The convective terms are computed using third-order upwind biased finite difference approximation hile the viscous terms are computed using a fourth-order entral difference approximation. The Poisson equation is olved numerically using a second order accurate elliptic olver that uses a four-level multigrid scheme to converge he solution. The finite difference equations are integrated n time using a second order scheme.

The G-equation discussed earlier, has the following form.

$$\frac{\partial G}{\partial t} + u_j\frac{\partial G}{\partial x_j} = S_l|\nabla G| \tag{3}$$

nd G lies between two constant values. When using akhot's model for LES, the advection velocity in the above quation if replaced by filtered velocity and the laminar lame speed by the turbulent flame speed. The Renormalzation Group theory [Yakhot,1988] provides the following xpression for the turbulent flame speed u_t.

$$\frac{u_t}{S_l} = exp\left[\frac{u'^2}{u_l^2}\right] \tag{4}$$

here u' here, is the *rms* of (incoming) subgrid velocity field (can be estimated using the subgrid kinetic energy). The numerical scheme used to calculate the gradient in the propagation term of eq.(3) is biased in the direction of maximum gradient.

3 LES Model

A K-equation model with dynamic evaluation of the model coefficients based on the Germano's filtering approach [11], is used as the subgrid model. The advantage of this model is that it solves a single scalar equation for the subgrid kinetic energy which characterizes the velocity scale of subgrid turbulence. This velocity scale along with the length scale (grid spacing or the filter width) provides a subgrid timescale representing the non-equilibrium relaxation of the subgrid scales. This is one level higher (in the direction of developing non-equilibrium models) than the equilibrium models (algebraic or the zero equation models), wherein the production and dissipation of the subgrid kinetic energy are assumed to balance instantaneously.

Menon and Kim [11] recently suggested a dynamic modeling approach using the K-equation. Only an outline of the model is provided here, since a more comprehensive description, including the implementation issues, can be found in Ref.11. The eddy viscosity and subgrid dissipation in physical space, for a characteristic filter width Δ, are given as follows.

$$\nu_t = C_\nu K^{\frac{1}{2}}\Delta, \tag{5}$$

$$\epsilon^{sgs} = C_\epsilon\frac{K^{\frac{3}{2}}}{\Delta} \tag{6}$$

For the transport term, a gradient diffusion model based on eddy diffusivity model (with unit eddy Prandtl number) has been proposed and studied by Menon and Kim. This approximation was found to adequately model the transport terms. Hence this is used in a similar form in this study. The dynamic equation for K can now be written as:

$$\frac{\partial K}{\partial t} + \overline{U_j}\frac{\partial K}{\partial x_j} = \tau_{ij}\frac{\partial\overline{U_i}}{\partial x_j} - \epsilon^{sgs} + \frac{\partial}{\partial x_j}\left[\nu_t\frac{\partial K}{\partial x_j}\right] \tag{7}$$

C_ν and C_ϵ are the model constants that need to be specified. These constants, however, are not universal and differ with flow fields in general. This suggests that these constants also depend on the local (supergrid) structure of the flow field. It is, then appropriate to refer to them as coefficients rather than constants. A dynamic approach is applied

here to evaluate these coefficients, thus removing the arbitrariness in prescribing these coefficients. The approach is based on the concept of subgrid stress similarity supported by experiments in jets (Liu et al. [12]). In this approach, a test filter(similar to the LES filter) of characteristic width 2Δ is defined and the corresponding filtered velocity field is denoted by $\widetilde{U_i}$. This new velocity field is obtained by convolution of the LES filtered velocity with the test filter. The subgrid stress corresponding to the scales in between the grid filter width and the test filter width can be written as [11]:

$$t_{ij} = \widetilde{\overline{U_i}}\ \widetilde{\overline{U_j}} - \widetilde{\overline{U_i}}\ \widetilde{\overline{U_j}} \tag{8}$$

and the corresponding dissipation is defined as

$$\epsilon = (\nu + \nu_t)\left[\frac{\partial \widetilde{\overline{U_i}}}{\partial x_j}\frac{\partial \overline{U_i}}{\partial x_j} - \frac{\partial \widetilde{\overline{U_i}}}{\partial x_j}\frac{\partial \widetilde{\overline{U_i}}}{\partial x_j}\right] \tag{9}$$

Assuming stress similarity and the present model to be valid for length scales between Δ and 2Δ (which imposes a further restriction that the test filter width is also in the inertial range of length scales), t_{ij} and ϵ can be written as follows.

$$t_{ij} = -\frac{2}{3}\tilde{K}\delta_{ij} + 2\tilde{\nu}_t\widetilde{\overline{S_{ij}}} \tag{10}$$

and

$$\epsilon = C_\epsilon\frac{\tilde{K}^{\frac{3}{2}}}{2\Delta}, \tag{11}$$

where $\tilde{K} = -\frac{1}{2}t_{ii}$ and $\tilde{\nu}_t$ is the eddy viscosity corresponding to the test filter of width 2Δ and is given by $C_\nu\tilde{K}^{\frac{1}{2}}(2\Delta)$. From eq.(11), the value of C_ϵ can be evaluated. There are, however, six equations represented by eq.(10) using which C_ν could be evaluated. This is a over-determined system of equations and in the present formulation, is solved using least-squares technique. These coefficients are then used for evaluation of eddy viscosity and to advance the dynamic equation for K in time, thus achieving complete closure.

Now, the turbulent flame speed needed for subgrid closure of G-equation is computed using eq.(4). The value of u' needed in this equation is computed using the subgrid kinetic energy.

4 Linear Eddy subgrid model

A subgrid model should be able to account for all the relevant physical phenomena and couple well with the supergrid simulation. It should further allow for simulation of real life physical problems efficiently within the constraints of available computational resources.

A subgrid model based on Linear eddy mixing model (Kerstein, 13-16) was proposed by Menon et al. (17-19). This model treats separately the two basic physical processes that govern the evolution of a reactive system: molecular diffusion (accounted for in the present formulation by prescribing the laminar flame speed) and turbulent stirring. The physics involved in the modeling procedure is outlined here and the mathematical detail is avoided.

The modeling is done on a representative one-dimensional spatially linear domain (contained in each LES cell). The effect of three dimensional eddies is accounted for, on this one dimensional domain using turbulent scaling laws [19]. This reduced representation was found to be fairly accurate for the purpose and leads to a substantial reduction in computational cost. The physical sense of the one dimensional domain depends on the investigation at hand. For example, it is a radial line while investigating the radial dispersion in circular jets, it is an axial line in studies involving axial tranport. In homogeneous turbulence, it is a space curve aligned with the local scalar gradient. In LES, it is an arbitrary curve contained within each finite volume cell.

On the one-dimensional domain, the propagation and stirring are carried out as follows. Propagation is implemented by numerical simulation of G-equation without the convective term, using a finite volume approach on the linear domain. The G-equation now has the following one dimensional form.

$$\frac{\partial G}{\partial t} = S_l|\nabla G| \tag{12}$$

This equation replaces the one dimensional diffusion-reaction equation in the original formulation (for the finite rate kinetics). $G = 0$ corresponds to an unburnt state and $G = 1$ corresponds to a fully burnt state. Any surface in between can be considered to be the flame. The subgrid domain has no particular orientation (no directional information is included) and hence, periodic boundary conditions can be prescribed at the boundaries. The length of the domain is fixed to be the characteristic filter width used in the LES. The way to prescibe the number of cells needed for a finite volume implementation of the above equation is explained later. So the linear domain is a periodic curve of length Δ with arbitary orientation and is fully contained in the LES cell. The convective term is dropped as the effect of subgrid fluid turbulence (stirring) is modeled separately.

More details are given elsewhere (Menon et al. 1993).

The turbulent stirring is modeled by a stochastic process. The sense of subgrid field is, hence, statistical. It is one realization of the field. A Lagrangian rearrangement is chosen as a means to model the effect of fluid dynamic eddies on the scalar gradient. The size of the eddy (needed to detemine the size of the segment in which rearrangement is to be done) and the frequency of occurance is determined using scaling laws characteristic of the inertial range. The rearrangement mapping can be chosen arbitrarily. It should mimic the effect of an eddy on scalar rearrangement in turbulence and also should be conservative (total species concentration should remain unaltered after the mapping). A triplet map [16] is chosen for the present study. In this mapping, the given segment of the linear domain is divided into three equal parts. The spatial gradients (of all properties) in the left and the right segments are increased by a factor of three. The middle segment is reversed and then the scalar gradients are scaled by a factor of three. As illustrated in the fig.1, the scalar field remains continuous and the mapping is conservative. Size of the subgrid finite volume cell is so chosen that a stirring event at the smallest relevant length scale could be executed using this mapping. In the present case, the smallest significant length scale is the Kolmogorov length scale and one need atleast six points to be contained in this length to perform stirring. So the number cells turn out be $6\frac{\Delta}{\eta}$. This mapping causes a particle dispersion with mean square displacement of $\frac{4}{27}l^2$, where l is the length of the segment. The diffusivity associated with this process can be determined to be $\frac{2}{27}\lambda l^3$, where λ is the frequency per unit length. The diffusivity associated with the eddies of length scale l is given by inertial range scaling laws as:

$$D_t = \left[\frac{l}{\eta}\right]^{\frac{4}{3}} \nu \tag{13}$$

where η is the Kolmogorov length scale. Let $f(l)$ be the probability density function of the length scale chosen for the mapping event. By equating the diffusivity associated with the length scale l to the expression in the previous equation, the form of the PDF can be arrived at as:

$$f(l) = \frac{5}{3}\frac{l^{-\frac{4}{3}}}{\eta^{-\frac{5}{3}} - L^{-\frac{5}{3}}} \tag{14}$$

where L is the largest scale for stirring. In the present context of LES, it would equal Δ (all the eddies larger than Δ stir the scalar field at the supergrid level). Solving for λ yeilds

$$\lambda = \frac{54}{5}\frac{\nu Re_L}{L^3}\frac{\left[\frac{L}{\eta}\right]^{\frac{5}{3}} - 1}{1 - \left[\frac{\eta}{L}\right]^{\frac{5}{3}}} \tag{15}$$

where $Re_L = \frac{Lu'}{\nu}$ (the subgrid Reynolds number in the present case).

Heat release causes density gradients in the subgrid linear domain. When the density changes in a finite volume cell, the size of the cell is increased to conserve the mass in each cell. The domain is regridded to a uniform domain for computational ease. In the present case, these is no heat release or density variation, so this procedure is not required. For details on issues regarding heat release, see Smith and Menon[20].

Advection due to the supergrid velocity field brings about transport of the chemical species into the neighbouring LES cells. This is modeled using a procedure called "splicing"(Menon et al., 1993). The scalar flux across each LES cell face is computed using the supergrid velocity field. The number of cells that need to be transferred from one cell (donor cell) to it's neighbouring cell (receiver cell) across this face is computed using this flux and the LES timestep. A segment with this number of cells is picked at random from the donor cell and inserted at a randomly chosen location on the linear domain in the receiver LES cell. This introduces discontinuities in the scalar concentration in the subgrid field. While this seems unphysical, splicing is rare event compared to the subgrid processes and any spurious effects of splicing on subgrid field is minimal. For further details on the implementation, see McMurtry et al. [21].

For each value of $\frac{u'}{S_l}$, simulations are conducted using various different realizations of a statistically stationary flow field as initial conditions. The flame is activated in a similar way in all the simulations. This is done by instantaneously changing the value of G from 0 to 1 in a cubical domain at the centre of the domain.

5 Results and discussion

LES of turbulent Couette flow at Re = 5200 (chosen due to availability of accurate data in literature) was conducted on two different grid resolutions. A streamwise length of πH and span-wise length of $\frac{1}{2}\pi H$, where H is the width of the channel, are used in these simulations. No slip boundary conditions are used in the wall normal direction and periodic boundary conditions are used in the other two directions. A 49x33x33 grid reproduces *rms* of fluctuating

velocities favorably with DNS due to Bech et al. [22]. The grid is clustered near the walls and a y^+ of 0.3 is used as minimum wall normal resolution. These single point statistics are shown in fig.2. There is significant amount of kinetic energy in the subgrid scales at this resolution, so *rms* values of fluctuating velocities should be underpredicted. As can be seen, *urms* is overpredicted by the LES. This is a well noted [23] fact that is true when the axial resolution is inadequate. This overprediction is not expected to alter greatly the flame evolution. The results corresponding to the 25x17x17 LES are presented in fig.3. The trends in prediction, in terms of single point statistics, are as expected. The predictions differ significantly, possibly due to a broad range of energetic scales (subgrid kinetic energy is found to be quite significant). The cutoff scale in these simulations borders on dissipation range of scales. Hence, for the sake of implementing LEM (which requires the cut off scale in the inertial range), a higher Re (=12000) is chosen. The LES resolution is increased accordingly to 65x49x49. The 25x17x17 grid is however retained. The subgrid kinetic energy predictions by LES on these grid resolution are shown in fig.4. The finer grid resolves the shear layer and captures the kinetic energy peak near the wall. The coarse grid does not have adequate resolution near the wall. A y^+ of 4.0 was used for wall normal resolution near the wall. The simulation retains stability but the near wall results are not expected to be correct. Since the focus here, is on the core region, this fact is not of much concern.

The variation of the model coefficients with the wall normal coordinate in this simulation is shown in fig.5. While the values are of the same order of magnitude as in constant coefficient K-equation models, they are found to be lower by a few times. The C_ϵ values are close to it's suggested value of 0.916, but C_ν values are about three times lower than recommended constant value of 0.0854.

While implementing LEM in LES, the laminar flame speed is fixed by prescribing $\frac{u'}{S_l}$, where u' is based on core region turbulent intensity (which is nearly a constant over a wide region).

For the 65x49x49 grid, the volume occupied by the burnt gases (volume integral of G over the whole domain) is plotted against time for three different values of $\frac{u'}{S_l}$: 1, 4 and 8, in fig.6. The corresponding predictions from LES using Yakhot's model are also presented for comparison. This gives the quantitative measure of the flame growth. The comparison is favorable for $\frac{u'}{S_l}$ of 4 and 8, but the flame growth seems to be faster in case of Yakhot's model for $\frac{u'}{S_l}$ of 1. This perhaps could be attributed to the incorrect flame propagation across the supergrid cells brought about by splicing. Splicing is a stochastic algorithm which works in the statistical sense (when averaged over several realizations). Further, the splicing should retain the same number of linear eddy cells in each of the LES cells since the fluid is incompressible. However, it is found that this is not the case. The number of cells in each LES cell is found to change by two cells in the worst case. The number of subgrid cells used in each LES cell is 50, which corresponds to the maximum subgrid Reynolds number (18.0) encountered in this LES. This is a conservation error that needs to be corrected in the future.

As mentioned earlier, each G-surface is considered a flame. Here iso-surfaces of G between 0.1 and 0.9 have been used as flames to collect flame statistics. The analysis of all geometric properties is considered next at a non-dimensional time of 0.4 (non-dimensionalized using channel width and laminar flame speed). Since the flow field is not stationary, several realizations corresponding to large eddy simulations with different initial fluid dynamic states (realizations of a statistically stationary fluid dynamic state) are used in calculation of these statistics.

A measure for characterizing the flame shape called the shape factor is defined as the ratio of smaller to higher eigen-values of the curvature tensor (Ashurst, 1993). It is bounded between -1 and 1. These extreme values correspond to a saddle and a spherical nature of the flame at a point, respectively . The value of 0 indicates a cylindrical structure. This value is computed at several points and a PDF is plotted for the three values of $\frac{u'}{S_l}$ in fig.7, fig.8 and fig.9. The figures indicate a cylindrical propagation of the flame, which is expected due to the shearing effect of Couette flow. There however, seem to be more locations on the flame predicted by LEM with locally spherical or saddle-type structure. This indicates more flame wrinkling by LEM. The Yakhot's model however is implemented using a supergrid field equation and wrinkling is based on the front propagation algorithm. It is difficult to distinguish between flame wrinkling due to turbulence and the spurious oscillations that are a characteristic of numerical methods used to capture scalar fronts using field equations. A DNS using G-equation with a more accurate numerical method for capturing scalar fronts would perhaps give the correct nature of the flame.

The mean curvature PDF is plotted for the three $\frac{u'}{S_l}$ values in fig.10, fig.11. and fig.12. This gives us a measure of local curvature of the flame. Predominant positive curvature indicates a convex flame growing outwards. In the

present study the PDF has a peak in the postive region. There however, are several points where the mean curvature is negative indicating that the flame shape is locally concave (and hence that the flame is wrinkled). Except for the lower value of $\frac{u'}{S_l}$, the results compare favorably to the Yakhot's model predictions.

The data from LES is now used to estimate the flame stretch (in the plane of the flame) which is defined as the rate of change of a Lagrangian flame surface element. It can be expressed in terms of local tangential strain rate, flame curvature and flame speed as (Candel and Poinsot, 1990):

$$\kappa = -n_i e_{ij} n_j - \frac{S_l}{R} \qquad (16)$$

where κ is the stretch, e_{ij} is the resolved scale strain tensor, in the plane of the flame and R is the mean priciple radius of curvature. Positive stretch tends to decrease the flame speed and replanarize the flame, while negetive stretch wrinkles the flame and increases propagation rate. The PDFs for flame stretch for the three $\frac{u'}{S_l}$ values are shown in fig.13, fig.14 and fig.15. As in the case of curvature, the results for the lower value of $\frac{u'}{S_l}$ do not compare well with Yakhot's model.

In case of $\frac{u'}{S_l}$ equal to 1.0, the laminar flame speed is a dominant factor in flame propagation. Turbulence effects are less significant in this case. The capability of a model such as LEM for predicting the correct propagation would depend greatly on the advection (splicing) algorithm. Since the present algorithm is stochastic, it perhaps is not suited for prediction of a near laminar (deterministic) propagation of the flame. An improvement to correct this inadequacy would be the objective of the future research, before the thermodynamics effects such as heat release are included.

The results from 25x17x17 grid are plotted against LES results obtained using Yakhot's on a 65x49x49 grid. It is very unlikely that the 25x17x17 grid would resolve the fine grain turbulent structure of the flame, but the large scale characteristics like the growth in size of the flame could turn out to be reasonably accurate. However, since the grid is coarse, if there exists an inertial range in Couette flow at Re = 12000, it is likely that the grid spacing would lie in the inertial range. Furthermore the subgrid Reynolds number in the core region is found to of the order of 100 as against 20 in the 65x49x49 LES. The LEM was designed as a high Reynolds number model, so it is better to have a high subgrid Reynolds number. The volume occupied by burnt gases versus the time is plotted in fig.16. The pdfs for the ratio of curvatures and flame stretch are plotted in fig.17 and fig.18 respectively. In all these plots, the corresponding results from 65x49x49 LES using Yakhot's model are presented for comparison. It is seen that net growth of the flame is predicted fairly well. Also the pdf for the ratio of curvatures compares favorably with results from Yakhot's model. It is surprising that this prediction is more accurate than in the high resolution simulation. A higher Reynolds number in the subgrid could be one of the reasons for this. The statistics from the low resolution are not expected to be very accurate since they are based on numerical derivatives which can only account for the large scale structures and not the wrinkling at small scales. As can be seen in fig.18, the pdf of flame stretch is not as accurate as in the case of higher resolution case. The accurate prediction of mean curvature pdf could purely be heuristic.

6 Conclusions

The Linear eddy model is found to capture all the trends in the evolution of the flame structure. For the two higher cases of $\frac{u'}{S_l}$, the results are found to be close predictions obtained using Yakhot's model. The only issue of concern seems to the difference in the prediction of the shape factor. This obviously is due to difference between the two methods in accouting for the advection due to supergrid velocity. In LES using Yakhot's model, the correct evolution of the sharp flame front is not captured in the early stages (due to reasons stated earlier). And in case of LEM, there is some randomness involved in the approach. There is no reason to believe one is more correct than the other. But the random nature of splicing is also the reason why the prediction of the flame structure in the case of near laminar (deterministic) propagation ($\frac{u'}{S_l}$=1) is found to be different. The splicing procedure may need to be modified in such cases.

The accurate prediction of flame growth in 25x17x17 is, however, very encouraging, a fact that warrants further research on LEM implementation in LES on grids coarse enough to be computationally efficient.

Acknowledgements

This research was supported by the NASA Lewis Research Center under Grant No. NAG3-1610 and by the Office of Naval Research under Grant N00014-93-1-0342. The authors acknowledge the help rendered by T. M. Smith, graduate student at the Georgia Institute of Technology, during the course of this research. The computer time was pro-

vided by the DoD on the SGI Power Challenge Array at the HPC Center, Army Research Laboratories, Maryland.

References

1. Patterson, G. K., Application of turbulence fundamentals to reactor modeling and scaleup. *Chem. Eng. Commun.* 1981, **8**, 25.

2. Pope, S. B., PDF methods for turbulent reactive flows. *Prog. Energy Combust. Sci.* 1985, **11**, 119.

3. Frankel, S. H., Adumitroaie, V., Madnia, C. K. and Givi, P. Large eddy simulation of turbulent reacting flows by assumed PDF methods. *Engineering Application of Large Eddy Simulations.* 1993, ASME-FED-Vol.**162**, 81-101.

4. Gao. F., and O'Brien, E. E. A large eddy simulation scheme for turbulent reacting flows. *Phys. Fluids A*, 1993, **5**, 1282-1284.

5. Pope, S. B. PDF methods for turbulent combustion: Progress and challenges, *Twenty third symposium (Int.) on combustion*, 1990, The Combustion Institute, 591-612.

6. Yakhot, V. Propagation velocity of premixed turbulent flames. *Combust Sci. Tech.* 1988, **60**, 443-450.

7. Menon, S. and Kerstein, A. R. Stochastic simulation of the structure and propagation rate of turbulent premixed flmaes. *Twenty fourth symposium (Int.) on combustion*, 1992, The Combustion Institute, 443-450.

8. Fureby, C. and Moller, S.-I. Large eddy simulation of reacting flows applied to bluff body stabilized flames. *AIAA J.*, 1995, **12**, 2339-2347.

9. Kerstein, A. R., Ashurst, W. and Williams, F. A. Field equation for interfacepropagation in an unsteady homogeneous flow field. *Physical Review*, 1988 **A37**, 2728-2731.

10. Yan Zang, R. L. Street, and J. R. Koseff. A non-staggered grid, fractional step method for the time-dependent incompressible Navier-Stokes equations in curvilinear coordinates, *J. Comp. Phys.*, 1994, **114**, 18-33.

11. Menon, S., and W.-W. Kim. High Reynolds number flow simulations using the localized dynamic subgrid scale model, *AIAA Paper 96-0425, 34th Aerospace Sciences Meeting and Exhibit*, Reno, NV.

12. Liu, S., Meneveau, S. and J. Katz, On the properties of similarity subgrid scale models as deduced from measurements in a turbulent jet," *J. Fluid Mech.*,1994 **275**, 83.

13. Kerstein, A. R. Linear eddy model of turbulent scalar transport and mixing. *Combust. Sci. Tech.*, 1988, **60**, 391-421.

14. Kerstein, A. R. Linear eddy model of turbulent transport II. Application to shear layer mixing. *Comb. Flame*, 1989, **75**, 397-413.

15. Kerstein, A. R. Linear eddy model of turbulent transport III. Mixing and differential molecular diffusion in round jets. *J.Fluid.Mech.*, 1990, **216**, 411-435.

16. Kerstein, A. R. Linear eddy model of turbulent transport. Part 6:i Microstructure of diffusive scalar fields. *J.Fluid.Mech.*, **231**, 361-394.

17. Menon, S. A new subgrid model for large eddy simulations of turbulent reacting flows,*QUEST Technical Report No. 595*, NASA Contract No. NAS2-13354, 1991.

18. Menon, S., McMurtry, P. A., and Kerstein, A. R. A linear eddy subgrid model for turbulent combustion: Application to premixed combustion, *AIAA paper 93-0107, AIAA 31st Aerospace Sciences Meeting*, Reno.

19. Menon, S., McMurtry, P. A. and Kerstein, A. R. A linear eddy mixing model for LES of turbulent combustion, in *LES of Complex Engineering and Geophysical flows* (Galerpin, B. and Orszag, S. ed.), Cambridge Univ. Press (1994).

20. Smith, T., and Menon, S. Model Simulations of freely propagating turbulent premixed flames. Paper No. 26-290, to be presented at the *Twenty sixth symposium (Int.) on combustion*, July28 - August2, 1996, Naples, Italy.

21. McMurtry, P. A., Menon, S., and Kerstein, A. R. A subgrid mixing model for LES of non-premixed turbulent combustion, *AIAA paper 92-0234, AIAA 30th Aerospace Sciences Meeting*, Reno.

22. Bech, K. H., Tillmark, N., Alfredson, P. H., and Anderson, H. I. An investigation of turbulent plane Couette flow at low Reynolds numbers, *Combust. Sci. Tech.*, 1995, **286**, 291-327.

23. Askelvoll, K. and Moin, P. Large eddy simulation of turbulent confined coannular jets, *J.Fluid.Mech.*, 1996, **315**, 387-412.

24. Ashurst, Wm. T. Constant density Markstein Flamelets in Navier Stokes turbulence, submitted to *Combust. Sci. and Tech.*

25. Candel, S. M. and Poinsot, T. J. Flame Stretch and the balance equation for the flame area, 1990, *Combust. Sci. and Tech.*, **70**, 1-15.

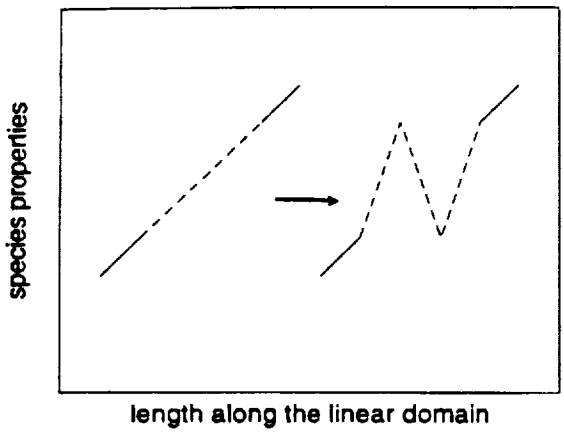

Figure 1: Illustration of triplet mapping

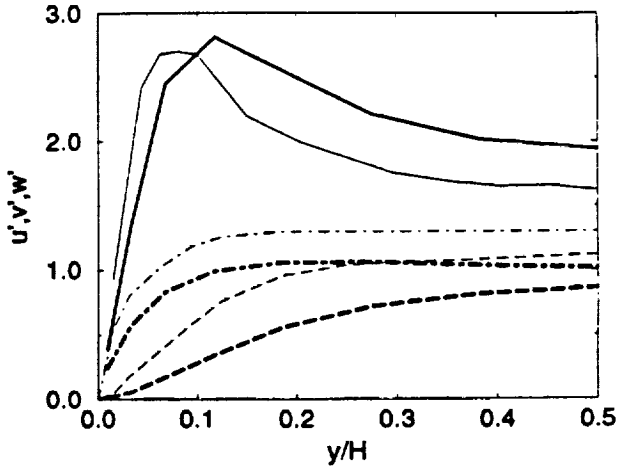

Figure 3: Rms velocities (non-dimensionalized by $u*$, the friction velocity) in LES of Couette flow(Re=5200) on 25x17x17 grid. Solid line: urms, dashed line: vrms, dotted-dashed line: wrms. Corresponding thinner lines indicate DNS data due to Bech et al.[22]

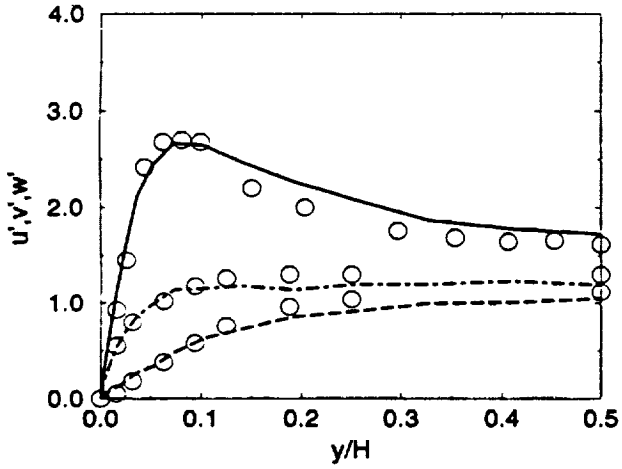

'igure 2: Rms velocities (non-dimensionalized by $u*$, the riction velocity) in LES of Couette flow(Re=5200) on 9x33x33 grid. Solid line: urms, dashed line: vrms, dotted-ashed line: wrms. Circles indicate DNS data due to Bech t al.[22].

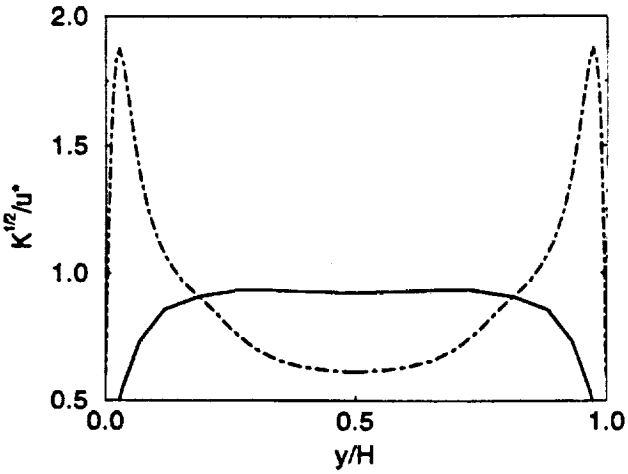

Figure 4: Subgrid kinetic energy in LES at Re = 12,000. Solid line: 25x17x17 grid, dotted-dashed line: 65x49x49 grid

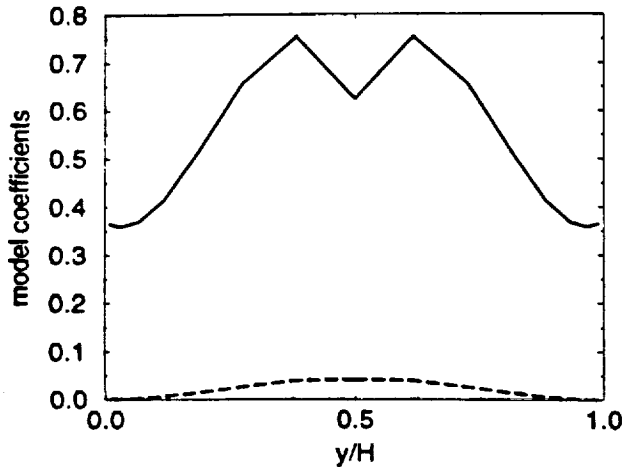

Figure 5: Variation of model coefficients computed using filtering approach. Solid line: C_ϵ, dashed line: C_ν

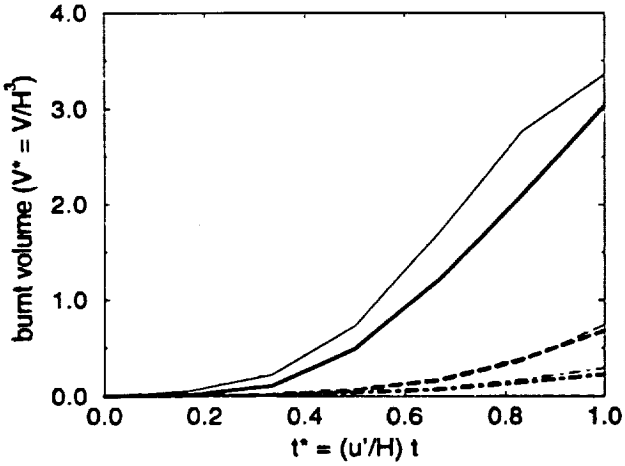

Figure 6: Temporal variation of volume occupied by burnt fluid in LES on a 65x49x49 grid. Solid line: $\frac{u'}{S_l} = 1$,dashed line: $\frac{u'}{S_l} = 4$, dotted-dashed line: $\frac{u'}{S_l} = 8$. The thinner lines indicate corresponding predictions from LES using Yakhot's model.

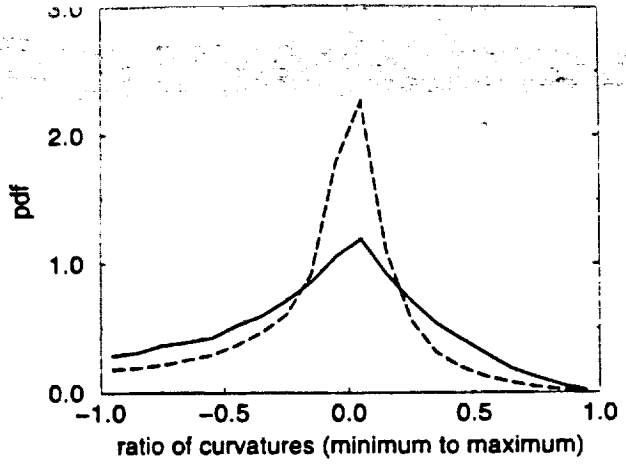

Figure 7: Pdf of the shape factor for $\frac{u'}{S_l} = 1$. Solid line: LEM, dashed line: Yakhot's model

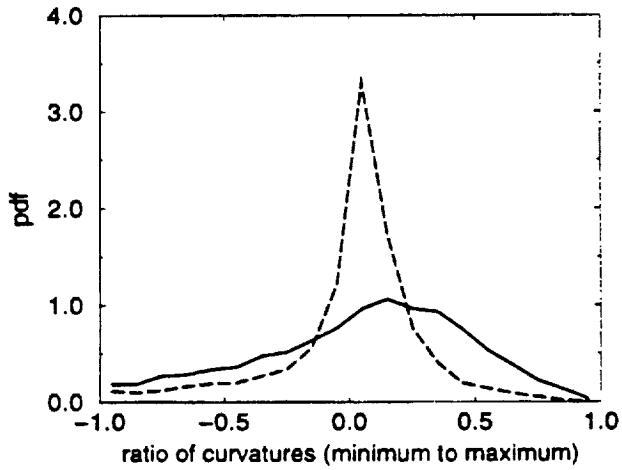

Figure 8: Pdf of the shape factor for $\frac{u'}{S_l} = 4$. Solid line: LEM, dashed line: Yakhot's model

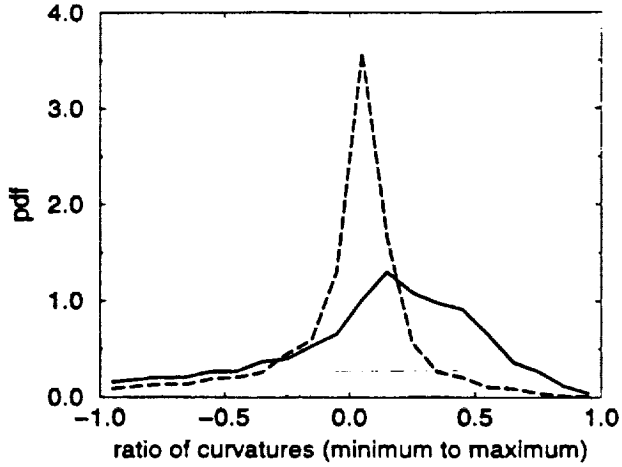

Figure 9: Pdf of the shape factor for $\frac{u'}{S_l} = 8$. Solid line: LEM, dashed line: Yakhot's model

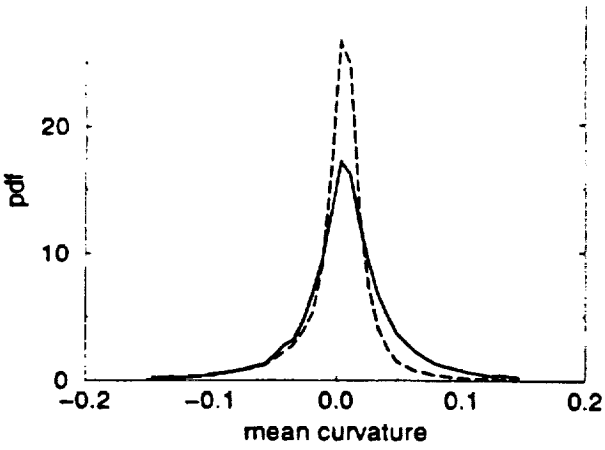

Figure 10: Pdf of the mean curvature for $\frac{u'}{S_l} = 1$. Solid line: LEM. dashed line: Yakhot's model

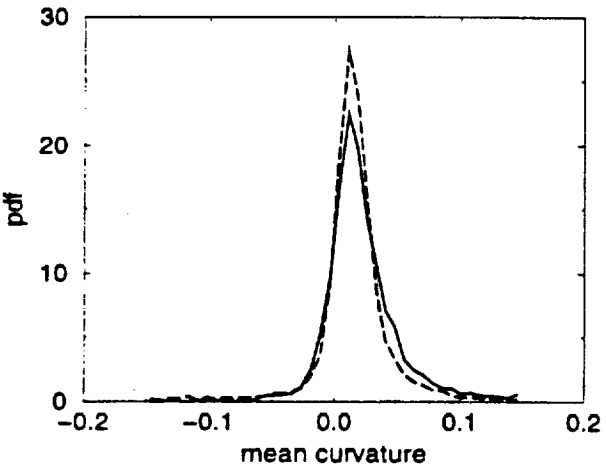

Figure 11: Pdf of the mean curvature for $\frac{u'}{S_l} = 4$. Solid line: LEM, dashed line: Yakhot's model

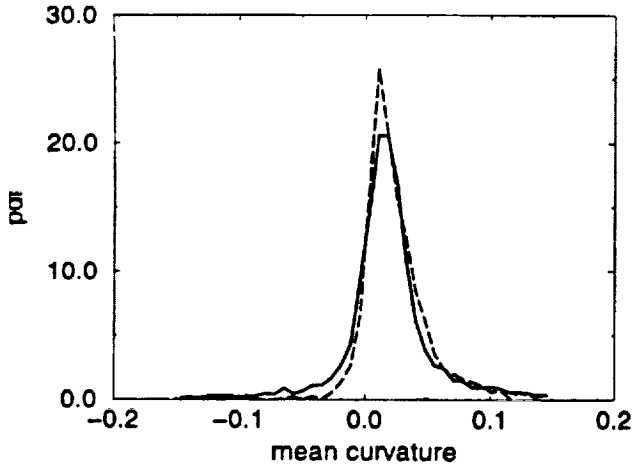

Figure 12: Pdf of the mean curvature for $\frac{u'}{S_l} = 8$. Solid line: LEM, dashed line: Yakhot's model

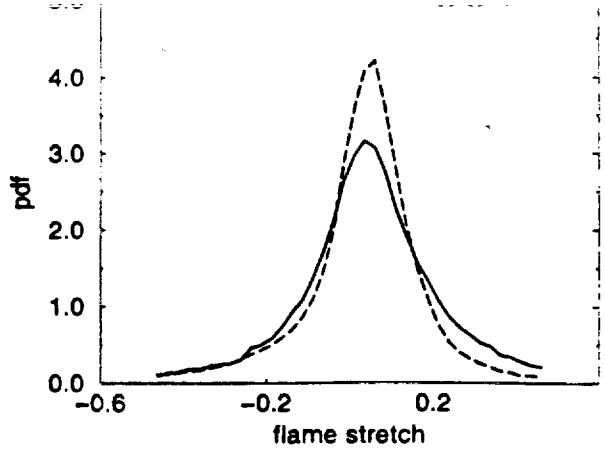

Figure 13: Pdf of the flame stretch for $\frac{u'}{S_l} = 1$. Solid line: LEM , dashed line: Yakhot's model

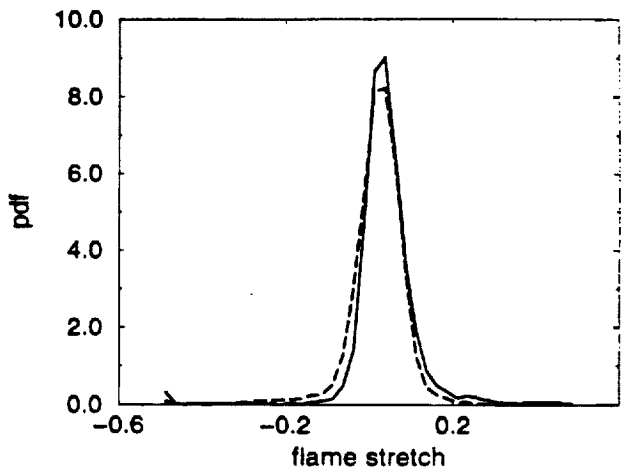

Figure 14: Pdf of the flame stretch for $\frac{u'}{S_l} = 4$. Solid line: LEM , dashed line: Yakhot's model

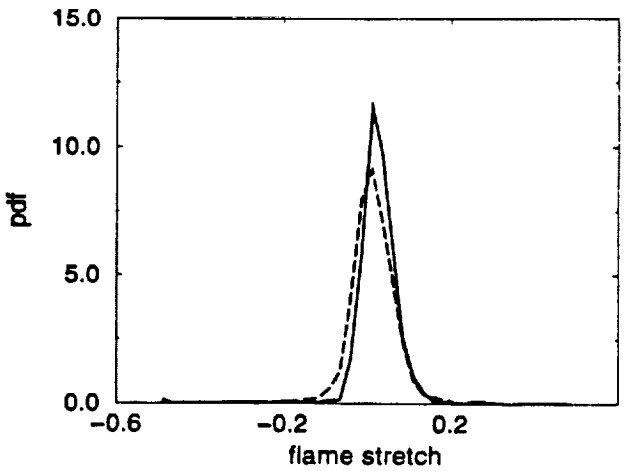

Figure 15: Pdf of the flame stretch for $\frac{u'}{S_l} = 8$. Solid line: LEM , dashed line: Yakhot's model

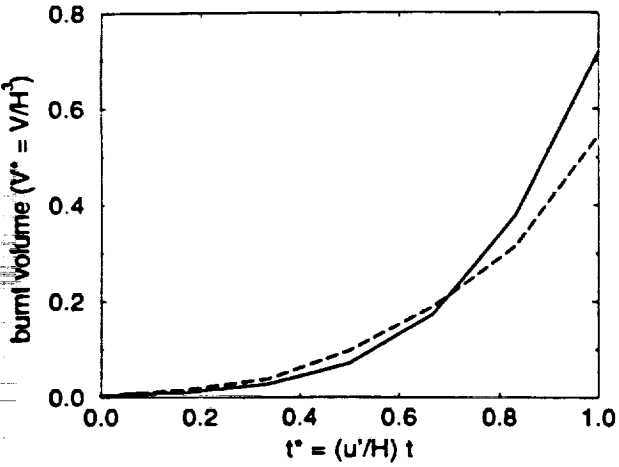

Figure 16: Temporal variation of volume occupied by burnt fluid in LES on a 25x17x17 grid. Solid line: LEM on a 25x17x17 grid, dashed line: Yakhot's model on a 65x49x49 grid.

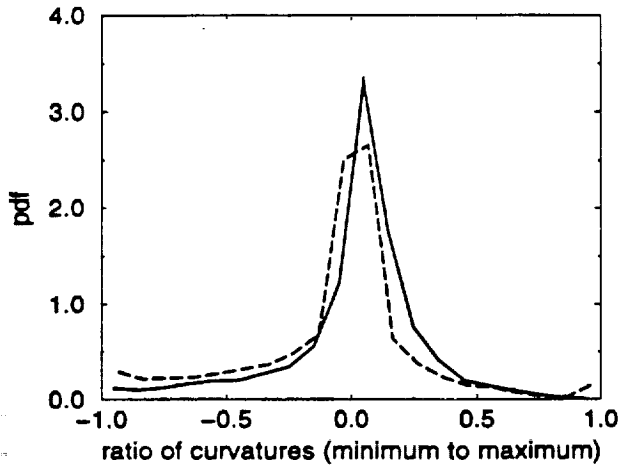

Figure 17: Shape factor of the flame predicted by LES on 25X17X17 grid. Solid line: LEM, dashed line: LES using Yakhot's model on 65x49x49 grid.

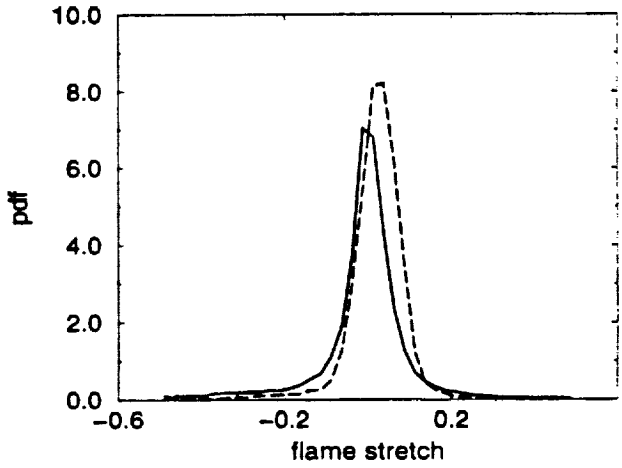

Figure 18: Pdf of flame stretch predicted by LES on 25X17X17 grid. Solid line: LEM, dashed line: LES using Yakhot's model on 65x49x49 grid.